A LABORATORY INVESTIGATION OF CONDUCTIVITY AND DIELECTRIC CONSTANT TENSORS OF ROCKS

Thesis for the Degree of Ph. D.
MICHIGAN STATE UNIVERSITY
DONALD GARDNER HILL
1969

THESIS

LIBRARY
Michigan State
University

This is to certify that the

thesis entitled

A Laboratory Investigation of
Conductivity and Dielectric Constant Tensors
in Rocks
presented by

Donald Gardner Hill

has been accepted towards fulfillment
of the requirements for

Ph.D. **degree in** Geology

William J. Hinze
Major professor

Date October 20, 1969

O-169

BINDING BY
HOAG & SONS'
BOOK BINDERY INC.
SPRI... MICHIGAN

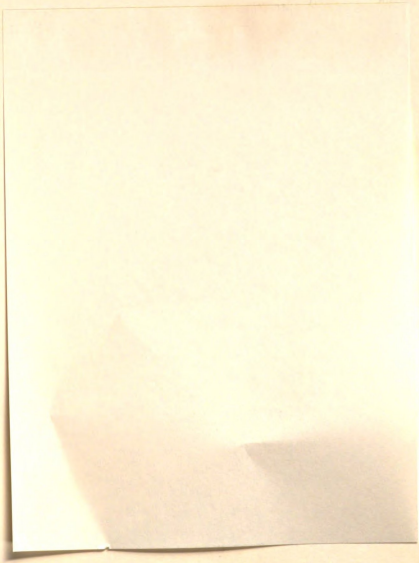

ABSTRACT

A LABORATORY INVESTIGATION OF CONDUCTIVITY AND DIELECTRIC CONSTANT TENSORS OF ROCKS

By

Donald Gardner Hill

The dielectric constant and conductivity of a material are symmetric second-rank tensors. These particular tensors are represented mathematically by a symmetric 3 x 3 matrix and geometrically by an ellipsoidal surface. Six independent coefficients must be determined to completely define these tensors. Thus, measurements of these properties must be made in at least six different directions, to completely define the tensors. Electrical anisotropy is studied by noting the orientations and magnitudes of the conductivity and dielectric constant tensors. An ordered arrangement, or symmetry, of the mineral grains composing a rock will be reflected in the orientation and symmetry of its conductivity and dielectric constant tensors.

Laboratory A.C. dielectric constant and electrical conductivity measurements were made on selected dry metasediments, meta-volcanics and meta-igeneous rocks from the Precambrian of Michigan and Ontario. Sample preparation and measurement followed A.S.T.M. standards D 150-65 (1965) for two electrode, low frequency bridge measurements of

lectric materials.

dielectric consta

ency range from 30

The results of

e rocks, particula

standing, are chara

trical properties

lower frequencies,

I.P. prospecting.

electric data gene

exhibit strong c

riate, and minimum

ue should be exerci

retation methods fo

dielectric materials. The anisotropy of the conductivity and dielectric constant tensors was studied over the frequency range from 30 to 100,000 cps.

The results of this laboratory study indicate that some rocks, particularly those with pronounced lineation, or banding, are characterized by strongly anisotropic electrical properties. This anisotropy tends to increase at lower frequencies, in the range of those used for E.M. and I.P. prospecting. Theoretical methods of interpreting geoelectric data generally assume that earth materials do not exhibit strong orthorhombic (distinct maximum, intermediate, and minimum principal values) anisotropy. Thus, care should be exercised when using theoretical interpretation methods for areas where anisotropy is suspected.

A LABORATORY INV

AND DIELECTRIC

Don

Mich
in partial fu

D

L

A LABORATORY INVESTIGATION OF CONDUCTIVITY AND DIELECTRIC CONSTANT TENSORS OF ROCKS

By

Donald Gardner Hill

PLEASE NOTE:

Not original text. Some pages have some Tables. Information [illegible] Appendix pages. Filled on [illegible]

UNIVERSITY MICROFILMS

A THESIS

Submitted to
Michigan State University
in partial fulfillment of the requirements
for the degree of

DOCTOR OF PHILOSOPHY

Department of Geology

1969

© Copyright by
DONALD GARDNER
1977

© Copyright by
DONALD GARDNER HILL
1970

AC

The author wishes

Dr. W. J. Hinze,
partment of Geology,
couragement, and cri

Dr. H. M. Mooney
partment of Geology
ance with the insigh
his study.

Dr. H. B. Stoneh
chigan State Univers
uggestions and critic
sults of this study.

Mr. T. D. Waggon
mpany, for his aid
ities.

The Michigan St
gineering, for the
dielectric sample hol

The National Ae
for financial support

GG1158
3-18-70

ACKNOWLEDGMENTS

The author wishes to express his sincere appreciation to:

Dr. W. J. Hinze, of the Michigan State University Department of Geology, for his patient guidance, advice, encouragement, and criticism throughout this study.

Dr. H. M. Mooney, of the University of Minnesota Department of Geology and Geophysics, for providing the author with the insight and inspiration needed to undertake this study.

Dr. H. B. Stonehouse and Dr. J. W. Trow, of the Michigan State University Department of Geology, for their suggestions and criticisms concerning the geological aspects of this study.

Mr. T. D. Waggoner, of the Cleveland-Cliffs Iron Company, for his aid and assistance in selecting sampling sites.

The Michigan State University Department of Electrical Engineering, for the loan of a General Radio type 1690-A dielectric sample holder.

The National Aeronautics and Space Administration, for financial support.

In addition, the

ssions with Mr. J. D.

.. A. Cowen, of the

nt of Physics; Mr. M

gh Dr. N. L. Hills,

rtment of Mathemat

rado School of Min

Macallister, of The

rth, of the Michig

matics to be ver

In addition, the author found written and oral discussions with Mr. J. D. Corbett, of The Anaconda Company; Dr. J. A. Cowen, of the Michigan State University Department of Physics; Mr. M. Halverson, of the Anaconda Company; Dr. N. L. Hills, of the Michigan State University Department of Mathematics; Dr. G. V. Keller, of the Colorado School of Mines Department of Geophysics; Mr. E. Macallister, of The Anaconda Company; and Dr. C. J. Martin, of the Michigan State University Department of Mathematics to be very helpful.

TA

TABLE OF CONTENTS

LIS

LIST OF TABLES

LIS

ure

1. Homogeneous, Is
Model . . .

2. Wenner Electro

3. Schlumberger E

4. Two-Layer Eart

5. Wenner Configu
Curves for H
Layered Eart
and Cook, 1

6. Schlumberger
Master Curv
tropic, Two
Orellana an

7. Wenner Electr
Arbitrary
Principal

8. Lossy Dielec
Circuit .

9. Lossy Dielec
Properties
1964; Kel

10. Block Diagr
Measureme

11. Analog Circ
Holder Co

12. Analog Circ
Holder W

LIST OF FIGURES

Anisotropy Rat

Deck Order for

Rationale

Electrically, ma

semiconductors.

nt of the actual p

Thompson (1964) a

ssification given

s most practical

, of rocks a

both the dielectr

erial are symmetr

completely defin

hen presented as

rticular symmetric

ted graphically b

e manner that the

ical properties o

ystals, the symme

operties they rep

e crystallographi

964). Thus, we ca

CHAPTER I

INTRODUCTION

Rationale for the Present Study

Electrically, most rocks are lossy dielectrics, or poor semiconductors. This is true, both from the standpoint of the actual physical definitions, as given by Wert and Thompson (1964) and Beam (1965), or the rule of thumb classification given by Keller (1966). For this reason, it is most practical to consider the electrical conductivity, σ, of rocks along with their dielectric constant, K. Both the dielectric constant and conductivity of a material are symmetric, second-rank tensors. As such, they are completely defined by six independent coefficients (often presented as a symmetric 3 x 3 matrix). These two particular symmetric second-rank tensors also can be represented graphically by ellipsoidal surfaces, in much the same manner that the optical indicatrix represents the optical properties of transparent materials. Within crystals, the symmetry of these surfaces and that of the properties they represent must parallel the symmetry of the crystallographic point group of the crystal (Nye, 1964). Thus, we can orient crystals by the symmetry of

physical p

onship in

fabric.

Theoretic

generally

orthorh

ute, and m

this, we ne

potential

orizontall

ters and B

schknecht

en, the as

rallel, ho

tial equat

ation and

solution

distance,

d in r, the

If, howe

otropic is e

no analytic

ar co-ordina

se, does not

on. A co-ord

ear to be iso

their physical properties. One would expect a similar relationship in rocks, particularly those with a pronounced fabric.

Theoretical methods of interpreting geoelectric data generally assume that earth materials do not exhibit strong orthorhombic anisotropy (distinct maximum, intermediate, and minimum principal values). For an example of this, we need look no further than the many papers on the potential distribution about a point electrode over a horizontally layered earth (cf., Stefansco et al., 1930; Peters and Bardeen, 1932; Grant and West, 1965; Keller and Frischknecht, 1966). In the isotropic layered earth problem, the assumption is made that the earth consists of parallel, homogeneous, and isotropic layers. The differential equation (D.E.) to be satisfied is Laplace's equation and the model has cylindrical symmetry. Thus, the solution is in terms of exponentials in z, the vertical distance, and zero order Bessel functions of the first kind in r, the radial distance from the source.

If, however, the requirement that the layers be isotropic is eliminated from the B.V.P., it apparently has no analytical solution. Conversion to cylindrical polar co-ordinates, which is so helpful in the isotropic case, does not yield a D.E. which has an analytical solution. A co-ordinate transformation so that the layers appear to be isotropic in the transformed system

...heim, 1947)
...B.C.), fo
...dinate syst
If the ele
...y be possi
...ds based o
...r. The pur
...possible o
...perties of
...s study wh
...e., those
...e absence
...eliminate
...y in roc
...portance as

There ha
...sotropy of
...sotropy (cf.
...acey, 1961) d
...sor properti
...ectrical prope
...estigation, w
...esent, uses fo
...rasnis, 1956;
...illett (1959) a

(Buchheim, 1947) produces very difficult boundary conditions (B.C.), for there will be discontinuities in the co-ordinate systems at the boundaries.

If the electrical anisotropy of rocks is not great, it may be possible to use theoretical interpretation methods based on the assumption of isotropy with little error. The purpose of this study will be to investigate the possible orthorhombic anisotropy in the electrical properties of vacuum dried rocks. Rocks were selected for this study which are most suspect of exhibiting anisotropy (i.e., those rock types which exhibit strong fabrics). The absence of anisotropy in the rock types studied would not eliminate the possibility of strong electrical anisotropy in rocks. It would, however, cast doubt on its importance as a geological phenomenon.

Previous Work

There has been very little previous work on electrical anisotropy of rocks. Those papers which did consider anisotropy (cf., Schlumberger et al., 1934; Rao, 1948; Stacey, 1961) did not attempt to completely define the tensor properties. There has, however, been more work on electrical properties in general. An early method of investigation, which has retained some popularity to the present, uses four point electrodes (cf., Harvey, 1928; Parasnis, 1956; Vacquier et al., 1957; Shaub, 1964). Collett (1959) attempted to overcome the problems involved

using point ele

ing strap potent

ectrodes. While

estion as to wh

e effects of po

ems. Ward (19

ems. Keller a

Bell and Licas

nd Siessman (1

1966) and Park

ulations of el

nd minerals.

talogued mea

A very t

nd oral discu

personnel, re

t is now att

nductivity

he discussio

xploration

hysicists n

econd-rank

s too ofte

nisotropy

ensor prop

irections.

in using point electrodes on inhomogeneous material by using strap potential electrodes and plate current electrodes. While he succeeded at this, there is some question as to whether or not he completely eliminated the effects of polarization at the sample-electrode contacts. Ward (1953) and Orr (1964) used inductive measurements. Keller and Licastro (1959), Arbogast et al. (1960), Howell and Licastro (1961), Stacey (1961), Simandoux (1963), and Liessman (1964) used capacitance measurements. Keller (1966) and Parkhomenko (1967) gave the most recent compilations of electrical properties determined for rocks and minerals. Heiland (1940) and Parkhomenko (1967) have catalogued measurement methods in some detail.

A very thorough literature search, as well as written and oral discussions with industrial research laboratory personnel, revealed that apparently no one has attempted, or is now attempting, to completely define the electrical conductivity or dielectric constant tensors of rocks. The discussions mentioned above, as well as those with exploration geophysicists have revealed that many geophysicists normally do not consider σ and K as symmetric second-rank tensors and thus fail to define them completely. All too often in the past, investigations of electrical anisotropy have consisted of measurements of the effective tensor properties in two or three mutually perpendicular directions. While this may give an indication of

ıtropy, it does no

ınd-rank tensor.

Purpos

The purpose of

ıption underlying

n interpretation,

t least have cyli

ıal in their anis

ıption will only

Before commenc

e that a theoreti

perty to be studi

the present study

ectrical model fo

ies. This model i

rocedure for measu

o give qualitative

dvantage of using

the laboratory pro

stimation theory

ill yield estimat

ased model and t

heory would be t

would yield only

have any physical

anisotropy, it does not completely define the symmetric second-rank tensor.

Purpose of the Investigation

The purpose of this study is to test the fundamental assumption underlying theoretical methods of geoelectric data interpretation, that rocks are essentially isotropic, or at least have cylindrical symmetry (two equal principal values) in their anisotropy. In the present study, this assumption will only be tested for vacuum dried rocks.

Before commencing a petrophysics study, it is imperative that a theoretical model be developed for the rock property to be studied. Thus, much of the early portion of the present study was devoted to developing a qualitative electrical model for rocks based on sound physical principles. This model is then used to design a laboratory procedure for measuring electrical anisotropy of rocks and to give qualitative predictions of expected results. The advantage of using a theoretically based model to design the laboratory procedure is that it allows the use of estimation theory in the interpretation of the data. This will yield estimates of parameters in the theoretically based model and their accuracy. Opposed to estimation theory would be tests of significance. This approach would yield only statistical parameters which need not have any physical significance. Tests of significance

...e used when littl...

...theoretically va...

...is more appropri...

The theoreticall...

...be that of the lo...

...story and data re...

...will completely ...

...tensors. Care ...

...ues which will al...

...reasonable amount ...

The effects of ...

...P. used in theor...

...also considered ...

...anisotropy to a ...

...ible, to solve ...

...be gained by pr...

...lytical solutio...

...ined by simplify...

...ution is possib...

...re complicated ...

must be used when little is known about a phenomenon, but when a theoretically valid model is available, estimation theory is more appropriate.

The theoretically based model developed for rocks will be that of the lossy dielectric. Thus, suitable laboratory and data reduction procedures must be developed which will completely define the symmetric second-rank σ and K tensors. Care must be exercised to develop procedures which will allow measurements to be repeated with a reasonable amount of precision.

The effects of strong orthorhombic anisotropy on a B.V.P. used in theoretical geoelectric data interpretation are also considered. As previously indicated, the addition of anisotropy to a B.V.P. makes it difficult, if not impossible, to solve analytically. However, some insight may be gained by proceeding as far as possible toward an analytical solution. Qualitative predictions may also be gained by simplifying the B.V.P. so that an analytical solution is possible and extending these results to the more complicated problem.

THE EFFECT OF OR

ANISOTROPI

The electrical c

symmetric second-r

periment to measure

to study their electr

sider the effect t

isotropy has on the

terpretation method

ced I.P.) problem is

his effect. Other

to this particular

matically the pro

thorhombic anisotr

undary value probl

he conductivity, σ

sistivity (conduc

be converted to I.P

ivity, $\sigma^* = j\omega\varepsilon +$

$= \tan^{-1}(\frac{\omega\varepsilon}{\sigma})$, or t

he resistivity pro

CHAPTER II

THE EFFECT OF ORTHORHOMBIC ANISOTROPY--THE ANISOTROPIC LAYERED EARTH PROBLEM

Introduction

The electrical conductivity and dielectric constant are symmetric second-rank tensors. Before designing an experiment to measure the electrical properties of rocks and study their electrical anisotropy, it is helpful to consider the effect that orthorhombic (low symmetry) anisotropy has on theoretically based geoelectric data interpretation methods. The layered earth resistivity (and I.P.) problem is chosen as a vehicle to demonstrate this effect. Other geoelectric problems could be used, but this particular problem is useful because it shows dramatically the problems involved when the condition of orthorhombic anisotropy is added to the layered earth boundary value problem (B.V.P.). In this chapter, only the conductivity, σ, will be considered. However, the resistivity (conductivity) results of this chapter can be converted to I.P. response by use of the complex conductivity, $\sigma^* = j\omega\varepsilon + \sigma = \sigma_o e^{j\phi}$, where $\sigma_o = \sqrt{\omega^2\varepsilon^2 + \sigma^2}$ and $\phi = \tan^{-1}(\frac{\omega\varepsilon}{\sigma})$, or the method of Seigel (1959a, 1959b). The resistivity problem for a horizontally layered,

...model will first ...

...problem will be co...

...anisotropy. The dis...

...ver about the bounda...

...potential distribut...

...ered earth. A boun...

...ined by a differenti...

...dary conditions (B...

...unction which satis...

...gion of interest an...

...del.

The Isotro...

Electric curre...

...rson and Lorrain, ...

...aces or sinks, th...

...ector, $\underline{J}$, vanishes ...

$$\nabla \cdot \underline{J} = 0.$$

...e current densit...

...field intensity ve...

...w, $\underline{J} = \sigma \underline{E}$, and $\underline{E}$ ...

...by $\underline{E} = -\nabla V$. Fo...

...that equation ...

$$\nabla \cdot \underline{J} = \nabla \cdot \sigma \underline{E}$$

...

earth model will first be briefly reviewed. Then, the same problem will be considered with the added condition of anisotropy. The discussions of this chapter will center about the boundary value problems concerned with the potential distribution about a point source in a layered earth. A boundary value problem (B.V.P.) is defined by a differential equation (D.E.) and a set of boundary conditions (B.C.). The solution to a B.V.P. is a function which satisfies the D.E. at every point in the region of interest and the B.C. at all boundaries of the model.

The Isotropic Differential Equation

Electric current acts as an incompressible fluid (Corson and Lorrain, 1962); thus, in the absence of current sources or sinks, the divergence of the current density vector, $\underline{J}$, vanishes, or:

$$\nabla \cdot \underline{J} = 0. \qquad 2.1$$

The current density vector, $\underline{J}$, is related to the electric field intensity vector, $\underline{E}$, by the vector form of Ohm's law, $\underline{J} = \sigma \underline{E}$, and $\underline{E}$ is related to the electric potential, V, by $\underline{E} = -\nabla V$. For isotropic materials, σ is a scalar, so that equation 2.1 becomes:

$$\nabla \cdot \underline{J} = \nabla \cdot \sigma \underline{E} = -\sigma \nabla \cdot \nabla V = -\sigma \nabla^2 V = 0,$$

or:

$$\nabla^2 V = \frac{\partial^2 V}{\partial x^2} + \frac{\partial^2 V}{\partial y^2} +$$

...is Laplace's equa...

...sitivity problem po...

...place's equation (2...

The Isotr...

The basic B.C. f...

...ctric current in ma...

...ponent of $\underline{E}$ and the...

...tinuous across all...

...de Lorrain, 1962).

...ponent of $\underline{E}$, it f...

...ction, V, should...

...ces (Grant and Wes...

...arating material...

$$V_1 = V_2.$$

For an isotr...

...or an isotropic m...

...rrent density v...

$$\underline{J} \cdot \hat{n} = -\sigma$$

...ld at the bounda...

...and 2, this B...

$$\sigma_1 \frac{\partial V_1}{\partial \hat{n}} = \sigma_2$$

$$\nabla^2 V = \frac{\partial^2 V}{\partial x^2} + \frac{\partial^2 V}{\partial y^2} + \frac{\partial^2 V}{\partial z^2} = 0, \qquad 2.2$$

which is Laplace's equation. Thus, the isotropic resistivity problem potential distributions must satisfy Laplace's equation (2.2).

The Isotropic Boundary Conditions

The basic B.C. for a B.V.P. involving the flow of electric current in materials are that the tangential component of $\underline{E}$ and the normal component of $\underline{J}$ must be continuous across all boundaries in the model (Corson and Lorrain, 1962). From the continuity of the tangential component of $\underline{E}$, it follows directly that the potential function, V, should also be continuous across all boundaries (Grant and West, 1965). For example, at a boundary separating material 1 from material 2, the B.C. would be:

$$V_1 = V_2. \qquad 2.3$$

For an isotropic material, σ is a scalar. Thus, for an isotropic material, the normal component of the current density vector may be written as:

$$\underline{J} \cdot \hat{n} = -\sigma \nabla V \cdot \hat{n} = -\sigma \frac{\partial V}{\partial \hat{n}},$$

and at the boundary separating the two isotropic materials, 1 and 2, this B.C. becomes:

$$\sigma_1 \frac{\partial V_1}{\partial \hat{n}} = \sigma_2 \frac{\partial V_2}{\partial \hat{n}}. \qquad 2.4$$

The above B.C. (eq
ensal B.C. for all i
, there are usually
ential function at t
m from the source.
ential function.

The Homogeneo

Consider a curre
ated on a plane bou
ace of conductivity,
on in Figure 2.1.
ace conductivity is
metry. It is thus
uation (2.2) into s
is isotropic, the p
$R = \sqrt{x^2 + y^2 + z^2}$

$$\nabla^2 V = \frac{d^2V}{dR^2} + \frac{2}{R}\frac{d}{d}$$

Fig. 2.1.--Hom
ath model.

The above B.C. (equations 2.3 and 2.4) are the most universal B.C. for all isotropic earth models. In addition, there are usually B.C. involving the values of the potential function at the source and at an infinite distance from the source. These serve to calibrate the potential function.

The Homogeneous, Isotropic Half-Space

Consider a current (point) source electrode, S, located on a plane bounding a homogeneous, isotropic half-space of conductivity, σ, from a half-space of $\sigma = 0$, as shown in Figure 2.1. Because only the half-space with finite conductivity is of interest, the model has spherical symmetry. It is thus convenient to convert Laplace's equation (2.2) into spherical polar co-ordinates. Because σ is isotropic, the potential function will be a function of $R = \sqrt{x^2 + y^2 + z^2}$ only and Laplace's equation becomes:

$$\nabla^2 V = \frac{d^2V}{dR^2} + \frac{2}{R}\frac{dV}{dR} = 0. \qquad 2.5$$

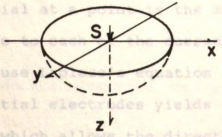

Fig. 2.1.--Homogeneous, isotropic half-space earth model.

olution of the B.V

and the earth model

, 1965; Keller and

$$V(R) = \frac{I}{2\pi\sigma R} ,$$

ere I is the current

face resistivity an

ly measured at t

ming $r = \sqrt{x^2 + y^2}$

tion about a point e

$$V(r,0) = \frac{I}{2\pi\sigma r} .$$

Appr

In the develop

is assumed to be in

ld operation

ur-point electrode

and two potential el

stances). For mu

ick) the potential

t that point due t

eparately (because

se of two potentia

ifference, ΔV, wh

e resistivity of

The solution of the B.V.P. defined by the D.E. of equation 2.5 and the earth model of Figure 2.1 is (cf., Grant and West, 1965; Keller and Frischknecht, 1966):

$$V(R) = \frac{I}{2\pi\sigma R} ,$$

where I is the current introduced at the source, S. For surface resistivity and I.P. prospecting, the potentials are only measured at the earth's surface, or at z = 0. Defining $r = \sqrt{x^2 + y^2}$, then the surface potential distribution about a point electrode is:

$$V(r,0) = \frac{I}{2\pi\sigma r} . \qquad 2.6$$

Apparent Resistivity

In the development of equation 2.6, the current sink was assumed to be infinitely distant from the source. Many field operations, however utilize variations of a four-point electrode configuration (two current electrodes and two potential electrodes, all separated by finite distances). For multiple current electrodes (source and sink) the potential at a point is the sum of the potentials at that point due to each of the current electrodes acting separately (because Laplace's equation is linear). The use of two potential electrodes yields the potential difference, ΔV, which allows the direct calculation of the resistivity of the half-space. For a generalized

point electrode co

distant r_1 and r_2 f

respectively) and P

pectively), the resi

Rechtnecht, 1966; Van

$$\rho = \sigma^{-1} = \frac{2\pi\Delta V}{I}\left(\frac{1}{r_1}\right.$$

practical field wor

which simplify e

duction, or both.

grations are the w

both of these con

a straight line a

configuration.

ues.

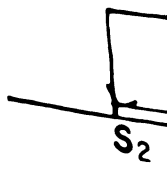

Fig. 2.2.--

the Wenner co

electrodes are e

four-point electrode configuration with potential electrodes P_1 (distant r_1 and r_2 from a current source, S_1, and sink, S_2, respectively) and P_2 (distant R_1 and R_2 from S_1 and S_2, respectively), the resistivity is given by (Keller and Frischknecht, 1966; Van Nostrand and Cook, 1966):

$$\rho = \sigma^{-1} = \frac{2\pi\Delta V}{I}\left(\frac{1}{r_1} - \frac{1}{r_2} - \frac{1}{R_1} + \frac{1}{R_2}\right)^{-1}. \qquad 2.7$$

In practical field work, certain geometrical patterns are used which simplify either the field procedures, data reduction, or both. Two of the most common electrode configurations are the Wenner and Schlumberger configurations. In both of these configurations, the electrodes are arranged in a straight line and are symmetrical about the center of the configuration. However, there are significant differences.

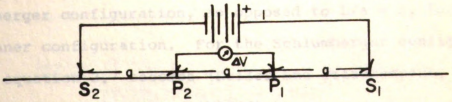

Fig. 2.2.--Wenner electrode configuration.

In the Wenner configuration (see Figure 2.2), all four electrodes are equally spaced and their common spacing,

is varied and $\frac{\Delta V}{I}$

ation, equatio

ler and Frischkr

ff:

$$\rho = 2\pi a \frac{\Delta V}{I} .$$

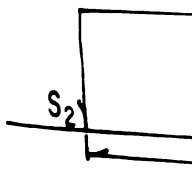

Fig. 2.3.-

In the Sc

the potential

urrent electr

chlumberger c

the Wenner co

ation, equati

1966; Van Nos

$$\rho = \frac{\pi}{4a}$$

For L>>a, t

becomes:

a, is varied and $\frac{\Delta V}{I}$ measured. For this electrode configuration, equation 2.7 becomes (Grant and West, 1965; Keller and Frischknecht, 1966; Van Nostrand and Cook, 1966):

$$\rho = 2\pi a \frac{\Delta V}{I} . \qquad 2.8$$

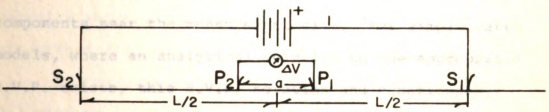

Fig. 2.3.--Schlumberger electrode configuration.

In the Schlumberger configuration (see Figure 2.3), the potential electrode spacing, a, is much less than the current electrode spacing, L. Usually, L/a>>5, for the Schlumberger configuration, as opposed to L/a = 3, for the Wenner configuration. For the Schlumberger configuration, equation 2.7 becomes (Keller and Frischknecht, 1966; Van Nostrand and Cook, 1966):

$$\rho = \frac{\pi \Delta V}{4aI} L^2 (1 - \frac{a^2}{L}) . \qquad 2.9$$

For L>>a, then $\rho \cong \frac{\pi}{I} (\frac{L}{2})^2 \frac{\Delta V}{I}$ and in the limit, a → 0, this becomes:

$$\rho = \frac{\pi}{I}\left(\frac{L}{2}\right)^2 \frac{\partial V}{\partial r} \cdot$$

The resistivities
...are true resistiv
...nably approximate
...measurement site.
...las yield apparen
...ted averages of t
...ments near the m
...s, where an anal
...exists, this B
...ugh 2.10 can be u
...stivity master c
...ratio of the app
...stivities versus
...me dimension of th
...such a manner ma
...creases their use

Review of
Hori
Bo

The B.V.P. f
...int electrode on
...homogeneous, is
...he 1930's and 194
...1931; Hummel, 193
...Colby, 1942). Mo

$$\rho \cong \frac{\pi}{I} \left(\frac{L}{2}\right)^2 \frac{\partial V}{\partial r} . \qquad 2.10$$

The resistivities given by equations 2.7 through 2.10 are true resistivities only if the earth can be reasonably approximated by the model of Figure 2.1 at the measurement site. Otherwise, the above resistivity formulas yield apparent resistivity values, ρ_a, which are weighted averages of the true resistivities of the earth's components near the measurement site. For simple earth models, where an analytical solution to the appropriate B.V.P. exists, this B.V.P. solution and equations 2.7 through 2.10 can be used to obtain theoretical apparent resistivity master curves. These are usually plotted as the ratio of the apparent resistivity to one of the true resistivities versus the ratio of the electrode spacing to some dimension of the model on logarithmic paper. Plotting in such a manner makes the master curves very flexible and increases their usefulness.

Review of the Homogeneous, Isotropic, Horizontally Layered Earth Boundary Value Problem

The B.V.P. for the potential distribution about a point electrode on the surface of an earth model consisting of homogeneous, isotropic, horizontal layers was solved in the 1930's and 1940's (cf., Stefanesco et al., 1930; Roman, 1931; Hummel, 1932; Peters and Bardeen, 1932; Keck and Colby, 1942). Modern summaries of the solution of this

...P. are given by ...

...schknecht (1966), ...

...le results have b...

...as many as four ...

...nce, the importan...

...lled two-layered ...

...lf-space) model, ...

...rties, σ_1 and σ ...

...erial above lay...

...with $\sigma = 0$, so...

At the boun...

...must be satis...

...e lower boundar...

...so, the potent...

...behave like ...

...The D.E. whi...

...2).

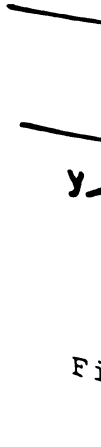

Fi...

B.V.P. are given by Grant and West (1965), Keller and Frischknecht (1966), and Van Nostrand and Cook (1966). While results have been obtained for models consisting of as many as four or more layers overlying a half-space, the important concepts are covered by the so-called two-layered (single horizontal layer overlying a half-space) model, shown in Figure 2.4. The conductivities, σ_1 and σ_2, are finite and isotropic, while the material above layer I (i.e., for $z < 0$) is taken to be air with $\sigma = 0$, so that no current will pass through it.

At the boundaries above and below layer I, equation 2.3 must be satisfied. Equation 2.4 must be satisfied at the lower boundary and at the upper boundary, $\frac{\partial V_1}{\partial n} = \frac{\partial V_1}{\partial z} = 0$. Also, the potential function, V, must vanish at infinity and behave like equation 2.6, with $\sigma = \sigma_1$, for points near S. The D.E. which V must satisfy is Laplace's equation (2.2).

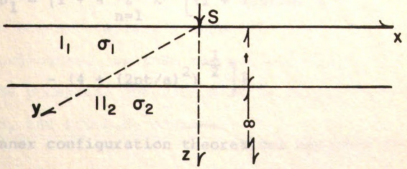

Fig. 2.4.--Two-layer earth model.

...e Solution to t...
...ered Earth Probl...

The method of ...

...ain B.V.P. with ...

...correct Green's ...

...correct Green' ...

...lace's equation ...

...image located ...

...B.C. of the m...

...ges has been u...

...rical optics, ...

...els with simpl...

...od is straigh...

...er, multiple b...

...e method can n...

Hummel (19...

...plied the meth...

...rth problem a...

$$\rho_a/\rho_1 = [$$

...s the Wenner ...

...vity functio...

...ven by:

Image Solution to the Isotropic Layered Earth Problem

The method of images is a direct method for solving certain B.V.P. with simple geometry by attempting to guess the correct Green's function for the B.V.P. By definition, the correct Green's function for a given B.V.P. satisfies Laplace's equation at all points except at its pole and the image located outside the region of interest, and all the B.C. of the model (Kellogg, 1929). The method of images has been used with considerable success in geometrical optics, seismology, and potential theory for models with simple geometry. For single boundaries, the method is straight forward and gives a single image. However, multiple boundaries result in multiple images and the method can not always be used.

Hummel (1932) and Keller and Frischknecht (1966) applied the method of images to the isotropic two-layered earth problem and obtained:

$$\rho_a/\rho_1 = \{1 + 4 \sum_{n=1}^{\infty} k^n \left[(1 + (2nt/a)^2)^{-\frac{1}{2}} - (4 + (2nt/a)^2)^{-\frac{1}{2}}\right]\} \qquad 2.11$$

as the Wenner configuration theoretical apparent resistivity function. The term, k, is a reflection coefficient given by:

$$k = \frac{\sigma_1 - \sigma_2}{\sigma_1 + \sigma_2}$$

two-layer Wenne

obtained from

Keller and K

$$\rho_a/\rho_1 = \{1 +$$

the Schlumberge

two-layer model

The theoret

quations 2.11 an

last term is the

urface, σ_1, while

the two-layer

ansformation t

lar Co-ordinat

The earth

metry about

nient to conv

lar co-ordina

opic, the po

zimuth, θ, an

$$\nabla^2 V = \frac{\partial^2}{\partial r}$$

$$k = \frac{\sigma_1 - \sigma_2}{\sigma_1 + \sigma_2} . \qquad 2.12$$

The two-layer Wenner master curves shown in Figure 2.5 were obtained from a form of equation 2.12.

Keller and Krischknecht (1966) obtained:

$$\rho_a/\rho_1 = \{1 + 2 \sum_{n=1}^{\infty} k^n [1 + (nt/L)^2]^{-3/2}\}, \qquad 2.13$$

as the Schlumberger theoretical resistivity function for a two-layer model, using the method of images.

The theoretical apparent resistivity functions of equations 2.11 and 2.13 both consist of two terms. The first term is the resistivity of a half-space of resistivity, σ_1, while the second term (series) modifies this to the two-layer model.

Transformation to Cylindrical Polar Co-ordinates

The earth model shown in Figure 2.4 has cylindrical symmetry about the z (vertical) axis. Thus, it is convenient to convert Laplace's equation into cylindrical polar co-ordinates. Because the conductivities are isotropic, the potential function will be independent of azimuth, θ, and the D.E. becomes:

$$\nabla^2 V = \frac{\partial^2 V}{\partial r^2} + \frac{1}{r}\frac{\partial V}{\partial r} + \frac{\partial^2 V}{\partial z^2} = 0. \qquad 2.14$$

Fig. 2.5.--We
nes for homogene
dels (after Van

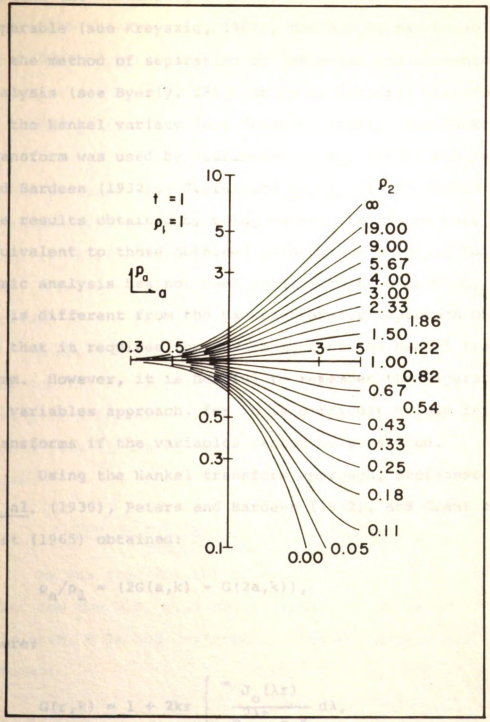

Fig. 2.5.--Wenner configuration resistivity master curves for homogeneous, isotropic, two-layered earth models (after Van Nostrand and Cook, 1966).

ause the variables
arable (see Kreys
the method of sep
alysis (see Byerly
the Hankel variet
nsform was used b
d Bardeen (1932).
e results obtaine
uivalent to those
ic analysis has
it is different fro
that it requires
ion. However, it
variables appro
nsforms if the

Using the Ha
et al. (1930), Pet
est (1965) obtai

$$\rho_a/\rho_1 = (2G$$

here:

$$G(r,k) = 1$$

is defined by e
Bessel function

Because the variables, r and z, in equation 2.14 are separable (see Kreyszig, 1967), the B.V.P. may be solved by the method of separation of variables and harmonic analysis (see Byerly, 1893) or by an integral transform of the Hankel variety (see Tranter, 1966). The Hankel transform was used by Stefanesco et al. (1930) and Peters and Bardeen (1932). Stefanesco et al. (1930) showed that the results obtained by using Hankel transforms were equivalent to those obtained using image theory. Harmonic analysis has not been applied to this problem, for it is different from the Hankel transform approach only in that it requires the development of the Hankel transform. However, it is helpful to remember the separation of variables approach, for it is difficult to use integral transforms if the variables cannot be separated.

Using the Hankel transform approach, Stefanesco et al. (1930), Peters and Bardeen (1932), and Grant and West (1965) obtained:

$$\rho_a/\rho_1 = (2G(a,k) - G(2a,k)), \qquad 2.15$$

where:

$$G(r,k) = 1 + 2kr \int_0^\infty \frac{J_o(\lambda r)}{e^{2\lambda t} - k}\, d\lambda,$$

k is defined by equation 2.2, and $J_o(\lambda r)$ is a zero order Bessel function of the first kind (see Gray and Mathews,

[illegible] Watson, 19[illegible]

[illegible]ration theor[illegible]

Mooney et [illegible]

$$[illegible]_a/[illegible]_1 = 1$$

[illegible] the Schlumber[illegible]

[illegible]ction for a t[illegible]

[illegible] is a firs[illegible]

[illegible]. The two-l[illegible]

[illegible]ained from a [illegible]

Comparing [illegible]

[illegible]y consist of [illegible]

[illegible]ity of a half-[illegible]

[illegible]cond term (inte[illegible]

[illegible]al.

The An[illegible]

As was true [illegible]

[illegible]ut for the D.P[illegible]

[illegible]is case, σ is n[illegible]

[illegible]comes:

$$\nabla \cdot \underline{J} = \nabla \cdot$$

1922; Watson, 1944; Bowman, 1958), as the Wenner configuration theoretical apparent resistivity function.

Mooney et al. (1966) obtained:

$$\rho_a/\rho_1 = 1 + \frac{L^2}{2} \int_0^\infty \frac{J_1(\lambda L/2)}{e^{2\lambda t} - k} \, d\lambda, \qquad 2.16$$

as the Schlumberger theoretical apparent resistivity function for a two-layer earth model. The function, $J_1(r)$ is a first order Bessel function of the first kind. The two-layer master curves of Figure 2.6 were obtained from a form of equation 2.16.

Comparing equations 2.15 and 2.16, it is seen that they consist of two terms. The first term is the resistivity of a half-space of conductivity, σ_1, while the second term (integral) modifies this to the two-layer model.

The Anisotropic Differential Equation and Boundary Conditions

As was true for the isotropic case, the starting point for the D.E. will be equation 2.1. However, in this case, σ is not isotropic. Thus the anisotropic D.E. becomes:

$$\nabla \cdot \underline{J} = \nabla \cdot \sigma \underline{E} = -\nabla \cdot \sigma \nabla V = -\sigma_{ij} \frac{\partial^2 V}{\partial x_i \partial x_j} = 0. \qquad 2.17$$

Fig. 2.6.--Sc
ter curves for h
th models (after

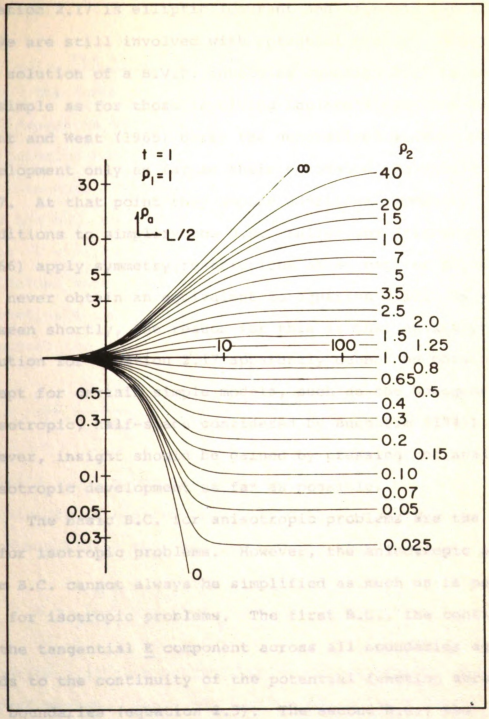

Fig. 2.6.--Schlumberger configuration resistivity master curves for homogeneous, isotropic, two-layered earth models (after Orellana and Mooney, 1965).

ation 2.17 is ellipt

we are still involv

a solution of a B.V.

ample as for those

ann and West (1965)

elopment only as f

. At that point

nditions to simplif

(1966) apply symmetry

never obtain an e

s seen shortly, the

ulation for equatio

except for certain s

isotropic, half-sp

However, insight sho

nisotropic develop

The basic B.C

s for isotropic pr

ese B.C. cannot al

ce for isotropic p

f the tangential p

leads to the contin

al boundaries (eq

ontinuity of the

ties cannot be fu

ortuitous circums

se of the co-ord

Equation 2.17 is elliptic (Courant and Hilbert, 1962), so we are still involved with potential theory. However, the solution of a B.V.P. involving equation 2.17 is not as simple as for those involving Laplace's equation (2.2). Grant and West (1965) carry the generalized anisotropic development only as far as their equivalent to equation 2.17. At that point they impose additional symmetry conditions to simplify the D.E. Keller and Frischknecht (1966) apply symmetry restrictions at an earlier point and never obtain an equivalent to equation 2.17. As will be seen shortly, the reason for this is that an analytical solution for equation 2.17 apparently cannot be obtained except for certain simple models, such as the homogeneous, anisotropic, half-space considered by Buchheim (1947). However, insight should be gained by pressing the analytic anisotropic development as far as possible.

The basic B.C. for anisotropic problems are the same as for isotropic problems. However, the anisotropic problem B.C. cannot always be simplified as much as is possible for isotropic problems. The first B.C., the continuity of the tangential $\underline{E}$ component across all boundaries again leads to the continuity of the potential function across all boundaries (equation 2.3). The second B.C., the continuity of the normal component of $\underline{J}$ across all boundaries cannot be further simplified, except under the very fortuitous circumstance where the boundary is normal to one of the co-ordinate axes. Thus, the second B.C. is:

$$\underline{J}_1 \cdot \hat{n}_1 = \underline{J}_2 \cdot$$

The Homoge

The earth mode

lf-space is that

striction that σ

ic tensor. The D

the B.C. to be

th $V \to 0$, as $x,$

cipal axes are

ordinate axes.

ained the D.E.:

$$\frac{\sigma_{ii}}{\sigma_o} \frac{\partial^2 V}{\partial x_i \partial x_i}$$

ere σ_o is a nor

self out in the

heim (1947)

$$X = \sqrt{\frac{\sigma_o}{\sigma_{11}}}$$

ation 2.19 th

med system.

out a point e

$$V(X,Y,0)$$

$$\underline{J}_1 \cdot \hat{n}_1 = \underline{J}_2 \cdot \hat{n}_2. \qquad 2.18$$

The Homogeneous, Anisotropic Half-Space

The earth model for the homogeneous, anisotropic half-space is that of Figure 2.1 with the additional restriction that σ be a generalized symmetric second-rank tensor. The D.E. to be satisfied is equation 2.17 and the B.C. to be satisfied are equations 2.3 and 2.18, and: $V \rightarrow 0$, as $x,y,z, \rightarrow \infty$. For convenience, the tensor principal axes are defined to be parallel to the model co-ordinate axes. With this situation, Buchheim (1947) obtained the D.E.:

$$\frac{\sigma_{ii}}{\sigma_o} \frac{\partial^2 V}{\partial x_i \partial x_i} = 0, \qquad 2.19$$

where σ_o is a normalization constant which will cancel itself out in the end, e.g., $\sigma_o = \frac{\sigma_{11} + \sigma_{22} + \sigma_{33}}{3}$. Buchheim (1947) then defined the transformation:

$$X = \sqrt{\frac{\sigma_o}{\sigma_{11}}}\, x \quad Y = \sqrt{\frac{\sigma_o}{\sigma_{22}}}\, y, \quad Z = \sqrt{\frac{\sigma_o}{\sigma_{33}}} \qquad 2.20$$

Equation 2.19 then becomes Laplace's equation in the transformed system. Then, the surface potential distribution about a point electrode is:

$$V(X,Y,0) = \frac{I}{2\pi\sigma_m R'}, \qquad 2.21$$

$r = \sqrt{X^2 + Y^2}$

ential function,

of the anisotr

, i.e.:

$$\rho_{a_x} = \sqrt{\rho_{22}}$$

$$\rho_{a_y} = \sqrt{\rho_{33}}$$

$$\rho_{a_z} = \sqrt{\rho_{11}}$$

sically, equati

stivity is mea

ration paralle

sistivity) dire

parent resistiv

tric mean of th

uations 2.21 in

sistivity measu

The

The earth m

with the adde

tric second-ra

equation 2.17

ach boundaries

atisfied at the

where $R' = \sqrt{x^2 + y^2}$ and $\sigma_m = \sqrt{\frac{\sigma_{11}\,\sigma_{22}\,\sigma_{33}}{\sigma_o}}$. With this potential function, Buchheim (1947) obtained the general form of the anisotropy paradox of Schlumberger et al. (1934), i.e.:

$$\rho_{a||x} = \sqrt{\rho_{22}\,\rho_{33}}, \qquad \sigma_{a||x} = \sqrt{\sigma_{22}\,\sigma_{33}},$$

$$\rho_{a||y} = \sqrt{\rho_{33}\,\rho_{11}}, \qquad \sigma_{a||y} = \sqrt{\sigma_{33}\,\sigma_{11}}, \qquad 2.22$$

$$\rho_{a||z} = \sqrt{\rho_{11}\,\rho_{22}}, \qquad \sigma_{a||z} = \sqrt{\sigma_{11}\,\sigma_{22}}.$$

Physically, equations 2.22 indicate that if the apparent resistivity is measured with a four point electrode configuration parallel to one of the principal conductivity (resistivity) directions, in an anisotropic medium, the apparent resistivity in that direction will be the geometric mean of the other two principal values. Thus, equations 2.21 indicate a possible serious error for resistivity measurements taken over anisotropic areas.

The Anisotropic Layered Earth Boundary Value Problem

The earth model for this B.V.P. is that of Figure 2.4 with the added restriction that σ_1 and σ_2 are symmetric second-rank tensors. The D.E. to be satisfied is equation 2.17. Equation 2.3 must be satisfied at both boundaries of the model. Equation 2.18 must be satisfied at the lower boundary and at the upper boundary:

$$\underline{J}_1 \cdot \hat{n} = 0.$$

The remaining B.C. are

ints near the source

are according to e

the B.V.P. as much as

rections in both ma

e model co-ordinate

nversion to Cylindr
ther Co-ordinates

Despite the fac

ase are symmetric s

ies have rotational

will be a function

nverting equation

or the case where

is principal axes

$$\sigma_{ij} \frac{\partial^2 V}{\partial x_i \partial x_i} =$$

$$\underline{J}_1 \cdot \hat{n} = 0. \qquad 2.23$$

The remaining B.C. are that $V \to 0$, as $x,y,z \to \infty$, and for points near the source, S, the potential function must behave according to equation 2.21. In order to simplify the B.V.P. as much as possible, the tensor principal directions in both materials will be required to parallel the model co-ordinate axes.

Conversion to Cylindrical Polar Co-ordinates

Despite the fact that the conductivities in this case are symmetric second-rank tensors, the earth model does have rotational symmetry about the z axis. However, V will be a function of azimuth, θ, as well as r and z. Converting equation 2.17 to cylindrical polar co-ordinates for the case where the conductivity tensor is relative to its principal axes yields:

$$\sigma_{ij} \frac{\partial^2 V}{\partial x_i \partial x_i} = \sigma_{11}(\cos^2\theta + \frac{\sigma_{22}}{\sigma_{11}} \sin^2\theta)\frac{\partial^2 V}{\partial r^2}$$

$$+ \sigma_{11}\left[\frac{\sin^2\theta + \frac{\sigma_{22}}{\sigma_{11}} \cos^2\theta}{r}\right]\frac{\partial V}{\partial r}$$

$$- \sigma_{11}\left[\frac{2\cos\theta \sin\theta\left(1 - \frac{\sigma_{22}}{\sigma_{11}}\right)}{r}\right]\frac{\partial^2 V}{\partial r \partial \theta}$$

+ c

+

+

ere the only requi

$\neq \sigma_{22} \neq \sigma_{33}$. Th

annot be separated.

e used. Also, this

possible to use i

s was done for the

.24 is in a form w

o a more symmetric

ove problem with

ere cylindrical s

$\sigma_{22}^{(i)} = \sigma_{22}^{(i)} =$

quation 2.24 beco

$$\sigma_{ii} \frac{\partial^2 V}{\partial x_i \partial x_i} =$$

n each layer, wh

efficient of anis

tant and West, 1

$$+ \sigma_{11}\left[\frac{2\cos\theta\ \sin\theta\left(1 - \frac{\sigma_{22}}{\sigma_{11}}\right)}{r^2}\right]\frac{\partial V}{\partial\theta}$$

$$+ \sigma_{11}\left[\frac{\sin^2\theta + \frac{\sigma_{22}}{\sigma_{11}}\cos^2\theta}{r^2}\right]\frac{\partial^2 V}{\partial\theta^2}$$

$$+ \sigma_{33}\frac{\partial^2 V}{\partial z^2} = 0, \qquad 2.24$$

where the only requirement on the principal values of σ is $\sigma_{11} \neq \sigma_{22} \neq \sigma_{33}$. The r and θ variables in equation 2.24 cannot be separated. Thus, separation of variables cannot be used. Also, this will make it very difficult, if not impossible to use integral transforms to solve this B.V.P. as was done for the isotropic case. However, equation 2.24 is in a form which allows consideration of the approach to a more symmetrical form of the tensor. Consider the above problem with the additional condition that σ_1 and σ_2 have cylindrical symmetry about the z axis, i.e., $\sigma_{11}^{(i)} = \sigma_{22}^{(i)} = \sigma_t^{(i)} \neq \sigma_{33}^{(i)} = \sigma_v^{(i)}$ (i = 1, 2). Then equation 2.24 becomes:

$$\sigma_{ii}\frac{\partial^2 V}{\partial x_i \partial x_i} = \left(\frac{\partial^2 V}{\partial r^2} + \frac{1}{r}\frac{\partial V}{\partial r}\right) + \frac{1}{\Lambda^2}\frac{\partial^2 V}{\partial z^2} = 0, \qquad 2.25$$

in each layer, where $\Lambda = \sqrt{\rho_v/\rho_t}$ is the classical coefficient of anisotropy (cf., Schlumberger et al., 1934; Grant and West, 1965; Keller and Krischknecht, 1966).

ing a mean resist

$= \sqrt{\rho_v \rho_t}$, the Wenne

ry is given by:

$$\rho_a = \rho_m^{(1)} (2H(a,$$

ere:

$$H(r,k') = 1 + 2k$$

$$k' = \frac{A_1\sigma_{(33)}^{(1)}}{A_1\sigma_{(33)}^{(1)}}$$

uation 2.26 is ver

uation 2.26 shows

izing master cur

uld be more appro

parent resistivit

isotropy coeffici

$\rho_t^{(i)}$, respecti

ilar results can

lectrode configura

The Method of Imag

The method o

e anisotropic la

rities are funct

tion of equatio

Defining a mean resistivity (Grant and West, 1965), $\rho_m = \sqrt{\rho_v \rho_t}$, the Wenner configuration apparent resistivity is given by:

$$\rho_a = \rho_m^{(1)} (2H(a,k') - H(2a,k')), \qquad 2.26$$

where:

$$H(r,k') = 1 + 2k'r \int_0^\infty \frac{J_o(\lambda r)}{e^{2\Lambda_1 \lambda t} - k'} \, d\lambda,$$

$$k' = \frac{\Lambda_1 \sigma(33)^{(1)} - \Lambda_2 \sigma(33)^{(2)}}{\Lambda_1 \sigma(33)^{(1)} + \Lambda_2 \sigma(33)^{(2)}} .$$

Equation 2.26 is very similar to equation 2.15. However, equation 2.26 shows that resistivity interpretations utilizing master curves based on equation 2.15, when 2.26 would be more appropriate, will yield thicknesses and apparent resistivities which will be the product of the anisotropy coefficient, Λ_i, with the true thicknesses and $\rho_t^{(i)}$, respectively (Keller and Krischknecht, 1966). Similar results can be obtained with any other four point electrode configuration.

The Method of Images

The method of images cannot be applied directly to the anisotropic layered earth B.V.P., for the conductivities are functions of direction. If the transformation of equation 2.20 is applied to equation 2.17, it

ossible to set up

layer. However,

co-ordinate syste

co-ordinate syste

complicate the

mean that the spec

ifficult, if not im

For the condit

nductivity (resist

mmer configuratio

pparently:

$$\rho_a = \rho_m^{(1)} \quad (1$$

$$- (4 +$$

ller and Krischk

bove situation, t

sing isotropic ma

he anisotropy coe

nd the ρ_t. Equa

o equation 2.11

gain, similar re

oint electrode c

is possible to set up the generalized image series for each layer. However, because each layer will have its own co-ordinate system, there will be discontinuities in the co-ordinate systems at the two boundaries. This will complicate the B.C. at these boundaries to such an extent that the specific solution to the B.V.P. may be difficult, if not impossible to obtain.

For the condition of cylindrical symmetry in the conductivity (resistivity) tensor about the z axis, the Wenner configuration apparent resistivity function is apparently:

$$\rho_a = \rho_m^{(1)} \{1 + 4 \sum_{n=1}^{\infty} k'^n [(1 + (2n\Lambda_1 t/a)^2)^{-\frac{1}{2}} - (4 + (2n\Lambda_1 t/a)^2)^{-\frac{1}{2}}]\}. \qquad 2.27$$

Keller and Krischknecht (1966) indicate that for the above situation, the resistivities and depths obtained using isotropic master curves will be the product of the anisotropy coefficients with the true thicknesses and the ρ_t. Equation 2.27 does have that relationship to equation 2.11 and it does satisfy equation 2.25. Again, similar results may be obtained with other four point electrode configurations.

Qualitative

The results of

ing the condition

ered earth B.V.P.

ficult to obtain.

ere appears to be

an a solution to t

heim (1947) may

ese qualitative ex

the expected resu

The apparent r

uations 2.22 are

ination where the

ne of the princ

he practical situ

e tensor principa

coordinate axes.

es not be paralle

rections. Consid

e Wenner electrod

with the x-axis.

$\frac{3a}{2}\cos\theta$, $-\frac{3a}{2}\sin$

strength, I, and p

and $p_2(\frac{a}{2}\cos\theta, \frac{a}{2}\sin$

esistivity is:

Qualitative Extension of Buchheim's Results

The results of the above section indicate that adding the condition of orthorhombic anisotropy to the layered earth B.V.P. makes its analytic solution very difficult to obtain. Short of using numerical methods, there appears to be little else that can be done to obtain a solution to this B.V.P. However, the results of Buchheim (1947) may be extended in a qualitative manner. These qualitative extensions may then indicate the form of the expected results of the layered earth B.V.P.

The apparent resistivity relationships given by equations 2.22 are useful only for the very fortuitous situation where the electrode configuration is parallel to one of the principal tensor directions. A somewhat more practical situation will now be considered. Again, the tensor principal directions will be parallel to the co-ordinate axes. However, the electrode configuration need not be parallel to one of the principal tensor directions. Consider the situation in Figure 2.7, where the Wenner electrode configuration line is at an angle, θ, with the x-axis. For current electrodes, $S_1(-\frac{3a}{2}\cos\theta, -\frac{3a}{2}\sin\theta, 0)$ and $S_2(\frac{3a}{2}\cos\theta, \frac{3a}{2}\sin\theta, 0)$, of strength, I, and potential electrodes, $P_1(-\frac{a}{2}\cos\theta, -\frac{a}{2}\sin\theta, 0)$ and $P_2(\frac{a}{2}\cos\theta, \frac{a}{2}\sin\theta, 0)$, the Wenner configuration apparent resistivity is:

Fig. 2.7.--Wen
itrary orientatio
ections.

$$\rho_a(\theta) = \sqrt{\rho_{33}}$$

Equation 2.28

ing structural tr
ent (e.g., glacial
nductivity (resis
nfigurations orie
mon center point
ferent resistivit
st minor semi-axes
sections. For ex
rrespond to the p
ipsoids used in
his approach may b
he simple anisotro
ase. In any even

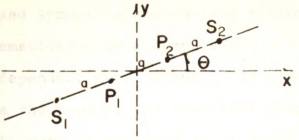

Fig. 2.7.--Wenner electrode configuration at some arbitrary orientation to the horizontal principal tensor directions.

$$\rho_a(\theta) = \sqrt{\rho_{33}} \Big/ \sqrt{\frac{\cos^2\theta}{\rho_{22}} + \frac{\sin^2\theta}{\rho_{11}}} \quad . \qquad 2.28$$

Equation 2.28 suggests a field procedure for determining structural trends in areas where they are not well known (e.g., glacial drift and alluvium covered areas). Conductivity (resistivity) measurements with electrode configurations oriented in more than one azimuth and a common center point are taken. Then, a ground surface apparent resistivity ellipse may be defined, whose major and minor semi-axes should correspond to major structural directions. For example, these structural directions may correspond to the principal axes of the stress or strain ellipsoids used in structural geology (Billings, 1954). This approach may be used even if the earth does not fit the simple anisotropic half-space model at the measurement site. In any event, the apparent resistivity ellipse will

define the tensor

ellipse, beca

A generalized s

esented mathemati

has six indepe

pletely define th

e equation 3.5) m

ifferent directions

six different d

be used to deter

apter VI). If it

stivity (conducti

ends, there will

ese trends when s

ost general form c

the origin, must

survey. The genera

ntered at the or

$$S_{ij}x_ix_j = S_1$$

completely defi

ellipse, apparent

at least three

determination, fo

the anisotropy pa

round surface ap

not define the tensor representation surface cross section ellipse, because of the anisotropy paradox.

A generalized symmetric second-rank tensor is represented mathematically by a symmetric 3 x 3 matrix, which has six independent coefficients. In order to completely define the tensor, the resultant property (see equation 3.5) must be measured in at least six different directions. If measurements are taken in more than six different directions, a least square procedure may be used to determine the tensor coefficients (see Chapter VI). If it is desired to use the apparent resistivity (conductivity) ellipse to determine structural trends, there will generally be no prior knowledge of these trends when setting up the field survey. Thus, the most general form of the equation for an ellipse, centered at the origin, must be considered when setting up a field survey. The general form for the equation of an ellipse centered at the origin is:

$$S_{ij}x_i x_j = S_{11}x_1^2 + S_{22}x_2^2 + 2S_{12}x_1x_2 = 1. \qquad 2.29$$

To completely define the surface apparent resistivity ellipse, apparent resistivity measurements must be taken in at least three different azimuths. For a least square determination, four or more must be taken. Because of the anisotropy paradox (equations 2.22 and 2.28), the ground surface apparent resistivity ellipse will not be

resistivity tenso

mmon ellipse. The

ained from surface

nal symmetry condi

.1 through 2.27) ca

tion on the true re

ion in advance.

If the apparen

s to be completely

rectional apparent

s taken in at least

e horizontal. The

ifferent attitudes.

epresentation surfa

ities can be determ

uations 2.22 to de

rsity) tensor princ

The above fie

ea where the struc

he field geophysic

he converse proble

e area where the s

ghly well known.

parallel to the str

determine an appare

he true resistivit

the resistivity tensor representation surface cross-section ellipse. The true resistivities cannot be obtained from surface measurements alone, unless additional symmetry conditions (such as those of equations 2.25 through 2.27) can be applied, or additional information on the true resistivity principal values are known in advance.

If the apparent resistivity representation surface is to be completely defined by field measurements alone, directional apparent resistivity measurements must also be taken in at least three additional directions out of the horizontal. These could be made in drill holes at different attitudes. After the apparent resistivity representation surface has been defined, its principal values can be determined (as in Chapter VI) and used with equations 2.22 to determine the true resistivity (conductivity) tensor principal values.

The above field procedure might be helpful in an area where the structural trends are unknown but suspected. The field geophysicist might equally well be faced with the converse problem, i.e., setting up a field program in an area where the structural trends, or anisotropy, are fairly well known. In this case, measurements normal and parallel to the structural trends would be sufficient to determine an apparent resistivity ellipse. However, if the true resistivities are desired and no additional

mation available

mation surface mus

information available, the apparent resistivity representation surface must be defined as above.

THE CON

The theoretica
perties of rocks
that of an anisot
rely heavily up
, K, and conduc
sors. Solkolnikc
lete discussions
sors. Nye (1964)
metric second-ra
s a symmetric se
45], DeGroot and
chalsky and Curr
cause the remaind
owledge of some p
and 3 tensors, a

One of the c
that they obey
ye, 1964):

CHAPTER III

THE CONDUCTIVITY AND DIELECTRIC CONSTANT TENSORS

Introduction

The theoretically based model for the electrical properties of rocks to be developed in Chapter IV will be that of an anisotropic lossy dielectric. This model will rely heavily upon the fact that the dielectric constant, K, and conductivity, σ, are symmetric second-rank tensors. Solkolnikoff (1951) and Nye (1964) have very complete discussions on the properties of second-rank tensors. Nye (1964) also establishes that K and σ are symmetric second-rank tensors. More thorough proofs that σ is a symmetric second-rank tensor are given by Casimir (1945), DeGroot and Mazur (1954a, 1954b), Callen (1961), Katchalsky and Curran (1965), and Smith et al. (1967). Because the remainder of this paper is dependent upon a knowledge of some properties of the symmetric second-rank K and σ tensors, a short review is now included.

One of the criteria for defining second-rank tensors is that they obey the rotational transformation laws (Nye, 1964):

$$T'_{ij} = \sum_{k=1}^{3} \sum_{m=1}^{3} l$$

$$T_{ij} = \sum_{h=1}^{3} \sum_{m=1}^{3} l$$

ing the Einstein s

$$T' = l\, T\, l^{T},$$

$$T = l^{T}\, T'\, l,$$

ing matrix notatio

ix tensor, (l_{ij}) i

the angles between t

the T superscript i

second-rank tensor,

3 x 3 matrix. If

symmetric and the re

its main diagonal.

coefficients from n

is rotated so that

rotation matrix va

to its principal ax

is called the prin

Symmetric sec

metrically by a

ly for the genera

to the origin:

$$T'_{ij} = \sum_{k=1}^{3} \sum_{m=1}^{3} l_{ik} T_{km} l_{jm} = l_{ik} T_{km} l_{jm},$$

$$T_{ij} = \sum_{h=1}^{3} \sum_{m=1}^{3} l_{ki} T'_{km} l_{mj} = l_{ki} T'_{km} l_{mj}, \qquad 3.1$$

using the Einstein summation convention (Nye, 1964), or:

$$T' = l\ T\ l^{T},$$

$$T = l^{T}\ T'\ l, \qquad 3.2$$

using matrix notation, where T is a generalized second-rank tensor, (l_{ij}) is a 3 x 3 direction cosine matrix for the angles between the co-ordinate axes, X'_i and X_j, and the T superscript indicates a matrix transpose. The second-rank tensor, T, is represented mathematically by a 3 x 3 matrix. If $T_{ij} = T_{ji}$, the tensor is said to be symmetric and the representation matrix is symmetric about its main diagonal. This reduces the number of independent coefficients from nine to six. If the co-ordinate axes are rotated so that the off-diagonal terms of the representation matrix vanish, the tensor is said to be referred to its principal axes. The remaining main diagonal terms are called the principal values of the tensor.

Symmetric second-rank tensors also may be represented geometrically by a second order surface. The coefficients, S_{ij}, for the general equation of such a surface, centered at the origin:

$S_{ij}x_ix_j = 1$, S

also obey the rotati

1 and 3.2. The ty

om the principal v

incipal values ar

s a real ellipsoid.

gative, the repre

e or two sheets,

alues are negative

aginary ellipsoid

The magnitude

n arbitrary direct

s Boye, 1964):

$$T_{11}\hat{l} = \hat{l}_i T_{ij}$$

sing the Einstein

$$T_{11}\hat{l} = \hat{l}^T T$$

sing matrix notat

he result is:

$$T_{11}\hat{l} = T_{11}\hat{l}$$

+ 2

$$S_{ij}x_i x_j = 1, \; S_{ij} = S_{ji} \qquad 3.3$$

also obey the rotational transformation laws of equations 3.1 and 3.2. The type of representation surface depends upon the principal values of the tensor. If all three principal values are positive, the representation surface is a real ellipsoid. If one or two principal values are negative, the representation surface is a hyperbaloid of one or two sheets, respectively. If all three principal values are negative, the representation surface is an imaginary ellipsoid.

The magnitude of a symmetric second-rank tensor in an arbitrary direction indicated by the unit vector, $\hat{l}$, is (Nye, 1964):

$$T_{ll}\,\hat{l} = \hat{l}_i T_{ij} \hat{l}_j, \qquad 3.4a$$

using the Einstein summation convention, or:

$$T_{ll}\,\hat{l} = \hat{l}^T \, T \, \hat{l}, \qquad 3.4b$$

using matrix notation. If equations 3.4 are expanded, the result is:

$$T_{ll}\,\hat{l} = T_{11}\hat{l}_1^2 + T_{22}\hat{l}_2^2 + T_{33}\hat{l}_3^2 + 2T_{23}\hat{l}_2\hat{l}_3 + 2T_{31}\hat{l}_3\hat{l}_1 + 2T_{12}\hat{l}_1\hat{l}_2. \qquad 3.5$$

ation 3.5 is of ba

used as a model to

m laboratory measu

principal values

ctions have been

The Die

The relationsh

ty vector, $\underline{E}$, and

isplacement, vector, $\underline{D}$

Corson and Lorra

$$\underline{D} = \varepsilon \underline{E} = \varepsilon_o K \underline{E},$$

ere $\varepsilon_o = 8.85 \cdot 1$

ivity of free space

terial, and $K = \frac{\varepsilon}{\varepsilon}$

terial. If the m

alars so that $\underline{D}$ i

terial is anisotr

n equation 3.6 be

$$D_i = \varepsilon_{ij} E_j,$$

hich is of the co

lating a depende

ector quantity (

and K are repres

he dielectric co

Equation 3.5 is of basic importance to this study. It is used as a model to obtain least square coefficients from laboratory measurements. It is also used to obtain the principal values of the tensor, once the principal directions have been determined.

The Dielectric Constant Tensor

The relationship between the electric field intensity vector, $\underline{E}$, and the electric flux density, or displacement, vector, $\underline{D}$, in a dielectric material is given by (Corson and Lorrain, 1962):

$$\underline{D} = \varepsilon \underline{E} = \varepsilon_o K \underline{E}, \qquad 3.6$$

where $\varepsilon_o = 8.85 \cdot 10^{-2}$ farad/m is the electric permittivity of free space, ε is the permittivity of the material, and $K = \frac{\varepsilon}{\varepsilon_o}$ is the dielectric constant of the material. If the material is isotropic, ε and K are scalars so that $\underline{D}$ is parallel to $\underline{E}$. If, however, the material is anisotropic, $\underline{D}$ is no longer parallel to $\underline{E}$ and equation 3.6 becomes:

$$D_i = \varepsilon_{ij} E_j, \qquad 3.7$$

which is of the correct form for a second-rank tensor relating a dependent vector quantity to an independent vector quantity (Nye, 1964). For the anisotropic case, ε and K are represented mathematically by 3 x 3 matrices. The dielectric constant, K, and permittivity, ε, do obey

rotational tra

. Thus, they a

In addition

scribe a materia

marized in the p

mplished with

defined by (Co

$$\underline{D} = \varepsilon \underline{E} = \varepsilon_o$$

here $\underline{P}$ is the el

is the 3 x 3 id

, it is clear

$$K = I + \chi.$$

addition to r

dependent vect

rmation laws,

is also a secc

ility, χ, is a

han K or ε. H

ent results ar

esults of the

lso be given a

development of

The diele

susceptibility

the rotational transformation laws of equations 3.1 and 3.2. Thus, they are second-rank tensors.

In addition to K and ε, it is often desired to describe a material's willingness to become electrically polarized in the presence of an $\underline{E}$ field. This is accomplished with the electric (volume) susceptibility, χ, defined by (Corson and Lorrain, 1962):

$$\underline{D} = \varepsilon\underline{E} = \varepsilon_o\underline{E} + \underline{P} = \varepsilon_o(I + \chi)\underline{E}, \qquad 3.8$$

where $\underline{P}$ is the electric (volume) polarization vector and I is the 3 x 3 identity matrix. From equations 3.6 and 3.8, it is clear that:

$$K = I + \chi. \qquad 3.9$$

In addition to relating a dependent vector, $\underline{P}$, to an independent vector, $\underline{E}$, χ also obeys the rotational transformation laws, given by equations 3.1 and 3.2. Thus, χ is also a second-rank tensor. The electric susceptibility, χ, is a more fundamental property of the material than K or ε. However, by tradition, laboratory measurement results are usually given as K rather than χ. The results of the laboratory portion of this study will also be given as K, though χ will be used during the development of an electrical model for rocks.

The dielectric constant, K, permittivity, ε, and susceptibility, χ, have all been shown to be second-rank

sors. However, i

ey are symmetric,

y straight forwar

rics. If a ther

perature, θ, elec

the electric dis

nic work at con

$$dW = -E_i dD_i .$$

e combined first

ven by (MacInnes,

$$dU = \theta dS + E_j$$

ere U is the tota

the entropy of

e system is defi

$$G = U + W -$$

ere $Q = \theta S$ is th

$$dG = dU - E_i$$

$$= - D_i dE_i$$

constant temper

$$dG = - D_i dE_j$$

tensors. However, it has not yet been established that they are symmetric, e.g., $K_{ij} = K_{ji}$. This is done in a very straight forward manner, using classical thermodynamics. If a thermodynamic system is defined by temperature, θ, electric field intensity vector, $\underline{E}$, and the electric displacement vector, $\underline{D}$, the thermodynamic work at constant $\underline{E}$ is given by:

$$dW = -E_i dD_i.$$

The combined first and second laws of thermodynamics are given by (MacInnes, 1961; Moore, 1964):

$$dU = \theta dS + E_i dD_i,$$

where U is the total internal energy of the system and S is the entropy of the system. The Gibbs free energy of the system is defined as (MacInnes, 1961; Moore, 1964):

$$G = U + W - Q,$$

where $Q = \theta S$ is the heat transferred. Thus:

$$dG = dU - E_i dD_i - D_i dE_i - \theta dS - S d\theta$$

$$= - D_i dE_i - S d\theta.$$

At constant temperature, this becomes:

$$dG = - D_i dE_i = - (D_1 dE_1 + D_2 dE_2 + D_3 dE_3).$$

ε_0 is a function

differential (MacInn

Type and DiPrima,

$$\left(\frac{\partial D_i}{\partial E_j}\right)_\theta = \left(\frac{\partial D_i}{\partial E_i}\right.$$

$$\varepsilon_0 K_{ij}(\theta) \frac{\partial E_i}{\partial E_j}$$

that:

$$K_{ij}(\theta) = K_{ij}$$

where the θ superso

start temperature.

for K, similar pro

Experimental

always given posit

the case for the l

Thus, the represer

The vector f

and Lorrain, 1962)

$$\underline{E} = \partial \underline{J},$$

But G is a function of state. Thus, dG is an exact differential (MacInnes, 1961; Moore, 1964), so that (Boyce and DiPrima, 1965):

$$\left(\frac{\partial D_i}{\partial E_j}\right)_\theta = \left(\frac{\partial D_i}{\partial E_i}\right)_\theta, \quad i,j = 1, 2, 3,$$

or:

$$\varepsilon_o K_{ij}^{(\theta)} \frac{\partial E_i}{\partial E_j} = \varepsilon_o K_{ij}^{(\theta)} \frac{\partial E_i}{\partial E_j},$$

so that:

$$K_{ij}^{(\theta)} = K_{ij}^{(\theta)}, \text{ q.e.d.,} \qquad 3.10$$

where the θ superscript indicates the condition of constant temperature. While the above proof of symmetry was for K, similar proofs could also be given for ε and χ.

Experimental measurements of K (Nye, 1964) have always given positive principal values. This was also the case for the laboratory portion of the present study. Thus, the representation surface for K is a real ellipsoid.

The Conductivity Tensor

The vector form of Ohm's law is given by (Corson and Lorrain, 1962):

$$\underline{E} = \rho \underline{J}, \qquad 3.11a$$

$$\underline{J} = \sigma \underline{E},$$

...re $\underline{J}$ is the curr...
...ductivity of the ...
...uctivity of the ...
...a or 3.11b is d...
...independent vec...
...sample shape.

For isotropic ...
...s parallel to $\underline{E}$.
...no longer paral...

$$J_i = \sigma_{ij} E_j,$$

...ch is of the sa...
...relating a depe...
...and σ also obey ...
...quations 3.1 and ...
...nsors.

The establis...
...straight forwar...
...ectrical conduct...
...ansport phenome...
...assical thermod...
...ated approach ...
...ocesses is Onsa...

or:

$$\underline{J} = \sigma\underline{E}, \qquad 3.11b$$

where $\underline{J}$ is the current density vector, ρ is the electrical resistivity of the material, and $\sigma = \rho^{-1}$ is the electrical conductivity of the material. The choice of equations 3.11a or 3.11b is dependent upon the choice of $\underline{E}$ or $\underline{J}$ as the independent vector. This, in turn, is governed by the sample shape.

For isotropic materials, σ (or ρ) is a scalar and $\underline{J}$ is parallel to $\underline{E}$. For anisotropic materials, $\underline{J}$ and $\underline{E}$ are no longer parallel and equations 3.11 become:

$$J_i = \sigma_{ij}E_j, \qquad 3.12$$

which is of the same form as equation 3.6. In addition to relating a dependent vector to an independent vector, σ and ρ also obey the rotational transformation laws of equations 3.1 and 3.2. Thus, σ and ρ are second-rank tensors.

The establishment of the symmetry of σ and ρ is not as straight forward as it was for K. This is because electrical conduction is a transport phenomenon. Since transport phenomena deal with irreversible processes, classical thermodynamics cannot be used. A more sophisticated approach which can be used for irreversible processes is Onsager's principle of microscopic

ersibility. The

given in the ori

; Casimir, 19

in most advance

, Callen, 1961

al., 1967).

To be able t

mic system and

itions. These

stem is consider

ergoing small f

e equilibrium en

$$S = P_i Q_i,$$

ere the P_i are g

stem and the Q_i

e system. Becau

quilibrium, there

ntropy (disorder)

is not conserv

t volume, per u

; Katchalsky a

$$\Phi = \frac{\partial \hat{S}}{\partial t} = F_i J$$

ere $\hat{s}$ is the loc

neralized affin

reversibility. The justification of Onsager's principle is given in the original papers (cf., Onsager, 1931a, 1931b; Casimir, 1945, DeGroot and Mazur, 1954a, 1954b) and in most advanced texts covering statistical physics (cf., Callen, 1961, Katchalsky and Curran, 1965; Smith et al., 1967).

To be able to use Onsager's principle, the thermodynamic system and its variables must satisfy certain conditions. These conditions will now be reviewed. The system is considered to be in statistical equilibrium undergoing small fluctuations about this equilibrium. The equilibrium entropy must be given by:

$$S = P_i Q_i, \tag{3.13}$$

where the P_i are generalized intensive parameters of the system and the Q_i are generalized extensive parameters of the system. Because of the local fluctuations from equilibrium, there will be an entropy current, J_s. Entropy (disorder) is a maximum at equilibrium. Thus, J_s, is not conservative and a local entropy creation per unit volume, per unit time, Φ, can be defined as (Callen, 1961; Katchalsky and Curran, 1965):

$$\Phi = \frac{\partial \hat{s}}{\partial t} = F_i J_i, \tag{3.14}$$

where $\hat{s}$ is the local (per volume) entropy, the F_i are generalized affinities (forces) due to the non-equilibrium

nditions

luxes (cur

, flowing

mper choi

):

$$\beta_i J_i^j =$$

$$F_i =$$

ere the $\hat{q}_j$

e fluxes,

-called ph

$$J_i = L$$

ere the L_i

r differen

ates that

tisfy equa

efficients

$$L_{ij} = I$$

For the

ve variable

d the inten

th this cho

n by dimens

conditions within the system, and the J_i are generalized fluxes (current densities) of the extensive variables, Q_i, flowing in response to the F_i. The criteria for the proper choices of fluxes and affinities are (Smith et al., 1967):

$$\partial_i J_i^j = \frac{\partial \hat{q}_j}{\partial t},$$

$$F_i = \partial_i P_i, \qquad 3.15$$

where the $\hat{q}_j$ are local (per volume) extensive variables. The fluxes, J_i, and affinities, F_i, are related by the so-called phenomenological equations (Onsager, 1931a) as:

$$J_i = L_{ij} F_j, \qquad 3.16$$

where the L_{ij} are called coupling coefficients and vary for different thermodynamic systems. Onsager's principle states that if the parameters of the thermodynamic system satisfy equations 3.13 through 3.16, the cross coupling coefficients are equal, i.e.:

$$L_{ij} = L_{ji}. \qquad 3.17$$

For the case of electrical conductivity, the extensive variable of the system is the electric charge, Q, and the intensive variable is the electric potential, V. With this choice of variables, equation 3.13 is satisfied, for by dimensional analysis (Halliday and Resnick, 1961):

$$[Q][V] = Q$$

equations 3.

$$\underline{F} = \underline{E} = -$$

$$\nabla \cdot \underline{J} = -$$

where $\hat{q}$ is the per

choice of flux and

$$[\underline{E}][\underline{J}] = \frac{ML}{t^2 Q}$$

because equation 3

the choice of syst

conditions, Onsage

the symmetry of the

i.e.:

$$\sigma_{ij} = \sigma_{ij}$$

Experimental

always given posit

the case for the 1

thus, the σ repres

ellipsoid.

$$[Q][V] = Q\,\frac{ML^2}{t^2 Q} = \frac{ML^2}{t^2} = [S], \quad \text{q.e.d.}$$

From equations 3.15, the flux and affinity are given by:

$$F = \underline{E} = -\nabla V,$$

$$\nabla \cdot \underline{J} = -\frac{d\hat{q}}{dt},$$

where $\hat{q}$ is the per unit volume charge density. This choice of flux and affinity satisfies equation 3.14, for:

$$[\underline{E}][\underline{J}] = \frac{ML}{t^2 Q}\,\frac{Q}{L^2 t} = \frac{M}{Lt^3} = \left|\frac{\partial \hat{s}}{\partial t}\right|, \quad \text{q.e.d.}$$

Because equation 3.12 is of the same form as 3.16, and the choice of system parameters do satisfy the Onsager conditions, Onsager's principle can be used to establish the symmetry of the conductivity (resistivity) tensor, i.e.:

$$\sigma_{ij} = \sigma_{ij} \quad \text{q.e.d.} \qquad 3.18$$

Experimental measurements of σ (Nye, 1964) have always given positive principal values. This was also the case for the laboratory portion of the present study. Thus, the σ representation surface will also be a real ellipsoid.

THE LO

Keller's (1
tion of materia
be physically
mpson (1964) a
in an applied
le 4.1, the re
perties of dry
kes, 1942; Jak
ller, 1966; Par
cks are high res
ctrics. Thus,
lossy dielectri

e 4.1.--Electr

terial Type
Insulators
Semi-conductors
Conductors

CHAPTER IV

THE LOSSY DIELECTRIC MODEL FOR ROCKS

Introduction

Keller's (1966) rule-of-thumb electrical classification of materials is given in Table 4.1. While it may not be physically as sound as those used by Wert and Thompson (1964) and Beam (1965), it is perhaps more useful in an applied sense. Using the classification of Table 4.1, the reported measurements of the electrical properties of dry rocks (cf., Heiland, 1940; Slichter and Telkes, 1942; Jakosky, 1950; Keller and Licastro, 1959; Keller, 1966; Parkhomenko, 1967) indicate that most dry rocks are high resistivity semi-conductors, or lossy dielectrics. Thus, it is desirable to consider the properties of lossy dielectrics.

TABLE 4.1.--Electrical classification of materials.

Material Type	Conductivity Range (mho/m)
Insulators	$\sigma < 10^{-8}$
Semi-conductors	$10^{-8} < \sigma < 10^{5}$
Conductors	$\sigma > 10^{5}$

Macr

The laborator

rmed with the bul

mples of dry rock

e individual dipo

ystals) composing

vestigation will

crophysics sense

terial science s

If a paralle

al separation, d,

ected across a si

e voltage will l

y a phase angle o

ct ideal, there v

e voltage, as we

e voltage by 90°

e complex sum o

ppel, 1954a, 19

$$I = I_1 + jI$$

here $j = \sqrt{-1}$, C

d $G = \sigma \frac{A}{d}$ is th

rm of equation

$$\underline{J} = \underline{J}_1 + j\underline{J}$$

Macroscopic Electrical Model

The laboratory portion of this study will be concerned with the bulk electrical properties of small samples of dry rock, but not directly concerned with the individual dipole centers (atoms, molecules, crystals) composing the rock. Thus, the laboratory investigation will be microscopic in nature, in the petrophysics sense, but macroscopic in nature, in the material science sense.

If a parallel plate capacitor, with plate area, A, and separation, d, containing an ideal dielectric is connected across a sinusoidal voltage source, $V = V_o e^{j\omega t}$, the voltage will lead the current through the capacitor by a phase angle of 90°. If the dielectric material is not ideal, there will be a loss current, I_l, in phase with the voltage, as well as a charging current, I_c, lagging the voltage by 90°. The total current, I, will then be the complex sum of the charging and loss currents (von Hippel, 1954a, 1954c):

$$I = I_l + jI_c = (G + j\omega C)V, \qquad 4.1$$

where $j = \sqrt{-1}$, $C = K\varepsilon_o \frac{A}{d}$ is the capacitance of the system, and $G = \sigma \frac{A}{d}$ is the loss factor of the system. The vector form of equation 4.1 is:

$$\underline{J} = \underline{J}_l + j\underline{J}_c = (\sigma + j\omega\varepsilon)\underline{E}, \qquad 4.2$$

...ch is the vector
...rics. The forr
...a parallel R-C
...this reason, a
...nalog for a los

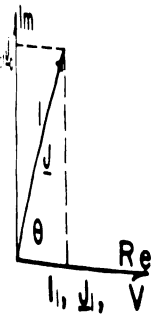

Fig. 4.1.--L
...circuit.

...s, the total cu
...apacitor with a
...rcuit, will be i
...inst the voltag
...itive imaginary
...ure 4.1). A c
...ossy capacitor
...t, or dissipat

$$D = \tan \delta =$$

which is the vector form of Ohm's law for lossy dielectrics. The form of equation 4.1 is the same as that for a parallel R-C circuit (von Hippel, 1954a, 1954b). For this reason, a parallel R-C circuit is often used as an analog for a lossy dielectric.

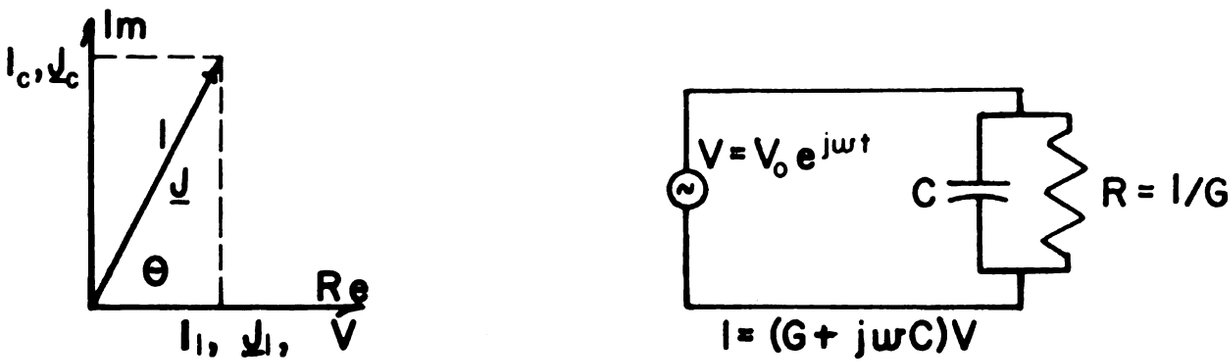

Fig. 4.1.--Lossy dielectric response and analog R-C circuit.

Thus, the total current, I, for such a lossy capacitor (capacitor with a lossy dielectric), or its R-C analog circuit, will be inclined at a power angle, $\theta < 90°$, against the voltage, or a loss angle, δ, against the positive imaginary axis of the phasor diagram (see Figure 4.1). A common method of describing the loss of a lossy capacitor or dielectric is to use the loss tangent, or dissipation factor, D, given by:

$$D = \tan \delta = \frac{1}{\omega CR} = \frac{R}{\omega C} = \frac{\sigma}{\omega \varepsilon} . \qquad 4.3$$

The frequency
generally not agree
results. This is
is exclusively to
in any energy cons
of out-of-phase a
with frequency.
admittance varies

Because of
the loss and char
incommittally by
to describe a los

$$\varepsilon^* = \varepsilon - j$$

where $\varepsilon' = \frac{\sigma}{\omega}$ is
as the approach
Harbaugh and Ro

Another ap
is to realize th
pendent for a lo
is effective, co
cavities instead
realistic for g
electrical meth
in the laborato
constant and ef
ained, accordin
42.

The frequency response of a lossy capacitor will generally not agree with that of any of its R-C analog circuits. This is because the loss current may not be due exclusively to the migration of change carriers, but to any energy consuming process. Thus, both the in-phase and out-of-phase admittances for the lossy capacitor vary with frequency. By contrast, only the out-of-phase admittance varies with frequency for the R-C analog.

Because of the ambiguity of the R-C analog circuit, the loss and charging currents are often lumped together noncommittally by the use of a complex permittivity, ε^*, to describe a lossy dielectric material, i.e.:

$$\varepsilon^* = \varepsilon - j\varepsilon', \qquad 4.4$$

where $\varepsilon' = \frac{\sigma}{\omega}$ is called the specific loss factor. This is the approach used by von Hippel (1954a, 1954c) and Sharbaugh and Roberts (1959).

Another approach to the ambiguity of the R-C analog is to realize that the conductivity will be frequency dependent for a lossy dielectric and call it the dielectric, or effective, conductivity. The use of effective conductivities instead of complex permittivities seems more realistic for geophysical problems because most geoelectrical methods involve A.C. measurements of some kind. In the laboratory portion of this study, the dielectric constant and effective conductivity of rocks will be determined, according to the lossy dielectric model of equation 4.2.

From equation

expressed as

$$\underline{P} = \varepsilon_0 \chi \underline{E}.$$

e volume polariz

idge between the

operties of a ma

ipole species of

iformly through

the polarizati

$$\underline{P} = N\underline{p}.$$

ese microscopic

cing field, E'

$$\underline{P} = \alpha \underline{E}',$$

ere α may be c

e inducing fie

count the eff

e local field

rrain, 1962)

$$\underline{E}' = \underline{E} +$$

Polarizability

From equation 3.8, the polarization vector, $\underline{P}$, can be expressed as

$$\underline{P} = \varepsilon_o \chi \underline{E}. \qquad 4.5$$

The volume polarization vector, $\underline{P}$, provides a convenient bridge between the macroscopic and microscopic electric properties of a material. If a material contains a single dipole species of microscopic dipoles, $\underline{p}$, distributed uniformly throughout the material with a volume density, N, the polarization vector may also be written as:

$$\underline{P} = N\underline{p}. \qquad 4.6$$

These microscopic induced dipoles are related to the inducing field, E', by the polarizability, α, as:

$$\underline{p} = \alpha \underline{E}', \qquad 4.7$$

where α may be due to a number of different mechanisms. The inducing field, $\underline{E}'$, is a local field which takes into account the effects of the other dipoles within the material. The local field is given (von Hippel, 1954c; Corson and Lorrain, 1962) as:

$$\underline{E}' = \underline{E} + g \frac{\underline{P}}{3\varepsilon_o}, \qquad 4.8$$

ere $g \geq 1$ is a co-

the dipole distr

ributions, g =

neral form of the

mple, 1954c; Cors

terials is obtai

$$\frac{N\alpha}{3\varepsilon_0} = \frac{K -}{gK + (}$$

hich, for highly

$$\frac{N\alpha}{3\varepsilon_0} = \frac{K - 1}{K + 2}$$

quation 4.9 is in

with a similar res

ective electric mo

Lossy D

Electrical

echanism. Three

ielectrics are c

elaxation polari

he shift of elec

nd physical orie

resence of an e

geneous lossy di

ation, due to c

where $g \geq 1$ is a coefficient which describes the symmetry of the dipole distribution. For highly symmetric dipole distributions, $g = 1$ (Corson and Lorrain, 1962). The general form of the Clausius-Mossotti equation (von Hipple, 1954c; Corson and Lorrain, 1962) for isotropic materials is obtained:

$$\frac{N\alpha}{3\varepsilon_o} = \frac{K - 1}{gK + (3 - g)} ,$$

which, for highly symmetric dipole distributions, becomes:

$$\frac{N\alpha}{3\varepsilon_o} = \frac{K - 1}{K + 2} . \qquad 4.9$$

Equation 4.9 is included at this point for later comparison with a similar result which can be obtained from the qualitative electric model proposed for rocks.

Lossy Dielectric Frequency Dependence

Electrical polarization is seldom due to a single mechanism. Three mechanisms common to homogeneous, lossy dielectrics are called electronic, ionic, and dipole relaxation polarization. These mechanisms are due to the shift of electron clouds, relative shift in ions, and physical orientation of permanent dipoles in the presence of an electric field, respectively. Inhomogeneous lossy dielectrics also exhibit interfacial polarization, due to charge build up at phase (inhomogenity)

ndaries. Some c

anisms are desc

anisms, and the

addition, they

frequencies ne

erial will have

will decrease ra

frequencies ab

$\ll f_c$. Also, ε

an it is for f

is an inertia

res a definite

e established in

A.C. field at

th the inducing

$\sim f_c$, the dipo

. For $f >> f_c$

eep up with $\underline{E}'$

ormant. When t

gain.

The resona

an be determine

. The specific

eak about the r

harply at f_c.

ersus f plot wi

, with local ma

boundaries. Some common theoretical models for these mechanisms are described in Appendix A. Each of these mechanisms, and their models, are frequency dependent. In addition, they exhibit resonance characteristics. For frequencies near the resonance frequency, f_c, the material will have a high specific loss factor, ε', and K will decrease rapidly with increasing frequency, f. For frequencies above f_c, K is much less than it is for $f << f_c$. Also, ε' is much smaller for $f >> f_c$ and $f << f_c$ than it is for $f \sim f_c$. Physically, the resonance phenomenon is an inertial one. Each polarization mechanism requires a definite relaxation time, τ, for its dipole to be established in the presence of the inducing field. For an A.C. field at $f << f_c$, the dipole can polarize in phase with the inducing field, and ε' assumes small values. As $f \longrightarrow f_c$, the dipole begins to lag $\underline{E}'$, creating an increased ε'. For $f >> f_c$, the dipole can no longer even begin to keep up with $\underline{E}'$ and the polarization mechanism becomes dormant. When this happens, ε' becomes insignificant again.

The resonance frequency of a polarization mechanism can be determined empirically from plots of K and ε' versus f. The specific loss factor, ε', will show a symmetric peak about the resonance frequency, f_c, and K will decrease sharply at f_c. From equation 4.4, $\sigma = \varepsilon'$, so that a σ versus f plot will be a steadily increasing function of f, with local maximas near the f_c. Because of the

ensions and mass

the four polari

dely separated fr

nance frequenci

erials, however,

lectronic polariza

ption of the elect

ation, f_c generall

ple relaxation fo

ption, but in sol

The f_c for interfa

the range of 1

shown in Figur

Fig. 4.
properties (a
Fröschknecht,

dimensions and masses involved, the resonance frequencies for the four polarization mechanisms described above, are widely separated from one another (see Figure 4.2). Resonance frequencies for a given mechanism in different materials, however, are generally close together. The electronic polarization f_c values occur in the ultraviolet region of the electromagnetic spectrum. For ionic polarization, f_c generally occurs in the infra-red range. Dipole relaxation for fluids has its f_c in the microwave region, but in solids it is much lower, if present at all. The f_c for interfacial polarization appear to be very low, in the range of 100 to 1000 cps. This frequency dependence is shown in Figure 4.2.

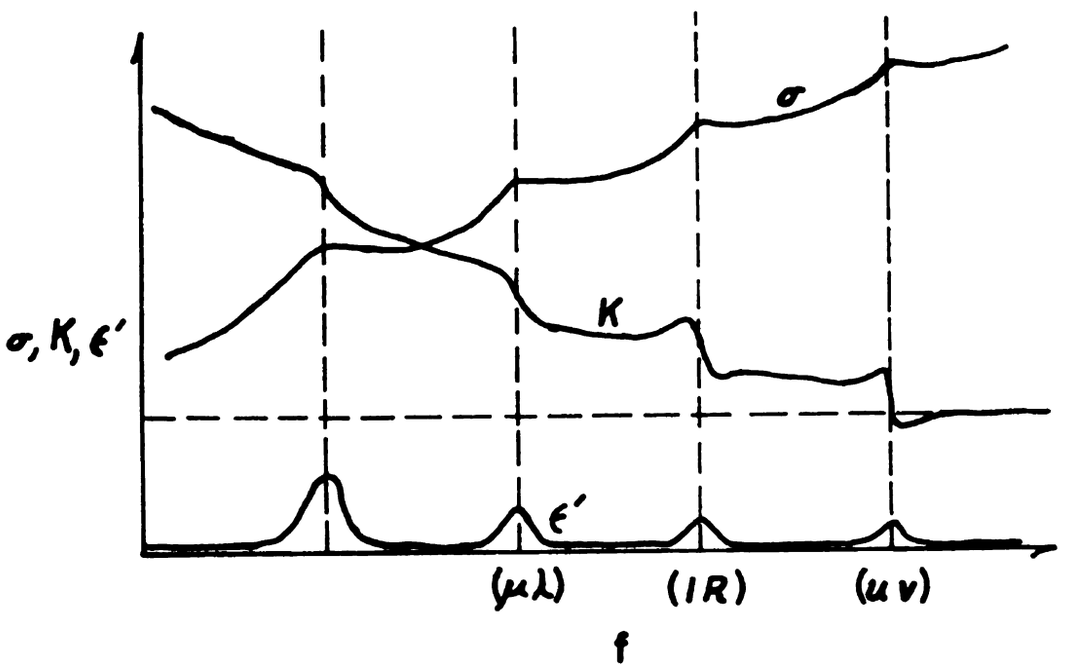

Fig. 4.2.--Lossy dielectric dispersion of electrical properties (after Wert and Thompson, 1964; Keller and Frischknecht, 1966).

Qualit

A quantitativ
ould be very diff
plexity needed for
croscopic model,
tting laboratory
terpreting them
uction to this ch
ery appropriate f
of anisotropy and
al lossy dielect
or the purposes
ock may be consi
rains, each spec
species of polar
ately heterogen
ock model be st
ely consider ro
statistical comp
he sub-sample
his implies th
niformly throu
scale of the su
hat the rock m
respect to comp
becomes:

Qualitative Microscopic Electric Model for Rocks

A quantitative microscopic electric model for rocks would be very difficult to develop because of the complexity needed for a realistic model. A qualitative microscopic model, however, can be very helpful for predicting laboratory results before experimentation and interpreting them afterward. As indicated in the introduction to this chapter, the lossy dielectric model is very appropriate for dry rocks. However, the conditions of anisotropy and inhomogenity must be added to the classical lossy dielectric model to make it applicable to rocks. For the purposes of the qualitative theoretical model, a rock may be considered to consist of its constituent grains, each species of which would constitute a separate species of polarization mechanism. Such a model is definitely heterogeneous, however we will require that the rock model be statistically homogeneous. Thus, we will only consider rock samples of sufficient size that the statistical composition will not vary significantly from the sub-sample to sub-sample taken from the parent sample. This implies that each mineral species be distributed uniformly throughout the parent sample (at least on the scale of the sub-sample). Borrowing terms, we can say that the rock model is statistically stationary with respect to composition. For such a model, equation 4.6 becomes:

$$\underline{P} = \sum_{i=1}^{n} N_i \underline{p}_i,$$

in a model consist

mbined) of dipol

n the model with

The second g

electric model i

nisotropy may be

istribution of is

istribution of a

istribution of a

odels may be phy

he use of the m

equires the cal

ster symmetry is

econd model is

he use of the

$$\underline{E}' = \underline{E} +$$

his is the app

lectric model

For isot

o $\underline{E}'$ and α of

olarization r

becomes a s

4.7 becomes:

$$\underline{P} = \sum_{i=1}^{n} N_i \underline{p}_i , \qquad 4.10$$

for a model consisting of n > 1 species and mechanisms (combined) of dipoles, $\underline{p}_i$, distributed uniformly throughout the model with densities, N_i.

The second generalization from the classical lossy dielectric model involves the condition of anisotropy. Anisotropy may be achieved by an anisotropic (low symmetry) distribution of isotropic dipole sources, an isotropic distribution of anisotropic sources, or an anisotropic distribution of anisotropic sources. The first and last models may be physically more realistic, but they require the use of the most general form of equation 4.8. This requires the calculation of the coefficient, g, using whatever symmetry is present in the dipole distribution. The second model is mathematically much simpler, for it allows the use of the high symmetry form of equation 4.8:

$$\underline{E}' = \underline{E} + \frac{\underline{P}}{3\varepsilon_o} . \qquad 4.11$$

This is the approach used to develop the qualitative electric model for rocks.

For isotropic polarization models, $\underline{p}$ is parallel to $\underline{E}'$ and α of equation 4.7 is a scalar. For anisotropic polarization models, $\underline{p}$ and $\underline{E}'$ are no longer parallel and α becomes a symmetric second-rank tensor. Then, equation 4.7 becomes:

$$p_i = \alpha_{ij} E'_j .$$

the polarizability

nsformation law

nk tensor. The

n for K. Inser

sults in:

$$\underline{p} = \sum_{i=1}^{n} N_i \alpha^{(i}$$

n:

$$\varepsilon_o \chi \underline{E} = \sum_{i=1}^{n}$$

$$= \left[\sum_{i=1}^{n} \right.$$

so that:

$$\frac{1}{3\varepsilon_o} = \sum_{i=1}^{n} N_i$$

which is the Cla

aterial with n

ipoles. In equa

$\alpha^{(i)}$, χ, and K a

appropriate symm

identity matrix,

inversion.

$$p_i = \alpha_{ij} E'_j. \qquad 4.12$$

The polarizability, α_{ij}, does satisfy the rotational transformation laws of 3.1 and 3.2 and thus is a second-rank tensor. The proof of its symmetry is similar to that for K. Inserting equations 4.12 and 4.11 into 4.10 results in:

$$\underline{p} = \sum_{i=1}^{n} N_i \alpha^{(i)} \underline{E}' = \sum_{i=1}^{n} \left[N_i \alpha^{(i)} \left(\underline{E} + \frac{\underline{P}}{3\varepsilon_o} \right) \right],$$

or:

$$\varepsilon_o \chi \underline{E} = \sum_{i=1}^{n} \left[N_i \alpha^{(i)} \left(I + \frac{\chi}{3} \right) \underline{E} \right]$$

$$= \left[\sum_{i=1}^{n} N_i \alpha^{(i)} \right] \left[\frac{K + 2I}{3} \right] \underline{E},$$

so that:

$$\frac{1}{3\varepsilon_o} = \sum_{i=1}^{n} N_i \alpha^{(i)} = (K - I)(K + 2I)^{-1}, \qquad 4.13$$

which is the Clausius-Mossotti equation for anisotropic material with n > 1 species and mechanisms (combined) of dipoles. In equation 4.13 and the steps leading to it, $\alpha^{(i)}$, χ, and K are 3 x 3 representation matrices for the appropriate symmetric second-rank tensors, I is the 3 x 3 identity matrix, and the -1 superscript indicates matrix inversion.

Predicti

El

A qualitative

ctrical characte

an alternating

roscopic study,

el is not needed

that developed

ming macroscop

For a unifor

ecies of isotro

ect to obtain

ch a model woul

on of the pola

olarization cen

requencies woul

be symmetri

hat for the an

on curves for

diate, and m

roperties. O

ecies of dip

and σ to var

For sin

ensor proper

as stated by

Predictions Based on the Qualitative Electric Model for Rocks

A qualitative working microscopic model for the electrical characteristics of dry rocks in the presence of an alternating $\underline{E}$ field has been developed. For a macroscopic study, such as the present, a quantitative model is not needed. However, a qualitative model, such as that developed above does aid in predicting and explaining macroscopic observations.

For a uniform, isotropic distribution of a single species of isotropic polarization centers, one would expect to obtain dispersion curves similar to Figure 4.2. Such a model would give unique resonance frequencies for each of the polarization mechanisms present. If the polarization centers were anisotropic, unique resonance frequencies would still be expected but K and σ would now be symmetric second-rank tensors. The result is that for the anisotropic model, there are three dispersion curves for K and σ, indicating the maximum, intermediate, and minimum principal values of the tensor properties. One would not, however, for a single species of dipoles, expect the principal directions of K and σ to vary with the frequency of $\underline{E}$.

For single crystals, the principal directions of tensor properties are controlled by the crystal lattice, as stated by Neumann's principle (Nye, 1964): "The

metry elements c

st include the s

the crystal."

For heteroge

uld expect to be

nciple, which m

nts of any phys

he symmetry elem

the rock.

Turner and

pect rock fabr

ffer no develo

o they attempt

little more

between the ro

he conductiv

Single

arallel and

axes for the

Neumann's p

be expected

-planes o

are statis

be very g

easureme

and line

these r

symmetry elements of any physical property of a crystal must include the symmetry elements of the point group of the crystal."

For heterogeneous materials, like rocks, one would expect to be able to use an extension of Neumann's principle, which might be stated as: The symmetry elements of any physical property of a rock must include the symmetry elements of the statistical symmetry (fabric) of the rock.

Turner and Weiss (1963) mention that they would expect rock fabric to control physical properties, but offer no development in support of this statement, nor do they attempt to follow it up. Let us now consider, in a little more detail, the relationships one might expect between the rock fabric and the principal directions of the conductivity and dielectric constant tensors.

Single lineations and S-planes in rock fabric are parallel and normal, respectively, to rotary symmetry axes for the fabric (and rock). Using the extension of Neumann's principle, the principal K and σ values would be expected to parallel any lineations and be normal to S-planes of the rock fabric. Since these relationships are statistically based, this correspondence might not be very good for small numbers of macroscopic fabric measurements on the field sample. Also, multiple S-plane and lineations present in some rocks may further confuse these relationships.

Let us now c

ock model propose

atistically uni

ultiple species

or this model, u

f the four types

ent) would not

equire that the

he different po

ery fortuitous

requency spect

tudy, it is re

ctions to the

come from diffe

encies. This

esonance freq

he rocks. Th

nd the maxima

s they are ir

he principal

should be coi

even differen

exhibit diffe

Combini

idual dipole

uency respon

n the princ

Let us now consider the expected results for the rock model proposed in the previous section, i.e., a statistically uniform and homogeneous distribution of multiple species of anisotropic polarization centers. For this model, unique resonance frequencies for each of the four types of polarization mechanisms (if present) would not be expected. For them to be unique would require that the corresponding resonance frequencies of the different polarization species would be identical; a very fortuitous occurrence. Thus, even for the short frequency spectrum used in the laboratory portion of this study, it is reasonable to expect that the dominant contributions to the dielectric constant and conductivity may come from different dipole species at different frequencies. This should result in spreading out the resonance frequencies of the bulk characteristics of the rocks. That is, the change in slope of the K curve and the maxima on the σ curve will not be as pronounced as they are in Figure 4.2. Also, there is no reason why the principal tensor directions for all the dipole species should be coincident. In rocks, different minerals, or even different sized grains of the same mineral, may exhibit different fabrics.

Combining the variations in anistropy of the individual dipole species and the variations in their frequency responses, one would logically expect variation in the principal directions of the bulk rock tensors

with frequency. Also, the relative σ and K contributions of the individual dipole species may vary with frequency. This may, in turn, lead to the condition where the principal directions for the σ and K tensors do not coincide for some frequencies of investigation. However, one would, in general, expect that lineations be sub-parallel and foliations (and other S-planes) be normal to the tensor principal axes, unless multiple S-planes and lineations lower the symmetry of the rock fabric.

The model developed above gives us considerable latitude in anticipated results. However, we must remember that the model is an analog for a material which, in itself, is quite variable.

E

A block diag

laboratory por

The elements

shunt capacit

W. Keller (19

pose is twofo

tion factor fo

stem capacitar

om the holder

e circuit for

ring data rec

rocedure

The lab

resent study

opic lossy

hapter IV.

lectrics a

he dielect

CHAPTER V

EXPERIMENTAL PROCEDURES

Instrumentation

A block diagram of the measurement circuit used for the laboratory portion of this study is shown in Figure 5.1. The elements of the circuit are given in Table 5.1. The shunt capacitor was included at the suggestion of Dr. G. V. Keller (1967), of the Colorado School of Mines. Its purpose is twofold. It decreases the holder system dissipation factor for high loss samples and provides sufficient system capacitance for balance when the sample was removed from the holder. Since the shunt capacitor remained in the circuit for all measurements, its value canceled out during data reduction.

Laboratory Measurements

Procedure

The laboratory measurement procedure used for the present study was governed by the inhomogeneous, anisotropic lossy dielectric model developed for rocks in Chapter IV. The electrical properties of lossy dielectrics are determined by simultaneous measurement of the dielectric constant, K, and (effective) conductivity,

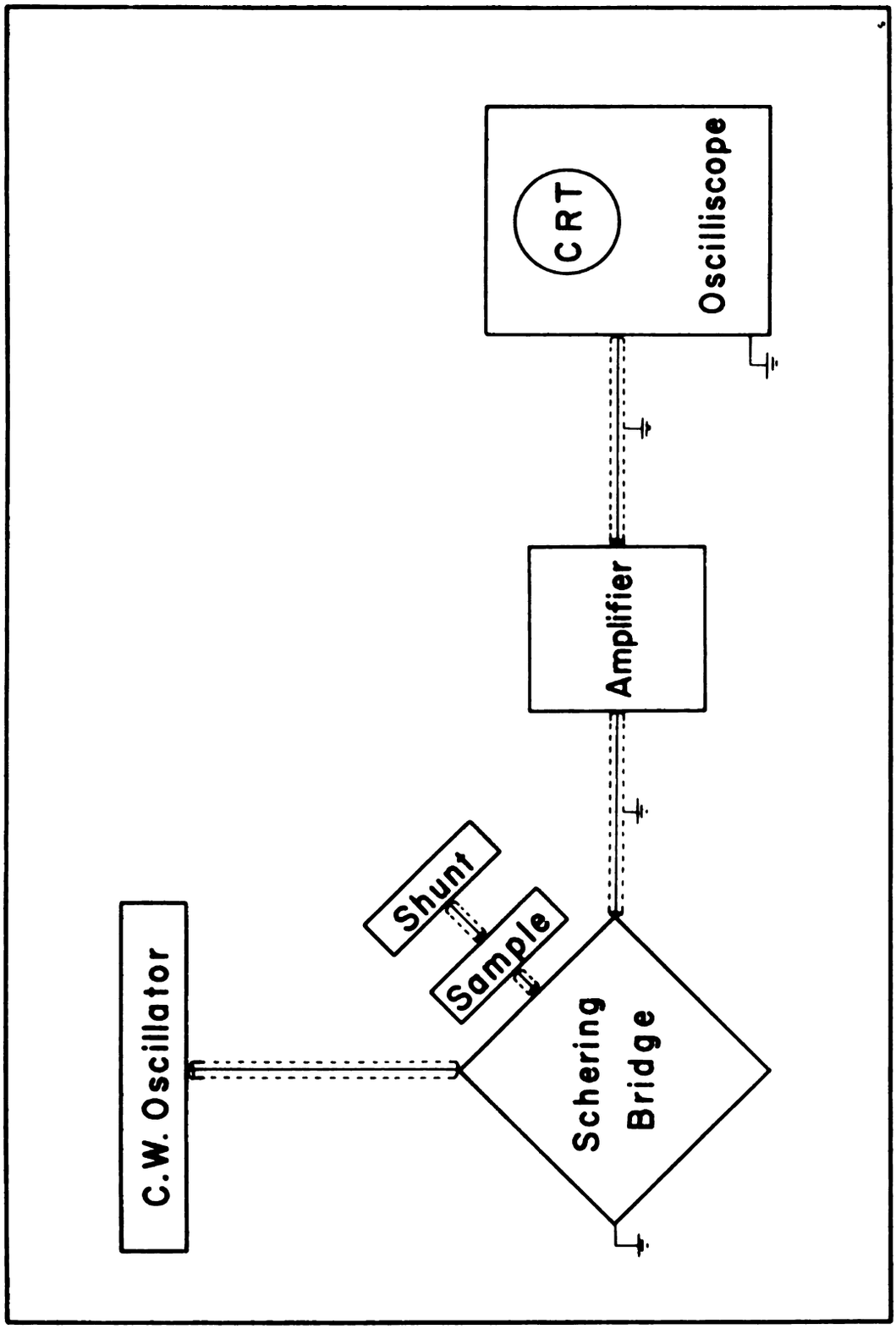

Fig. 5.1.--Block diagram of electrical properties measurement circuit.

TABLE 5.1.--Instrumentation for the electrical properties study.

Element	Description	Input Impedance	Output Impedance	Range
			600 ohm	10 cps-

TABLE 5.1.--Instrumentation for the electrical properties study.

Element	Description	Input Impedance	Output Impedance	Range
C. W. Oscillator	Hewlet-Packard 650-A Audio Oscillator	---	600 ohm	10 cps-10 Mcps
Schering Bridge	General Radio 716-C Capacitance Bridge	600 ohm	low (~ 200 ohm)	100-1100 pf, 30 cps-300 Kcps
Amplifier	Hewlet-Packard 450 Stabalized Amplifier	1 Mohm	150 ohm	10 cps-1 Mcps
Oscilliscope	Tectronix 564 Dual Trace Oscilliscope	1 Mohm	---	---
Micrometer Sample Holder	General Radio 1690-A Dielectric Sample Holder	---	---	---
Shunt	Shielded Ceramic Capacitor	---	---	330-670 pf

von Hippel, 19

or low frequency

plished by measur

efer of material

rm of an A.C. br

4b; Sharbaugh

he A.S.T.M. sta

idge measureme

llowed, the e

orn and Ward,

berts, 1959;

aking two mea

terest. The

older and the

he sample fa

easurement,

Fig.
older cont

assumed fo

balance, t

factor, D

σ (von Hippel, 1954a, 1954c; Sharbaugh and Roberts, 1959). For low frequency measurements, this is usually accomplished by measuring the electrical properties of a thin wafer of material in a micrometer sample holder as one arm of an A.C. bridge (Hartshorn and Ward, 1936; Field, 1954b; Sharbaugh and Roberts, 1959; A.S.T.M., 1965). If the A.S.T.M. standards (D-150-65T, 1965) for low frequency bridge measurements using a micrometer sample holder are followed, the edge and lead effects are eliminated (Hartshorn and Ward, 1936; Field, 1954a, 1954b; Sharbaugh and Roberts, 1959; A.S.T.M., 1965). This is accomplished by taking two measurements at every signal frequency of interest. The sample wafer is inserted into the sample holder and the movable electrode brought into contact with the sample face for the first measurement. For this measurement, the analog circuit shown in Figure 5.2 is

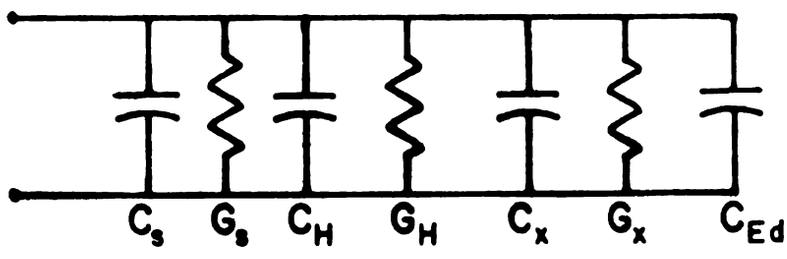

Fig. 5.2.--Analog circuit for micrometer sample holder containing sample.

assumed for the sample-holder system. From the initial balance, the system capacitance, C_1, and dissipation factor, D_1, are obtained as:

$$C_1 = C_H + C_x$$

$$G_1 = G_H + G_x$$

$$D_1 = \frac{G_H}{xC_1} +$$

ere G_H is the c
ads, G_x is the
ckness, d, and
ant, C_H is the
ads, C_x is the
e air capacit
d separation,
e sample is
easurement ta
d an air di
alance is sh
, and diss
e then:

$$C_2 =$$

$$G_2 =$$

$$D_2$$

$$C_1 = C_H + C_x + C_{Ed} + C_s = C_H + C_x + C_{od}(1 - \frac{A_x}{A_E}) + C_s,$$

$$G_1 = G_H + G_x + G_s, \qquad 5.1$$

$$D_1 = \frac{G_H}{\omega C_1} + \frac{G_x}{\omega C_1} + \frac{G_s}{\omega C_1},$$

where G_H is the combined loss factor for the holder and leads, G_x is the loss factor for the sample wafer of thickness, d, and area, A_x, G_s is the loss factor for the shunt, C_H is the combined capacitance for the holder and leads, C_x is the capacitance of the sample wafer, C_{od} is the air capacitance of the capacitor with plate area, A_E, and separation, d. After the initial balance is obtained, the sample is removed from the holder and a second balance measurement taken with the same electrode separation, d, and an air dielectric. The analog circuit for the second balance is shown in Figure 5.3. The system capacitance, C_2, and dissipation factor, D_2, for the second balance are then:

$$C_2 = C_H + C_s + C_{od},$$

$$G_2 = G_H + G_s, \qquad 5.2$$

$$D_2 = \frac{G_H}{\omega C_2} + \frac{G_s}{\omega C_2}.$$

Fig. 5.3.--
:lder without sa

:e sample diele

:ivity, σ, are t

$$K = \frac{C_x d}{\varepsilon_o A_x}$$

$$\sigma = \frac{G_x d}{A_x}$$

: the diamet

:ameter of

eliminated b

:954b; Shark

The m

for this s

and is ver

(1959), H

and Scott

properti

dried s

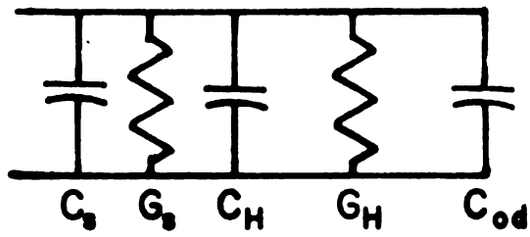

Fig. 5.3.--Analog circuit for micrometer sample holder without sample.

The sample dielectric constant, K, and (effective) conductivity, σ, are then obtained from equations 5.2 and 5.2 by:

$$K = \frac{C_x d}{\varepsilon_o A_x} = \frac{(C_1 - C_2)d}{\varepsilon_o A_x} + 1, \qquad 5.3$$

$$\sigma = \frac{G_x d}{A_x} = \frac{\omega d (D_1 C_1 - D_2 C_2)}{A_x} .$$

If the diameter of the sample wafer is smaller than the diameter of the holder electrodes, the edge effect is eliminated by the use of this procedure (Field, 1954a, 1954b; Sharbaugh and Roberts, 1959).

The measurement procedure described above was used for this study. It follows the A.S.T.M. standards (1965) and is very similar to that used by Keller and Licastro (1959), Howell and Licastro (1961), Simandoux (1963), and Scott et al. (1967) in their studies of the electrical properties of rocks. Measurements were made on vacuum dried sample wafers at room temperature and pressure.

addition, these

six, or more, d

is resulted in d

ich allowed the

nsor coefficien

. Measurement

een 30 and 3000

easurements were

ionale for Tw
easurements

For anisot

econd-rank ten

le to specify

for the pre

e done most e

in disk-shap

isk faces. A

ysical prope

ividuals c

ccuracy. Th

ollow A.S.T.

and c, are

aboratory m

older syste

ncreases t

ncrease th

In addition, these measurements were taken on wafers cut in six, or more, different directions from each sample. This resulted in directional measurements of K and σ, which allowed the least square determination of the tensor coefficients according to the model of equation 3.5. Measurements were made at several frequencies between 30 and 30000 cps for all samples. In addition, measurements were made at 100000 cps on two samples.

Rationale for Two-Electrode Measurements

For anisotropy measurements involving symmetric second-rank tensors, it is of utmost importance to be able to specify the direction of the independent vector ($\underline{E}$, for the present study) within the sample. This can be done most easily with two-electrode measurements on thin disk-shaped samples, for then, $\underline{E}$ is normal to the disk faces. A.S.T.M. measurement standards for a given physical property represent the combined efforts of many individuals concerned, primarily, with measurement accuracy. The measurement procedures outlined above do follow A.S.T.M. standards (1965). The material properties, K and σ, are not measured directly. Instead, the direct laboratory measurements are of C and G for the sample-holder system. The choice of the thin wafer sample shape increases the system C and G values, which in turn, will increase the measurement sensitivity for K and σ. Another

nsideration invo

ley (1948), Co

954), and Knox

ns on equipoten

ues. Because

ces in the vici

electrodes should

n opposite faces

ove, will be at

his method is l

mogenities. F

nts were used

perimental Li

The great

edure outlined

ut with the i

ct. Most sat

ble amounts o

with the 716-C

problem appea

pedance bridg

samples, but

sliding null

obtain.

Another

it operates

consideration involves the effects of inhomogenities. Bewley (1948), Cook and Van Nostrand (1954), Deppermann (1954), and Knox (1964) discuss the effects of inhomogenities on equipotential surfaces and apparent resistivity values. Because of the distortion of equipotential surfaces in the vicinity of inhomogenities, the use of point electrodes should be avoided. The two large electrodes on opposite faces of the thin wafer sample, as described above, will be at constant potentials at all times. Thus this method is least susceptible to the effects of inhomogenities. For these reasons, two-electrode measurements were used for the laboratory study.

Experimental Limitations

The greatest problems with the experimental procedure outlined above lay not with the procedure, itself, but with the instrumentation with which it was carried out. Most saturated samples and those containing appreciable amounts of metallic minerals could not be measured with the 716-C bridge because of their high loss. This problem appears to plague all capacitance bridges. Impedance bridges will allow the measurement of higher loss samples, but balance is then obtained by means of a sliding null (Stout, 1960) which is very difficult to obtain.

Another limitation to the above procedure is that it operates very close to the limits of sensitivity of

ne instrumentati
stout, 1960) sho
values may be a
between 15 per c
me same point w
ent. Greater a
ation measureme
propagated error
greatest when K
values, the erro
remembered, that
pessimistic in r
they should sho
ics and the re
a disk of green
were measured r
The discrepanci
all much less t
propagation (Δ

The

Sample Prepara

The samp
bical in sha
a side. Care
weathered, su
collected fro

the instrumentation. A statistical propagation of error (Stout, 1960) showed that the error in the directional σ values may be as high as 49 per cent, though most were between 15 per cent and 25 per cent. The K errors at the same point were fairly constant at about 10-15 per cent. Greater accuracy in the capacitance and dissipation measurements would help this situation. The propagated error for the directional σ and K values is greatest when K is very small ($K \sim 5$). For larger K values, the errors become much less. It should also be remembered, that a statistical propagation of error is pessimistic in nature. If the errors are indeed random, they should show up in repeated measurements. To check this and the repeatability of the measurement procedure, a disk of greenstone schist and one of syenite gneiss were measured repeatedly over the period of a month. The discrepancies between the different measurements were all much less than that predicted by the above error propagation ($\Delta K \sim 3\%$, $\Delta\sigma \sim 7\%$).

The Laboratory Measurement Samples

Sample Preparation

The samples collected in the field were roughly cubical in shape, approximately ten to twelve inches on a side. Care was taken to collect only from fresh, non-weathered, surfaces. Thus, most of the samples were collected from road cuts.

The sample
udy closely fol
(#1) and the A.
ld make some mod
tion was more ap

From the fi
ne different d
rresponded to
pothetical cub
is reference s
bserved fabric
mpletely succe
olved in slab
ere cut in this
ne the measure
alue determina
irections dist
ents uniformly
eference syste

Disks, 1.
ut, and lapped
rom 35 to 235
ides of the di
amples were th
oated with con
desiccated cont
be made.

The sample preparation procedures used for this study closely followed those of Howell and Licastro (1961) and the A.S.T.M. standards (1965). The author did make some modifications so that the sample preparation was more applicable to the present study.

From the field samples, slices were cut normal to nine different directions in the rock. These directions corresponded to the face normals and face diagonals of a hypothetical cube (co-ordinate system). Whenever possible, this reference system was oriented with respect to an observed fabric in the rock. However, this was never completely successful because of the mechanical problems involved in slabbing such large rock samples. The rocks were cut in this manner because the slab normal then became the measurement direction for the directional tensor value determinations. The use of these particular nine directions distributed the directional K and σ measurements uniformly over the quadrants of the laboratory reference system.

Disks, 1.6 in. in diameter were cored from the slices, cut, and lapped down to constant thicknesses, which ranged from 35 to 235 mills. During this process, the opposite sides of the disks were taken to a 600 grit polish. The samples were then vacuum dried at 60° C for 24 hours, coated with conducting silver paint, and stored in a desiccated container until electrical measurements could be made.

tionale for Mea
Dry Samples

The samples
his study were v
heir natural sta
lectrolyte solut
turation of the
f the saturating
alk electrical
950; Wyllie, 19
Fatt, Kruschknecht, 19
1957). This pr
f electrical p
in-situ conditi
ere that even
ikely that
ples will dupl
laboratory sam
condition duri
study, suffici
and measureme
Also, during
flushed with
not be recrea
Geertsma, Veevil and Wa
conditions, b
solutions. S

Rationale for Measurements on Dry Samples

The samples measured in the laboratory portion of this study were vacuum dried. However, most rocks in their natural state contain moisture in the form of electrolyte solutions. The effective porosity, per cent saturation of the available pore space, and the salinity of the saturating solution can drastically affect the bulk electrical properties of the rock (cf., Jakosky, 1950; Wyllie, 1963; Grant and West, 1965; Keller and Frischknecht, 1966; Parkhomenko, 1967; Ward and Fraser, 1967). This presents a strong case for the measurement of electrical properties in saturated rocks to duplicate in-situ conditions. However, Simmons and Nur (1968) indicate that even with the most careful precautions, it is unlikely that laboratory measurements of physical properties will duplicate in-situ results. This is because the laboratory sample is generally altered from its in-situ condition during sample preparation. For the present study, sufficient time elapsed between sample collection and measurement that most of the in-situ water evaporated. Also, during sample preparation, the rock was thoroughly flushed with cutting fluid so that in-situ solutions could not be recreated by saturating with distilled water. Keevil and Ward (1962) did not attempt to recreate in-situ conditions, but studied the effects of various electrolyte solutions. Such a study is certainly worth doing, but it

s such a large p

udy.

The presenc

ditional consid

MacInnes, 1961;

the electrical

e taking place.

ersible, or can

with the current

will become pola

within the rock

which we are mo

ertain valid me

egligible, any

electrode cont

on-polarizing

electrodes are

ay to predict

hase boundary

and effort ha

et al., 1957;

1959; Keevil

1967; Scott e

develop non-p

so-called nor

mote testimor

is such a large problem that it constitutes a separate study.

The presence of aqueous solutions requires the additional consideration of electrochemical problems (MacInnes, 1961; Moore, 1964). At every phase boundary in the electrical circuit, electrochemical reactions will be taking place. If these reactions are not truly reversible, or cannot take place fast enough to keep up with the current flow, the junctions at which they occur will become polarized. When these polarizations occur within the rock, they are a property of the rock (I.P.) which we are most interested in measuring. However, to obtain valid measurements, we must eliminate, or make negligible, any polarizations occurring at the sample-electrode contact. This is accomplished by the use of non-polarizing electrodes (Moore, 1964). Non-polarizing electrodes are not universal and there is apparently no way to predict, theoretically, whether or not a particular phase boundary will be polarizing in advance. Much time and effort has been spent by various workers (cf., Mandel et al., 1957; Collett, 1959; McEven et al., 1959; Mayper, 1959; Keevil and Ward, 1962; Simandoux, 1963; Quraishi, 1967; Scott et al., 1967; Scott and West, 1969) trying to develop non-polarizing electrodes. The great variety of so-called non-polarizing electrodes now in use stands as mute testimony to the fact that most of these have not

...completely s...

...a very carefu...

...lecting a non-p...

...their study in...

...ple system mus...

...e electrodes ar...

Schering br...

...nce, C, and di...

...ich generally ...

...e bridge used ...

...ssipation fac...

...only 29°. S...

...ons has the e...

...is very easy ...

...operties of ...

...strumentatio...

The rock ...

...eta-sediment...

...hould have ve...

...C. resistivi...

...reenstone sc...

...e vacuum dr...

...both cases ...

...e low curre...

...i.e., J ~ 20 ...

...ensities (J ...

...cm and a s...

been completely successful. Scott et al. (1967) carried out a very careful and detailed investigation aimed at selecting a non-polarizing electrode system. The results of their study indicate that each electrode-electrolyte-sample system must be tested before it can be assumed that the electrodes are indeed non-polarizing.

Schering bridges are designed to measure the capacitance, C, and dissipation factor, D, of real capacitors which generally have a finite, but low, loss factor, G. The bridge used for this study could measure a maximum dissipation factor which corresponded to a loss angle, δ, of only 29°. Saturating samples with electrolyte solutions has the effect of increasing the loss angle. Thus, it is very easy to reach a condition where the electrical properties of the rocks can no longer be measured with the instrumentation available.

The rock types selected for this laboratory study (meta-sediments, meta-volcanics, and meta-igneous rocks) should have very low porosities. As a check on this, D.C. resistivity measurements were made on a core of greenstone schist (M-2). This core was measured in both the vacuum dried condition and saturated with tap water. In both cases, it was impossible to make measurements with the low current densities used for the bridge measurements (i.e., $\underline{J} \sim 20$ ma/m^2). However, with much larger current densities ($\underline{J} \sim$ 3-4 amp/m^2), a dry resistivity of $2.28 \cdot 10^2$ ohm-m and a saturated resistivity of $1.66 \cdot 10^2$ ohm-m were

ained. Both c

se obtained us

sistivities pro

se of the hig

op needed to p

ilar results

mation collec

mples used for

at these samp

lation of the

ake Superior r

of Tammemogi (

ery high appa

f this area u

Howell

ifficulty re

ver extended

ey construc

he author's

ll sample d

t all times

sing the va

within the

Until

samples has

bad situati

obtained. Both of these resistivities are much lower than those obtained using the A.C. bridge. However, these D.C. resistivities probably represent dielectric breakdown because of the high current densities and the high voltage drop needed to produce a measurable current (V = 500v). Similar results were also obtained for a core of iron formation collected from Northern Michigan along with the samples used for this study. These results would indicate that these samples do indeed have low porosity. Extrapolation of these low porosities to the Precambrian of the Lake Superior region appears to be confirmed by the results of Tammemogi (1969a, 1969b) and Dowling (1969) who observed very high apparent resistivities in the Precambrian rocks of this area using magneto-telluric measurements.

Howell and Licastro (1961) encountered considerable difficulty repeating rock electrical property measurements over extended periods of time. To overcome this problem, they constructed a sample holder which could be evacuated. The author's solution to this problem was to vacuum dry all sample disks and store them in a desiccated container at all times except when taking electrical measurements. Using the vacuum dried samples, measurements were repeated within the accuracy described above ($\Delta K \sim 3\%$, $\Delta\sigma \sim 7\%$).

Until now, electrical measurements on vacuum dried samples has been considered as the best alternative to a bad situation. As such their results should be applied

field resu

ese result

th the Apo

ronautics

nts on dr

lar explo

The

plicable

mated

rosities

se of va

lication.

Limitati
reparat

Th

bove is

his to

inimum

repara

irect

even l

repar

altere

time

easu

ause

to field results in only a qualitative manner. However, these results may be used directly for dry environments. With the Apollo and post-Apollo programs of the National Aeronautics and Space Administration, laboratory measurements on dry samples should be directly applicable to lunar exploration (see Strangway, 1969).

The lossy dielectric model for rocks is particularly applicable for dry rocks, however, it may also be used for saturated rocks (cf., Bacon, 1965). With the very low porosities found in the rocks chosen for this study, the use of vacuum dried samples is not an unreasonable simplification.

Limitations of the Sample Preparation Procedure

The greatest limitation to the sample procedure given above is that it is very time consuming. The author found this to be the most frustrating aspect of the study. A minimum of forty-two man-hours was required, in sample preparation, to produce measurement disks for nine different directions. For most samples, the preparation time was even longer because of damage during one, or more, of the preparation steps. While it is possible that a slightly altered preparation procedure might reduce the preparation time somewhat, it is unlikely that electrical anisotropy measurements will ever be made on a production basis because of the preparation time involved.

The data ob

apacitance and

ignal frequenci

ask orientation

he K and σ ten

re the desired

aboratory data

and σ values

dication of

he symmetric

ore, differe

ndependent t

least squar

he least sq

eveloped in

ensor coeff

with respec

t does not

his is acc

edure to

CHAPTER VI

DATA ANALYSIS

Introduction

The data observed in the laboratory consist of capacitance and dissipation factor values at different signal frequencies, sample disk dimensions, and sample disk orientations. This data is greatly removed from the K and σ tensor principal values and directions, which are the desired information of the study. The original laboratory data must first be converted into directional K and σ values. The directional K and σ values give an indication of anisotropy, but do not define the appropriate symmetric second-rank tensors. However, if six, or more, different directional values are available, the six independent tensor coefficients can be obtained by use of a least square reduction process based upon equation 3.5. The least square tensor coefficient process will be developed in this chapter. The output of the least square tensor coefficient reduction process defines the tensors with respect to the laboratory co-ordinate system, however, it does not give the tensor principal values and directions. This is accomplished by a successive approximation procedure to be described later in this chapter.

Thus, the

successive reduc

ation is obtain

t least, would

y hand. For th

esses were prog

vailable at Mic

This program wa

the successive

diate outputs

reduction. Th

were then pres

Least

While t

electrical ar

1956; Stacey

completely d

primary goal

of investiga

the dielect

The K

rock are di

1.5) in the

directiona

indication

Thus, the original data must pass through three successive reduction processes before the desired information is obtained. The last two reduction processes, at least, would be very tedious and error prone if done by hand. For this reason, all of the reduction processes were programmed for the CDC 3600 digital computer available at Michigan State University (see Appendix B). This program was written so that the results of each of the successive reduction processes were output. The intermediate outputs allowed the data to be monitored during reduction. The tensor principal directions and values were then presented in graphical and tabulated form.

Least-Square Determination of Symmetric Second-Rank Tensor Coefficients

While there have been previous investigations of electrical anisotropy of rocks (cf., Rao, 1948; Parasnis, 1956; Stacey, 1961), none of these were concerned with completely defining the tensor properties. One of the primary goals of the present study is to develop a method of investigation which will allow complete definition of the dielectric constant and conductivity tensors in rocks.

The K and σ values obtained from a single disk of rock are directional values of the tensor (after equation 3.5) in the direction normal to the parallel disk faces. Directional measurements in several directions give an indication of anisotropy but do not, by themselves, define

ne tensor. The

e used to obtai

Consider f

$\{q_i\}_{i=1}^{q}$ unknown

efficients, {b

n experiment is

xperimental err

alue of a.

Now, if o

et up to measu

, this will re

nowns. It is

o determine t

least square

hosen such th

s minimized,

$$E = \sum_{i=1}^{p}$$

here B = (b

olumn vecto

uperscript,

Equati

inimized.

problem woul

the tensor. These directional measurements can, however, be used to obtain a set of least square tensor coefficients.

Consider first, the general problem where there are $\{z_i\}_{i=1}^{q}$ unknown quantities which, when multiplied by the coefficients, $\{b_i\}_{i=1}^{q}$, give the quantity, $a = \sum_{i=1}^{q} b_i z_i$. If an experiment is set up to measure a, there will be an experimental error, $\delta = a - m$, where m is the measured value of a.

Now, if other experiments, p in number ($p > q$), are set up to measure a, each with a different set of b_i and m, this will result in a system of p equations and q unknowns. It is desired to use this system of equations to determine the best set of values for the z_i. If $p > q$, a least square procedure can be used, i.e., the z_i are chosen such that the sum of the squares of the errors, E, is minimized, where:

$$E = \sum_{i=1}^{p} \delta_i^2 = \sum_{i=1}^{p} \left[\sum_{j=1}^{q} b_{ij} z_j - m_i \right]^2 = (BZ - M)^T (BZ - M), \qquad 6.1$$

where $B = (b_{ij})$ is a p X q matrix, $Z = (z_j)$ is a q X 1 column vector, $M = (m_i)$ is a p X 1 column vector and the superscript, T, indicates matrix transpose.

Equation 6.1 is positive definite, and will now be minimized. The classical approach to the least square problem would be to differentiate equation 6.1 with

spect to each

ations equal

unknowns which

es just such a

qual to zero d

deed give a m

inimum, or infl

eed have a mini

econd derivati

ubstitute in t

ifferentiation

econd derivati

xtremum is a

rocedure is,

or it does no

oints. Thus,

minimize e

The mat

he p X p ide

$I = (I - B(B^T$

both sides of

$M = (I$

or a shortha

$G = (I$

$H = (B^T$

respect to each of the z_j and set each of the resulting equations equal to zero. This would give q equations and q unknowns which are then solved for the z_j. Nye (1964) uses just such a procedure. Setting the first derivatives equal to zero does not insure that the z_j so determined do indeed give a minimum, but only an extremum (maximum, minimum, or inflection point). To insure that we do indeed have a minimum using this approach, we must take the second derivative of E with respect to each of the z_j and substitute in the values of the z_j determined by the first differentiation to test for the type of extremum. If the second derivative is positive at an extremum point, the extremum is a minimum (Sherwood and Taylor, 1957). This procedure is, at best, tedious and, at worst, tenuous, for it does not protect against local minima and saddle points. Thus, matrix operations will be used exclusively to minimize equation 6.1.

The matrix, $B(B^TB)^{-1}B^T$, is a p X p matrix. Thus, the p X p identity matrix, I, can be written as: $I = (I - B(B^TB)^{-1}B^T) + B(B^TB)^{-1}B^T$. Post multiplying both sides of this equation by M yields:

$$M = (I - B(B^TB)^{-1}B^T)M + B(B^TB)^{-1}B^TM.$$

For a shorthand notation, define:

$$G = (I - B(B^TB)^{-1}B^T)M, \qquad 6.2$$

$$H = (B^TB)^{-1}B^TM.$$

Then:

$$M = G + B$$

and equation 6.

$$E = (BZ -$$

$$= (BZ -$$

but:

$$B^T G = B^T$$

Thus, equation

$$E = (BZ$$

which will be

the right han

definite and

the R.H.S. of

mized only if

$$Z = H$$

Then E become

$$E = G^T$$

Then:

$$M = G + BH$$

and equation 6.1 can be written as:

$$E = (BZ - BH - G)^T (BZ - BH - G)$$

$$= (BZ - BH)^T (BZ - BH) + G^TG + 2(Z - H)^TB^TG. \qquad 6.3$$

But:

$$B^TG = B^T(I - B(B^TB)^{-1}B^T)M = (B^T - B^T)M = 0.$$

Thus, equation 6.3 becomes:

$$E = (BZ - BH)^T(BZ - BH) + G^TG, \qquad 6.4$$

which will be minimized by varying Z. The first term on the right hand side (R.H.S.) of equation 4.6 is positive definite and therefore non-negative. The second term on the R.H.S. of 6.4 is independent of Z. Thus, E is minimized only if Z is chosen such that:

$$Z = H = (B^TB)^{-1}B^TM. \qquad 6.5$$

Then E becomes the least square error and is given by:

$$E = G^TG = ((I - B(B^TB)^{-1}B^T)M)^T((I - B(B^TB)^{-1}B^T)M). \qquad 6.6$$

Now that t

ltiple indepen

pecific case of

n be considere

termination of

s equation 3.5.

alue is assumed

re than six T

e above least

e measured va

$$b_{i1} = \hat{2}_i$$

$$b_{i2} = \hat{1}$$

$$b_{i3} =$$

here the re

ate summat

least squar

espective

1968) is o

$$s^2 =$$

and the r

$$s$$

Now that the generalized least square problem for multiple independent variables has been solved, the specific case of the symmetric second-rank tensor model can be considered. The model used for the least square determination of symmetric second-rank tensor coefficients is equation 3.5. For this model, the directional tensor value is assumed to be measured parallel to $\hat{l}$. Thus, if more than six $T_{||\hat{l}}$ were measured for different $\hat{l}$, then the above least square procedure would be used, with m_i, the measured value to $T_{||\hat{l}i}$ and:

$$b_{i1} = \hat{l}^2_{i1}, \quad b_{i4} = 2\hat{l}_{i2}\hat{l}_{i3}, \quad z_1 = T_{11}, \quad z_4 = T_{23},$$

$$b_{i2} = \hat{l}^2_{i2}, \quad b_{i5} = 2\hat{l}_{i3}\hat{l}_{i1}, \quad z_2 = T_{22}, \quad z_5 = T_{31}, \qquad 6.7$$

$$b_{i3} = \hat{l}^2_{i3}, \quad b_{i6} = 2\hat{l}_{i1}\hat{l}_{i2}, \quad z_3 = T_{33}, \quad z_6 = T_{12},$$

where the repeated subscripts in equations 6.7 do not indicate summation. The least square tensor coefficients and least square error are then given by equations 6.5 and 6.6, respectively. The mean square error (Jenkins and Watts, 1968) is obtained from equation 6.6 by:

$$s^2 = \frac{E}{p + 2 - q} = \frac{E}{p - 4}, \qquad 6.8$$

and the root mean square (rms) error by:

$$s = \sqrt{s^2}. \qquad 6.9$$

The rms er

rror. Physical

irectional valu

sing the least

ms error can be

principal tenso

he least squar

1.5.

The deri

given above is

sults of this

y Nye (1964)

above develop

classical dev

surround tha

The le

estimation t

model possil

qualitative

It uses the

the analysi

estimation

To b

of rocks,

The rms error was chosen as the tensor determination error. Physically, it represents the probable error in a directional value of T given by equations 3.4 and 3.5, using the least square tensor coefficients. Thus, the rms error can be used as an uncertainty factor for the principal tensor values, for they will be determined from the least square tensor coefficients by equations 3.4 and 3.5.

The derivation of the least square tensor coefficients given above is somewhat academic. This is because the results of this development are the same as those obtained by Nye (1964) using the classical approach. However, the above development serves to confirm the results of the classical development with none of the uncertainties which surround that approach.

The least square procedure developed above uses estimation theory. The model of equation 3.5 is the only model possible for a symmetric second-rank tensor. The qualitative electric model developed for rocks in Chapter IV uses the symmetric second-rank K and σ tensors. Thus, the analysis of the laboratory data should consist of the estimation of the parameters of equation 3.5.

Principal Coefficients and Directions for a Generalized Symmetric Second-Rank Tensor

To be able to compare the electrical anisotropies of rocks, it is necessary to determine the orientations

nd values of th

second-rank K ar

ng the eigenval

ermation matri

rank tensor, th

1965) is a cubi

olve on a rou

tive procedure

equation. Thi

basis are out

Conside

$$u_i = T$$

where $\underline{v} = v$

is relative

vector is $\underline{u}$

surface for

$$T_{11}x$$

Figure 6.1

surface fo

e in Figu

where r i

Equation

$f(x_1, x_2,$

and values of the principal coefficients of the symmetric second-rank K and σ tensors. This is equivalent to finding the eigenvalues and eigenvectors of the 3 x 3 representation matrix. For a generalized symmetric second-rank tensor, the characteristic equation (Marcus and Minc, 1965) is a cubic equation, which is rather difficult to solve on a routine basis. Nye (1964) suggests an iterative procedure as an alternative to solving the cubic equation. This iterative procedure and its theoretical basis are outlined below.

Consider the tensor relationship:

$$u_i = T_{ij}v_j, \qquad 6.10$$

where $\underline{v} = v(l_1, l_2, l_3)$ is the independent vector and T is relative to its principal axes. Then, the dependent vector is $\underline{u} = v(T_{11}l_1, T_{22}l_2, T_{33}l_3)$ and the representation surface for T is:

$$T_{11}x_1^2 + T_{22}x_2^2 + T_{33}x_3^3 = 1. \qquad 6.11$$

Figure 6.1 shows a cross-section of the representation surface for T containing both $\underline{u}$ and $\underline{v}$. If the vector, $\underline{p}$, in Figure 6.1 is parallel to $\underline{v}$, then: $\underline{p} = r(l_1, l_2, l_3)$, where r is representation surface radius at the point, p. Equation 6.11 is of the form for an isotimic surface, $f(x_1, x_2, x_3) = C$, where C is a constant (Davis, 1961).

Fig. 6.1.
surface in the

he (unit) norr

rl_1, rl_2, rl

$$\hat{n} = \frac{\nabla f}{\|\nabla f}$$

which is paral

is more near

cross sectiona

Now, cor

second-rank te

information fr

can now be use

maximum princ

axis of the e

approximation

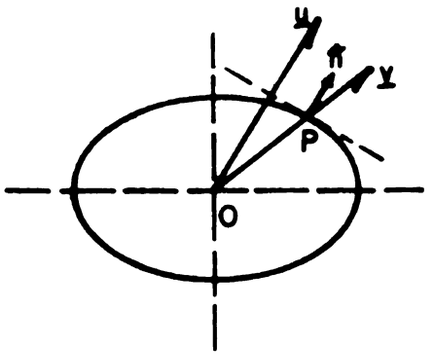

Fig. 6.1.--Cross-section through the T reference surface in the plane containing both $\underline{u}$ and $\underline{v}$.

The (unit) normal to such a surface at the point, $P(rl_1, rl_2, rl_3)$ is given by:

$$\hat{n} = \frac{\nabla f(P)}{||\nabla f(P)||} = \frac{(T_{11}l_1, T_{22}l_2, T_{33}l_3)}{\sqrt{(T_{11}l_1)^2 + (T_{22}l_2)^2 + (T_{33}l_3)^2}} \quad 6.12$$

which is parallel to $\underline{u}$. As can be seen in Figure 6.1, $\underline{u}$ is more nearly parallel to the minor semi-axis of the cross sectional ellipse than $\underline{v}$.

Now, consider the case of a generalized symmetric second-rank tensor, T_{ij} ($T_{ij} \neq 0$, for all i, j). The information from Figure 6.1 and equations 6.10 and 6.12 can now be used in an iterative sense to determine the maximum principal direction of the tensor (minimum semi-axis of the ellipsoid). The iterative, or successive approximation procedure is as follows:

i. Take a

and pr

matri

whose

minor

maxim

if $\hat{l}_1$

$\underline{\omega}_1$ wi

ii. Norma

paral

with each succe

the orientation

semi-axis of th

direction) thar

successive $\hat{l}_{i'}$

zero. Because

the iteration

the decreasing

This study was

the maximum pr

of the ellips

the maximum p

inserting $\hat{l}_{mx}$

$$T_{mx} = \frac{}{}$$

i. Take an arbitrary unit column vector, $\hat{l}_1$, and pre-multiply it by the representation matrix for T to obtain a new vector, $\underline{\omega}_1$, whose orientation is closer to that of the minor semi-axis of the ellipsoid (i.e., maximum principal axis of the tensor), e.g., if $\hat{l}_1$ is parallel to $\underline{v}$ in Figure 6.1, then $\underline{\omega}_1$ will be parallel to $\underline{u}$.

ii. Normalize $\underline{\omega}_1$ to obtain a new unit vector, $\hat{l}_2$, parallel to $\underline{\omega}_1$ and repeat step i.

With each successive application of the above procedure, the orientation of $\underline{\omega}_i$ is closer to that of the minor semi-axis of the ellipsoid (maximum principal tensor direction) than was the case for $\underline{\omega}_{i-1}$. Also, with each successive $\hat{l}_i$, the vector, $\underline{dl}_i = \hat{l}_i - \hat{l}_{i-1}$, approaches zero. Because of this, an appropriate cutoff point for the iteration procedure can be chosen on the basis of the decreasing magnitude of $\underline{d\hat{l}}_i$. The cutoff used for this study was $\frac{\sqrt{\sum_{i=1}^{3} T_{ii}^2}}{10^9}$. The last $\hat{l}_i$ is then taken as the maximum principal tensor direction (minor semi-axis of the ellipsoid), $\hat{l}_{mx}$. Once $\hat{l}_{mx}$ has been determined, the maximum principal tensor value is determined by inserting $\hat{l}_{mx}$ and T into equation 3.4, i.e.:

$$T_{mx} = \hat{l}_{mx}^T \; T \; \hat{l}_{mx}. \qquad 6.13$$

To find the

$_m$, the above it

atrix inverse of

inimum principal

ix T (not T^{-1}) i

The interme

is obtained by ta

ed normalizing

is then found

.4 (6.13).

To find the minimum principal tensor direction, $\hat{l}_{mn}$, the above iterative procedure is applied to the matrix inverse of the representation matrix for T. The minimum principal value of T is found by inserting $\hat{l}_{mn}$ and T (<u>not</u> T^{-1}) into equation 3.4 (6.13).

The intermediate principal tensor direction, $\hat{l}_{int}$, is obtained by taking the vector cross product, $\hat{l}_{mx} \times \hat{l}_{mn}$, and normalizing it. The intermediate principal value of T is then found by inserting $\hat{l}_{int}$ and T into equation 3.4 (6.13).

SAMPLE

Most of the
rtion of this st
e Precambrian o
ited for a deta
egional geology
1957; Van Hise ar
1959; Boyum, 196
accessible to ro
area, there is a
amorphic zone
1965). Also, pr
been carried out
Whitaker, 1966)
physics studies
selection in th

Figure 7.
showing the san
broken line in
Animike contac
Marquette sync

CHAPTER VII

SAMPLE LOCATIONS AND DESCRIPTIONS

Most of the samples considered in the laboratory portion of this study were collected by the author from the Precambrian of Northern Michigan. This area is well suited for a detailed petrophysics investigation. The regional geology is quite well known (Van Hise and Bayley, 1897; Van Hise and Lieth, 1911; Martin, 1937; Bayley, 1959; Boyum, 1963). Outcrops are abundant and easily accessible to roads. Within a rather small geographic area, there is a wide variety of rock types in several metamorphic zones (James, 1955; Henrickson, 1956; Willar, 1965). Also, previous petrophysics investigations have been carried out on rocks from this area (Merritt, 1963; Whitaker, 1966). The results of these previous petrophysics studies were used as a guide for rock type selection in the present study.

Figure 7.1 is a map of a portion of Northern Michigan showing the sample collection sites for this study. The broken line in Figure 7.1 indicates the Pre-Animikie-Animike contact (after Martin, 1937; Boyum, 1963). The Marquette synclinorium is the major structural feature


U.S.-41
M-11
M-6
MICHIGAMME
M-10
SUPERIOR
MARQUETTE
M-2

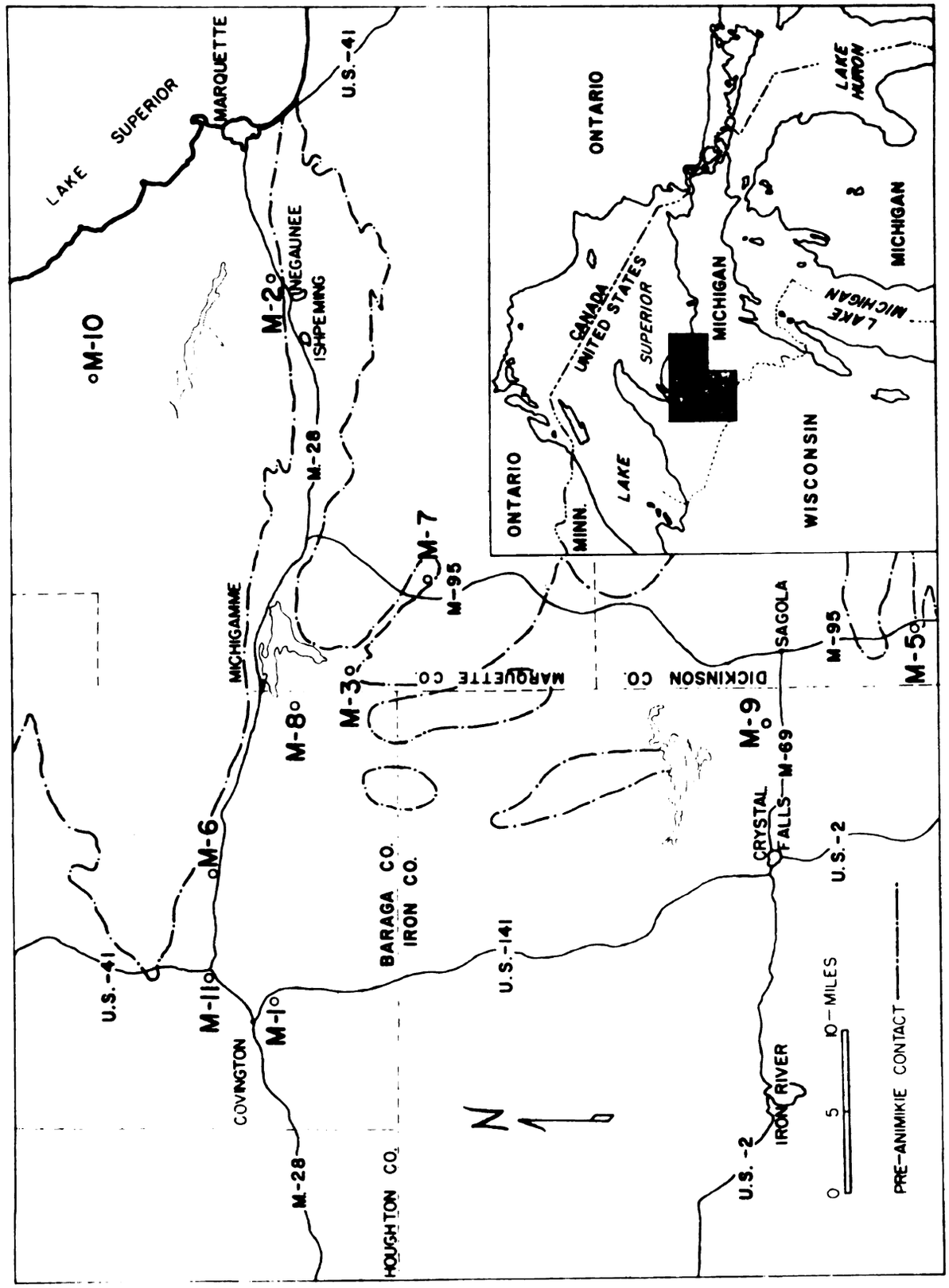

Fig. 7.1.--Northern Michigan sample location map.

f the area, extend

st axis from a po

f Marquette. The

kinikie Series me

kinikie meta-igne

s nderlain by a

gneisses, meta-vo

Keweenawan sedime

nd Paleozoic sec

rea.

Sample M-

ide of U.S. 14

Baraga County,

ame formatio

ones of James

onsists of a

sh-graywacke

ormal to the

Sample

orth side o

nd about o

Michigan.

schist (po

collectio

and Henri

chlorite

of the area, extending roughly forty miles along an east-west axis from a point on the Lake Superior shore south of Marquette. The rocks filling the basin consist of Animikie Series meta-sediments, meta-volcanics, and post Animikie meta-igneous rocks of Keweenawan age. The basin is underlain by a Pre-Animikie complex of granites, gneisses, meta-volcanics, schists and minor quartzites. Keweenawan sediments and volcanics outcrop to the west and Paleozoic sediments to the east of the sample collection area.

Sample M-1 was collected from a road cut on the east side of U.S. 141, about one mile south of Covington in Baraga County, Michigan. This sample is from the Michigamme formation and the site is located in the biotite zones of James (1955) and Henrickson (1956). The sample consists of a light gray, fine grained, meta-argillite to sub-graywacke. Slaty cleavage (C in Figure 8.1) is sub-normal to the [001] (z) laboratory direction.

Sample M-2 was collected from a road cut on the north side of U.S. 41-M. 28, just west of the Carp River and about one mile east of Negaunee in Marquette County, Michigan. This sample is from a Pre-Animikie greenstone schist (possibly Mona) containing pillow structures. The collection site is in the chlorite zones of James (1955) and Henrickson (1956). The sample is a fine grained, chlorite schist with calcite in veins. Epidote and some

gnite are also pr

s sub-normal to

ock cleavage (C

ntersect forming

[110].

Sample M-3

side of county r

section 10, T47

ample is from

olite. The sa

of James (1955)

staurolite-qua

facies. The s

dark green amp

chlorite or e

labeled F in

Sample

ct on count

section 10,

ample is a

two feldsp

is located

gneissic

Sam

north si

Saraga C

pyrite are also present. The foliation (f in Figure 8.2) is sub-normal to the [100] (x) laboratory direction. The rock cleavage (C in 8.2) is sub-normal to [001]. These intersect forming a lineation (L in 8.2) sub-parallel to [010].

Sample M-3 was collected from an outcrop on the east side of county road 607 near the west section line of section 10, T47N, R30W in Marquette County, Michigan. This sample is from a medium grained, dark greenish-black amphibolite. The sample site is located in the sillimanite zones of James (1955) and Henrickson (1956) and Villar's (1965) staurolite-quartz sub-facies of the almandine amphibolite facies. The sample consists primarily of medium grained dark green amphiboles (probably hornblende) with some chlorite or epidote and pyrite. There is a fracture set labeled F in Figure 8.3.

Sample M-5 was collected from the rubble of a road cut on county road 607 near the north section line of section 10, T41N, R30W in Dickinson County, Michigan. The sample is a granite-tourmaline gneiss, containing quartz, two feldspars, tourmaline, and mica. The collection site is located in the chlorite zone of James (1955). The gneissic banding is labeled B in Figure 8.5.

Sample M-6 was collected from a road cut on the north side of U.S. 41-M.28, just west of Tioga Creek in Baraga County, Michigan. This sample is from the

Michigamme Formation and the site is located in the biotite zones of James (1955) and Henrickson (1956). The sample is a light gray sub-graywacke with slaty cleavage (C in Figure 8.6) sub-normal to the [001] laboratory direction.

Sample M-7 was collected in the pit of the Republic Mine, Marquette County, Michigan. This sample is from the Negaunee formation and the site is located in the silliminate zones of James (1955) and Henrickson (1956) and Villar's (1965) staurolite-quartz sub-facies of the almandine amphibolite facies. The mineralogy of sample M-7 is given in Table 7.1. A microscopic petrofabric

TABLE 7.1.--Mineralogy of M-7.

Mineral	% Volume
Quartz	63.6
Hornblende	12.5
Epidote	8.6
Augite	6.3
Grunerite (?)	4.3
Hemitite and other	1.9
Total	100.0

analysis of quartz c-axes based on 400 grains in two thin sections is presented in Figure 7.2. The > 5 per cent maximum indicates a strong lineation (L in Figure 8.7) in

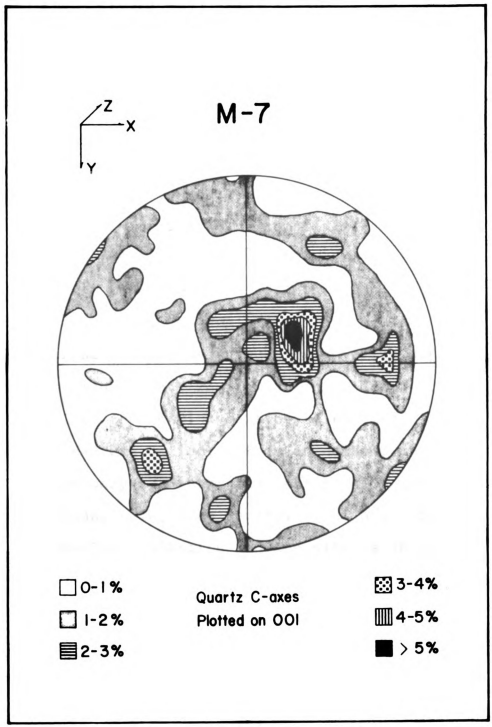

Fig. 7.2.--Microscopic petrofabric analysis of M-7.

is direction.

ircle (G in Fig

indicate a symme

there are faint

labeled B in Fi

Sample M-

est side of a

n Baraga Coun

gneiss formatio

Jones (1955) a

brown muscovi

staurolite cr

are shown in

is sub-normal

Sample

side of a se

section 27,

is from the

ite zone of

Bayley (195

grayish-gre

crystals ar

rocks at th

or washed

labeled F l

form linea

this direction. There also appears to be a petrofabric girdle (G in Figure 8.7) sub-normal to [110] which may indicate a symmetry plane in the rock. In addition, there are faint alternating quartz and epidote rich bands labeled B in Figure 8.7.

Sample M-8 was collected from an outcrop on the east side of a secondary road in section 36, T48N, R31W in Baraga County, Michigan. The sample is from the Michigamme formation and the site is in the staurolite zones of James (1955) and Henrickson (1956). The sample is a medium brown muscovite-staurolite schist with large euhedral staurolite crystals. These euhedral staurolite crystals are shown in Figure 7.3. The foliation (f in Figure 8.8) is sub-normal to the [010] laboratory direction.

Sample M-9 was collected from an outcrop on the west side of a secondary road near the east section line of section 27, T43N, R31W, Iron County, Michigan. This sample is from the Hemlock formation and the site is in the chlorite zone of James (1955) and the green schist facies of Bayley (1959). The sample consists of a fine grained grayish-green matrix containing many small feldspar crystals and some possible epidote and chlorite. The rocks at this collection site all had an over-all leached, or washed out, appearance. There are three fracture sets, labeled F_1, F_2, and F_3 in Figure 8.9. Their intersections form lineations, labeled L_1, L_2, and L_3 in Figure 8.9.

Fig. 7.3.--Euhedral staurolite crystals in M-8.

Sample M-10 was collected from the road bed of a logging trail near the north section line of section 5, T49N, R27W, Marquette County, Michigan. The sample is a dark green amphibole schist containing quartz, hornblende or actinolite, two feldspars, chlorite, and epidote, with calcite in veins. The collection site is in the chlorite zone of James (1955). The foliation (f in Figure 8.10) is sub-normal to [001] and the lineation of the amphibole crystals (L in Figure 8.10) is sub-parallel to [010].

Sample M-11 was collected from a road cut on the west side of U.S. 141-M. 28, about 0.3 miles south of their intersection with U.S. 41 in Baraga County, Michigan.

This sample is from the Michigamme formation and the site is in the biotite zones of James (1955) and Henrickson (1956). The sample is a massive, light-gray, sub-graywacke to siltstone. There is a fracture set marked F in Figure 8.11.

Sample B-4 was the only sample investigated in this study which was not collected from Northern Michigan. It was collected by the author from the Cardiff complex, Cardiff Township, Ontario (Hewit, 1959; Stonehouse, 1967). The collection site was at stop number eight on the 1967 Institute on Lake Superior Geology, Cardiff Complex field trip (Stonehouse, 1967). The sample is a syenite gneiss, containing two feldspars, some quartz, agerine-augite, micas, and opaques. The gneissic banding (B in Figure 8.4) is sub-normal to the [010] laboratory direction and there is a slight lineation (L in 8.4) due to the apparent alignment of the agerine-augite crystals sub-parallel to [100].

CHAPTER VIII

DISCUSSION AND INTERPRETATION OF THE LABORATORY MEASUREMENTS

Presentation of the Data

The electrical measurement data for each sample investigated in the laboratory portion of this study are presented in Tables 8.2 through 8.13 and Figures 8.1 through 8.12. The tabulated data consists of the K and (effective) conductivity, σ, principal values, rms errors and direction angles for the tensor principal axes. This data is given for each measured signal frequency for each of the rock samples considered in this study. The signal frequency, principal value, and rms error presentation is self explanatory. The presentation of the direction angles for the tensor principal axes is demonstrated by Table 8.1.

TABLE 8.1.--Direction angles for tensor principal axes.

α_{11}	α_{21}	α_{31}
α_{12}	α_{22}	α_{32}
α_{13}	α_{23}	α_{33}

TABLE 8.2.--M-1 (meta-argillite) electrical anisotropy data.

f (cps)	K Principal Values	F rms Error	K Principal Axes Direction Angles (°)			σ Principal Values $x10^9$ (mho/m)	σ rms Error $x10^9$ (mho/m)	σ Principal Axes Direction Angles (°)		
	6.480		137.4	58.8	64.2	1430.8		115.5	154.2	86.3
100,000	6.376	0.227	99.0	60.2	148.6	1008.9	174.0	154.2	64.3	87.9
	6.281		48.8	45.9	73.4	653.1		86.5	87.5	4.2
	6.741		146.5	86.7	123.2	588.2		114.4	155.0	84.9
30,000	6.436	0.196	123.4	91.3	33.4	461.0	62.0	155.6	65.6	90.6
	6.332		88.0	3.5	87.1	299.1		88.4	85.1	5.1
	6.967		137.8	77.4	129.4	239.5		114.0	154.7	82.6
10,000	6.645	0.240	130.8	90.9	40.8	193.4	29.6	115.9	66.1	92.6
	6.552		81.1	12.6	81.1	127.4		89.3	82.2	7.8
	7.342		135.4	45.5	87.8	94.42		74.0	162.3	82.6
3,000	6.868	0.285	134.1	135.4	84.8	73.13	9.16	16.0	74.3	92.7
	6.833		84.9	87.8	5.6	50.00		89.4	82.2	7.8
	7.754		131.2	41.3	92.1	37.24		79.6	168.9	86.2
1,000	7.222	0.315	138.1	130.1	80.0	28.61	3.50	10.5	79.7	92.0
	7.017		83.8	81.9	10.2	19.28		88.7	86.0	4.2
	8.261		125.1	144.6	85.6	14.860		84.6	8.0	96.0
300	7.657	0.372	144.8	54.8	90.3	11.404	1.595	6.7	95.7	93.4
	7.345		87.8	86.2	4.3	7.000		86.0	84.4	6.9
	8.629		121.3	148.4	86.2	8.020		89.6	172.4	82.4
150	7.974	0.410	148.6	58.6	90.5	6.082	0.889	2.3	90.0	92.3
	7.533		88.5	86.5	3.8	3.312		87.7	82.4	8.0
	8.862		118.6	151.1	85.9	5.675		88.0	2.5	91.5
100	8.173	0.430	151.4	61.4	91.4	4.485	0.561	4.0	92.1	93.3
	7.654		89.2	85.7	4.3	2.493		86.6	88.6	3.7
	9.168		117.1	152.8	87.7	3.775		92.2	3.8	93.0
60	8.422	0.459	152.9	62.9	90.2	2.954	0.406	4.6	88.0	94.1
	7.798		89.1	87.8	2.3	1.627		86.0	86.8	5.1
	9.465		66.1	155.9	86.8	2.2012		94.4	175.4	88.7
30	8.844	0.518	23.9	66.2	91.7	1.7899	0.2736	6.0	94.5	94.0
	8.021		89.7	86.4	3.6	0.9569		85.9	89.0	4.2

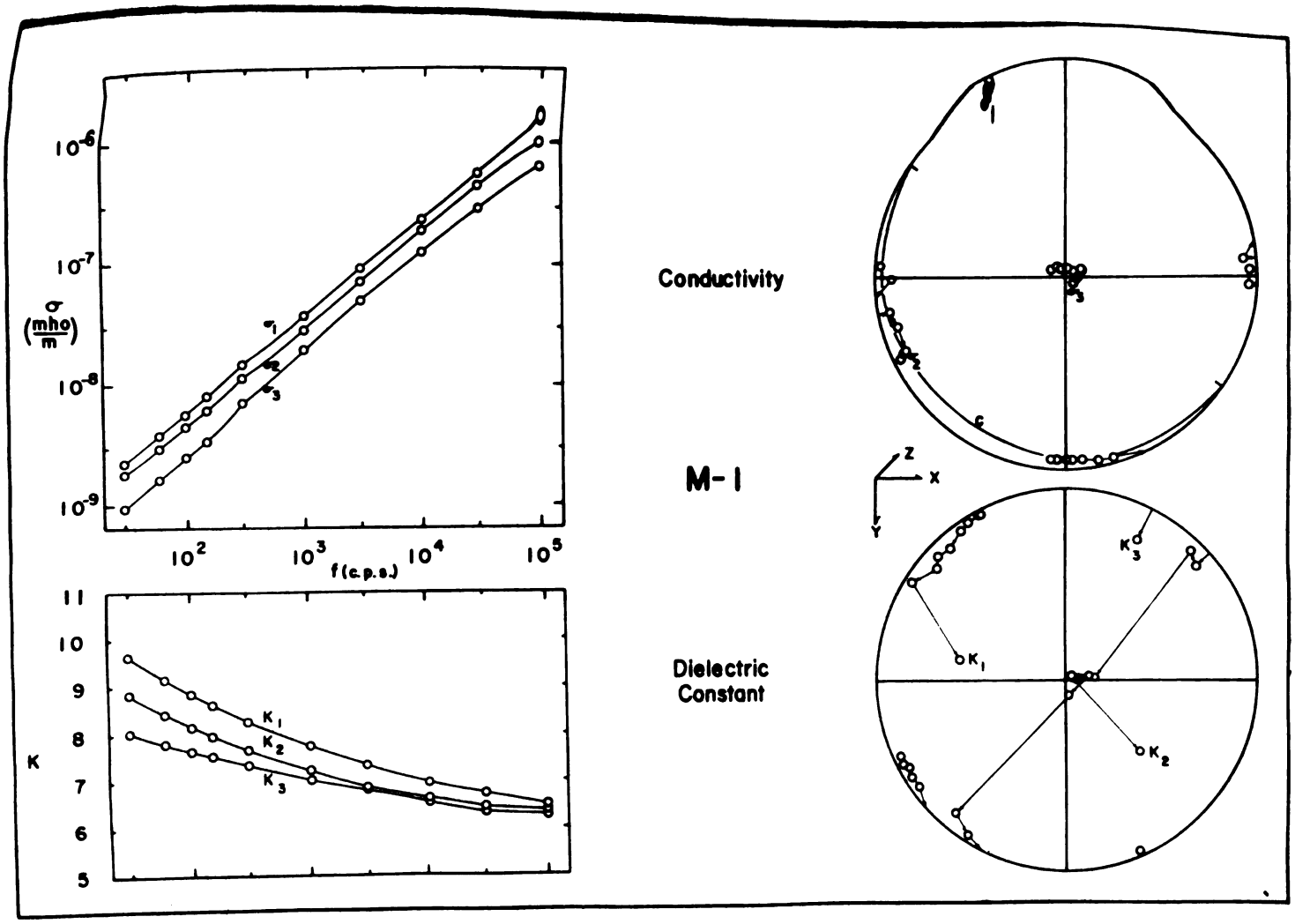

Fig. 8.1.--M-1 (meta-argillite) electrical anisotropy data.

TABLE 8.3 . ——M-2 (greenstone) electrical anisotropy data.

f (cps)	K Principal Values	K rms Error	K Principal Axes Direction Angles (°)			σ Principal Values $x10^8$ (mho/m)	σ rms Error $x10^8$ (mho/m)	σ Principal Axes Direction Angles (°)		
	10.776		109.4	119.2	36.1	1064.8		99.8	76.7	163.4
100,000	8.866	0.196	160.5	78.5	105.5	490.6	29.0	166.5	83.2	78.4
	8.126		88.2	31.8	58.3	378.0		80.8	15.0	78.3
	12.316		107.0	133.6	48.5	389.6		94.0	90.0	4.0
30,000	9.542	0.276	162.4	74.5	98.2	158.8	17.2	174.4	86.1	94.0
	9.040		85.4	47.7	42.7	148.2		86.1	3.9	89.7
	14.015		102.1	138.8	51.4	148.61		94.7	69.6	159.0
10,000	10.301	0.313	167.3	78.2	94.7	57.86	4.30	172.2	85.8	83.4
	9.754		86.2	51.2	39.0	52.72		83.8	20.9	70.1
	16.15		99.8	130.0	41.7	58.88		97.7	78.9	166.4
3,000	11.10	0.32	169.4	80.6	94.8	23.86	0.73	169.7	84.8	81.1
	10.54		86.0	41.6	48.7	18.11		83.2	12.3	79.8
	18.71		99.2	119.4	31.1	27.299		99.4	80.2	166.4
1,000	12.14	0.37	169.7	81.4	95.6	10.442	0.782	167.2	83.0	79.3
	11.42		85.6	30.9	59.5	8.266		81.4	12.0	81.6
	22.48		98.9	96.0	10.8	13.482		103.1	75.7	160.4
300	13.49	0.40	169.3	83.1	98.2	5.703	0.478	163.7	83.8	75.0
	12.79		84.1	9.1	83.1	3.734		80.5	15.6	77.7
	25.68		99.5	85.0	169.2	9.224		103.6	72.1	157.2
150	14.76	0.42	168.5	84.4	80.0	3.780	0.453	161.9	82.9	73.5
	13.84		83.6	7.5	86.0	2.121		78.4	19.3	74.8
	28.18		99.5	89.6	9.5	7.664		105.0	74.1	157.9
100	15.77	0.49	168.2	83.1	99.5	3.078	0.450	160.6	82.3	72.4
	14.60		83.2	6.9	89.2	1.574		78.0	17.7	77.1
	32.07		99.0	92.5	9.3	6.106		104.1	72.0	156.8
60	17.21	0.56	168.3	82.1	98.6	2.382	0.370	160.7	81.8	72.6
	16.00		82.6	8.3	86.3	1.297		77.1	19.8	75.2
	38.29		99.6	79.1	165.4	4.6528		104.7	68.3	153.4
30	20.16	0.59	167.3	83.7	79.0	1.8300	0.2757	159.4	82.0	71.1
	18.23		81.9	12.6	80.4	0.8812		75.9	23.2	71.9

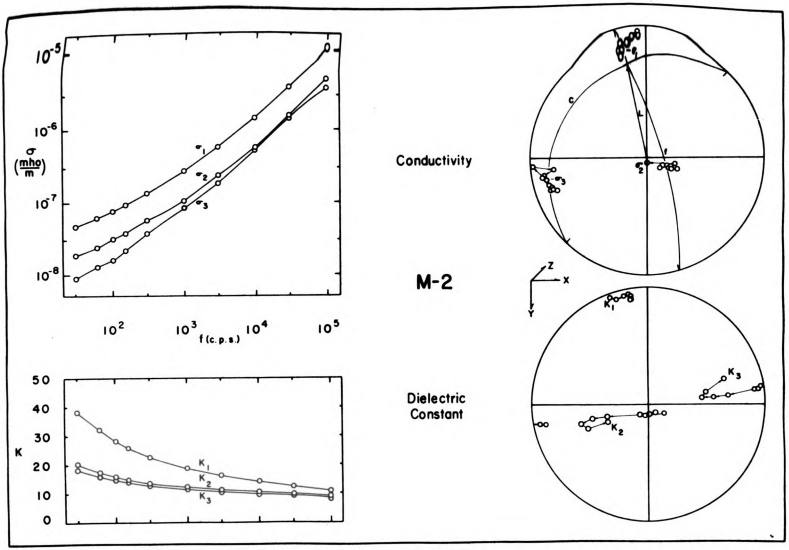

Fig. 8.2.--M-2 (greenstone) electrical anisotropy data.

TABLE 8.4 . ——M-3 (amphibolite) electrical anisotropy data.

f (cps)	K Principal Values	K rms Error	K Principal Axes Direction Angles (°)			σ Principal Values x10^9 (mho/m)	σ rms Error x10^9 (mho/m)	σ Principal Axes Direction Angles (°)		
	10.290		20.8	108.5	80.9	2193.9		24.8	114.2	95.2
30,000	9.276	0.802	99.4	89.3	9.4	1110.8	623.3	94.6	112.5	23.0
	8.416		71.6	18.5	87.7	395.0		65.7	34.1	67.6
	11.220		23.2	112.3	84.2	769.5		26.4	115.8	95.0
10,000	9.689	1.035	99.2	97.2	11.7	381.2	210.3	95.5	112.6	23.4
	8.857		68.9	23.6	79.9	130.8		64.3	35.5	67.2
	12.310		24.9	114.7	87.1	257.84		27.2	116.8	94.4
3,000	10.235	1.312	98.2	101.0	13.8	126.39	68.36	96.2	111.6	22.6
	9.066		66.6	27.4	76.5	47.44		63.6	35.6	67.9
	13.462		25.3	115.3	88.7	94.64		28.6	118.4	93.4
1,000	10.761	1.629	97.8	103.7	15.8	45.09	24.44	97.4	110.7	22.1
	9.290		66.1	29.2	74.2	19.05		62.5	36.3	68.2
	14.775		26.2	116.2	99.6	34.952		29.7	119.5	92.9
300	11.386	1.972	97.6	104.8	16.7	16.982	8.333	97.9	109.7	21.4
	9.556		65.1	30.6	73.3	9.147		61.6	36.7	68.8
	15.725		26.6	116.6	90.2	18.618		30.0	119.9	91.4
150	11.813	2.211	97.4	105.3	17.0	9.201	4.404	98.4	107.3	19.3
	9.761		64.5	31.3	73.0	5.303		61.4	35.5	70.7
	16.237		26.9	116.9	90.0	13.344		30.4	120.4	90.9
100	12.088	2.337	97.8	105.5	17.5	6.465	3.095	98.8	106.7	19.0
	9.912		64.4	31.7	72.5	4.006		61.1	35.6	71.0
	17.03		27.0	117.0	89.9	8.929		31.7	121.7	90.0
60	12.44	2.51	97.7	105.1	17.0	4.207	2.040	98.6	104.2	16.7
	10.10		64.3	31.5	73.0	2.931		59.8	35.4	73.2
	18.18		27.5	117.5	90.7	5.232		32.7	122.6	87.6
30	13.04	2.78	98.0	107.0	18.8	2.645	1.216	100.0	101.3	15.2
	10.35		63.9	33.1	71.2	1.923		59.2	35.0	75.0

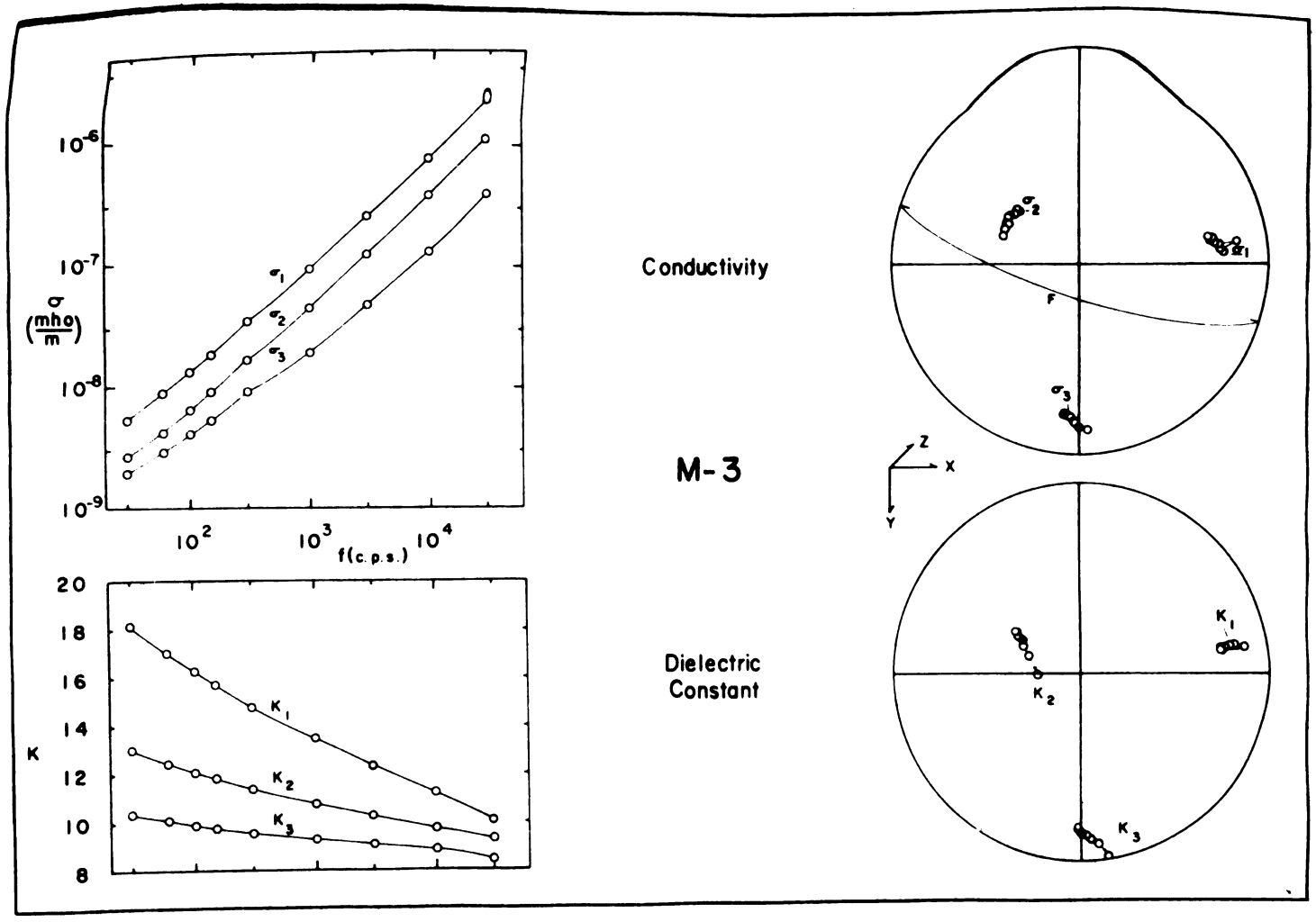

Fig. 8.3.--M-3 (amphibolite) electrical anisotropy data.

TABLE 8.5.--B-4 (syenite gneiss) electrical anisotropy data.

f (cps)	K Principal Values	K rms Error	K Principal Axes Direction Angles (°)			σ Principal Values $x10^9$ (mho/m)	σ rms Error $x10^9$ (mho/m)	σ Principal Axes Direction Angles (°)		
	7.516		148.6	62.9	104.8	591.8		143.4	77.9	56.1
30,000	7.417	0.159	73.0	89.4	163.0	350.9	123.3	65.3	118.1	39.0
	6.761		64.4	27.1	81.8	235.4		64.8	31.0	73.1
	7.842		150.2	65.1	105.4	287.35		148.8	80.6	60.6
10,000	7.524	0.199	72.9	89.8	162.9	162.42	40.12	74.4	132.1	46.3
	6.836		66.3	24.9	82.8	51.78		63.8	43.7	58.0
	8.228		151.6	68.6	107.7	116.88		153.1	84.8	63.7
3,000	7.692	0.256	72.2	93.3	161.9	53.65	20.84	72.7	128.5	43.6
	6.974		68.7	21.6	86.5	16.59		70.1	39.0	58.1
	8.802		151.2	70.4	110.3	55.177		149.6	82.4	60.7
1,000	7.887	0.349	71.0	96.9	159.7	18.668	9.142	72.2	129.4	44.8
	7.075		69.1	20.9	89.8	7.951		66.2	40.4	59.5
	9.755		146.4	66.1	67.8	25.063		148.8	83.8	59.5
300	8.189	0.512	73.4	105.7	23.2	9.222	4.376	71.7	132.2	47.8
	7.184		61.6	29.2	83.6	3.006		65.6	42.9	57.3
	10.322		148.1	70.3	66.0	15.114		148.9	82.2	60.1
150	8.271	0.590	71.6	107.1	25.6	5.292	2.646	73.3	132.6	47.3
	7.372		64.9	26.6	81.8	1.450		64.6	43.6	57.3
	10.732		149.6	73.4	65.3	11.454		149.0	83.0	60.0
100	8.428	0.684	72.0	110.9	28.2	3.817	2.028	73.4	134.1	48.8
	7.387		66.4	27.2	77.3	0.927		64.6	45.0	55.8
	11.357		149.3	74.4	64.2	8.0440		149.0	84.1	59.7
60	8.612	0.778	71.8	113.5	30.4	2.6606	1.476	72.6	134.2	49.4
	7.450		66.1	28.7	75.0	0.5644		65.2	44.8	55.5
	12.427		149.2	75.7	63.3	5.4058		149.1	83.8	59.8
30	8.905	0.966	72.4	117.6	33.6	1.6591	0.9937	73.5	135.8	50.4
	7.566		65.6	31.7	71.1	0.2925		64.6	46.5	54.2

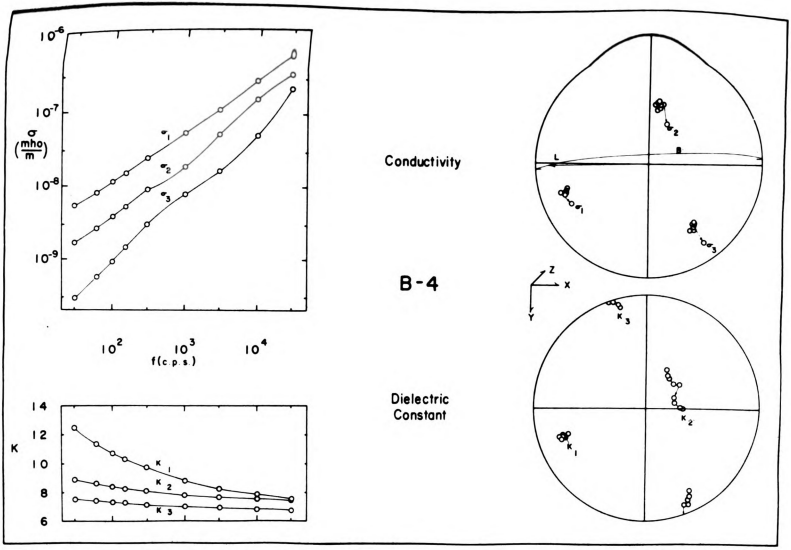

Fig. 8.4.--B-4 (syenite gneiss) electrical anisotropy data.

TABLE 8.6.--M-5 (granite gneiss) electrical anisotropy data.

f (cps)	K Principal Values	K rms Error	K Principal Axes Direction Angles (°)			σ Principal Values $x10^9$ (mho/m)	σ rms Error $x10^9$ (mho/m)	σ Principal Axes Direction Angles (°)		
30,000	6.763	0.053	98.9	28.9	117.2	1135.9	135.3	90.0	168.2	78.2
	6.197		105.1	65.7	29.1	732.4		116.1	79.4	28.4
	5.873		17.6	75.3	80.5	630.7		26.1	84.8	64.5
10,000	7.300	0.145	97.9	26.9	115.6	488.4	66.1	89.9	154.8	64.8
	6.515		107.4	67.8	28.8	327.9		126.1	69.9	42.9
	6.185		19.2	75.5	77.6	255.1		36.1	75.4	57.8
3,000	8.126	0.257	95.9	21.7	110.8	211.91	33.32	90.2	11.1	101.1
	7.004		110.2	72.5	27.3	124.38		116.9	80.2	28.9
	6.596		21.2	77.6	73.1	99.53		26.9	84.8	63.7
1,000	9.179	0.428	94.3	18.9	108.4	88.82	16.00	89.0	17.6	107.6
	7.612		112.0	74.5	27.4	51.63		115.6	73.7	31.0
	7.073		22.5	79.3	70.4	39.08		25.6	83.4	65.4
300	10.556	0.678	92.9	19.9	109.7	32.88	6.51	88.4	7.0	96.8
	8.382		113.0	73.1	29.1	19.58		116.1	83.2	27.1
	7.643		23.2	79.8	69.4	15.46		26.2	88.4	63.9
150	11.458	0.850	92.1	17.8	107.7	17.197	3.650	83.5	168.8	99.1
	8.931		113.2	74.6	28.3	10.364		114.3	101.0	26.9
	8.096		23.3	81.3	68.6	8.079		25.2	87.9	64.9
100	11.943	0.917	92.8	15.7	105.4	11.779	2.677	85.0	173.8	93.6
	9.239		114.5	77.1	28.1	7.132		114.8	95.4	25.4
	8.363		24.7	81.2	67.1	5.724		25.3	87.0	64.9
60	12.708	1.136	92.5	19.7	109.6	7.434	1.732	81.4	171.3	91.2
	9.613		113.8	73.2	29.8	4.594		114.0	94.6	24.5
	8.691		24.0	80.0	68.4	3.640		25.7	82.6	65.5
30	13.695	1.384	90.3	14.9	104.9	3.986	1.010	75.0	163.1	82.3
	10.308		113.3	76.4	27.4	2.608		113.6	88.8	23.7
	9.186		23.3	83.8	67.6	2.011		28.5	73.1	67.8

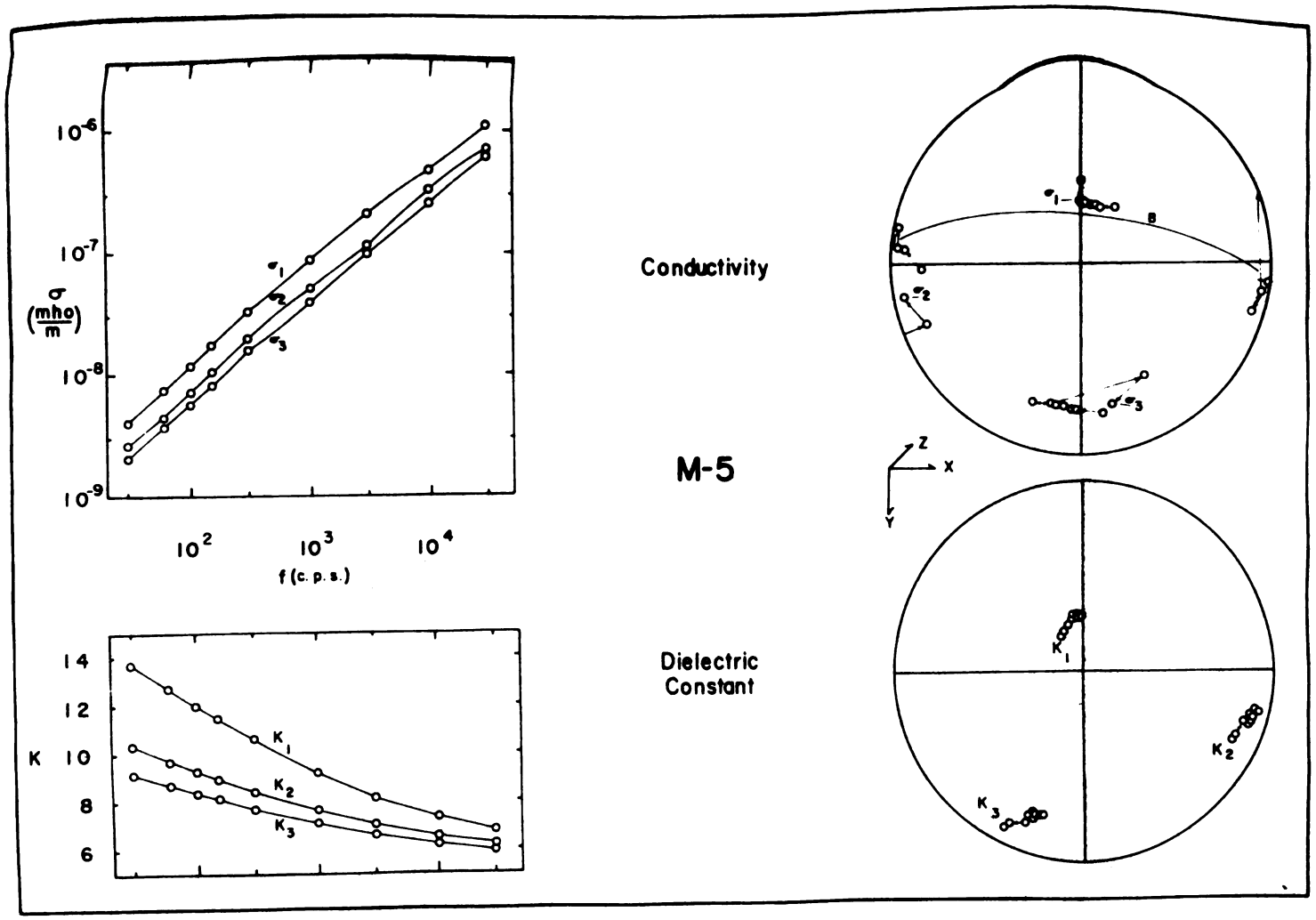

Fig. 8.5.--M-5 (granite gneiss) electrical anisotropy data.

TABLE 8.7.--M-6 (sub-graywacke) electrical anisotropy data.

f (cps)	K Principal Values	K rms Error	K Principal Axes Direction Angles (°)			σ Principal Values $\times 10^9$ (mho/m)	σ rms Error $\times 10^9$ (mho/m)	σ Principal Axes Direction Angles (°)		
	7.240		165.2	102.1	81.7	1198.6		155.2	114.3	85.5
30,000	6.640	0.078	104.1	21.5	105.9	410.0	32.5	114.6	24.7	92.8
	5.952		85.6	72.5	18.0	172.0		87.1	85.6	5.2
	7.818		161.6	106.5	82.0	528.77		157.9	111.5	85.3
10,000	6.839	0.102	108.0	22.2	102.5	189.28	12.56	111.8	22.1	93.3
	6.040		86.2	75.6	14.9	66.57		86.8	85.2	5.8
	8.726		159.8	109.1	83.8	206.53		159.6	109.8	85.1
3,000	7.116	0.127	109.7	20.5	95.6	78.12	6.48	110.0	20.1	92.0
	6.156		86.0	82.6	8.4	25.66		86.1	86.5	5.3
	9.731		160.4	108.5	83.9	80.294		162.1	106.9	84.2
1,000	7.495	0.154	109.1	20.0	95.6	31.951	2.505	107.3	17.6	93.0
	6.261		86.0	82.7	8.3	8.711		85.4	85.4	6.5
	10.931		160.6	108.3	83.9	28.958		163.9	104.2	82.6
300	7.986	0.188	108.8	19.5	94.7	12.644	0.751	104.6	14.9	92.7
	6.380		85.8	83.6	7.7	3.480		83.5	85.5	7.9
	11.698		161.4	107.6	84.0	14.855		166.9	101.2	83.4
150	8.327	0.214	108.0	18.4	93.8	7.011	0.696	101.7	12.2	93.5
	6.480		85.5	84.5	7.1	1.838		84.3	85.3	7.4
	12.175		161.7	107.2	84.0	10.265		168.4	99.3	83.2
100	8.535	0.228	107.6	18.1	93.9	4.804	0.511	99.8	10.3	93.3
	6.512		85.4	84.5	7.2	1.292		83.8	85.6	7.6
	12.775		161.9	106.9	83.8	6.6091		170.2	96.7	82.9
60	8.862	0.264	107.4	17.8	93.6	3.1410	0.3831	97.3	8.6	94.5
	6.583		85.1	84.7	7.2	0.8413		83.5	84.7	8.4
	13.576		163.6	105.1	83.8	3.8716		169.4	95.8	81.2
30	9.287	0.316	105.6	16.0	93.4	1.7982	0.3157	96.6	8.1	94.7
	6.685		84.9	85.1	7.1	0.5235		81.7	84.4	10.0

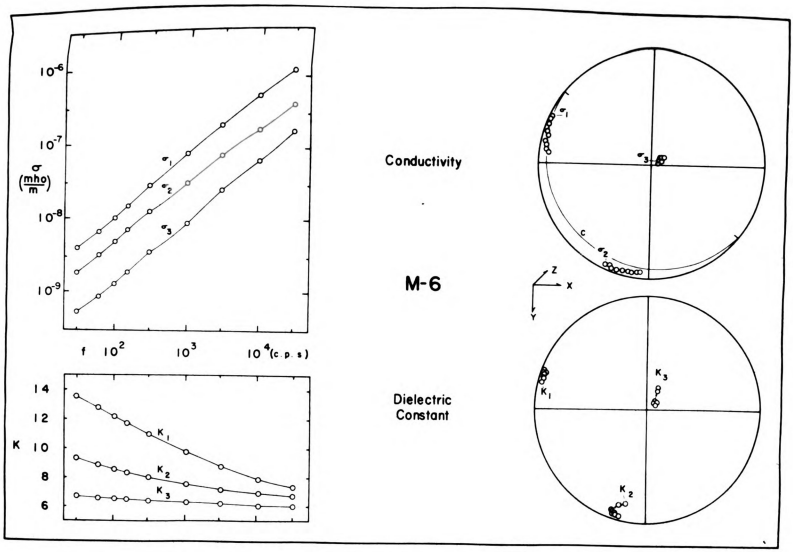

Fig. 8.6.--M-6 (sub-graywacke) electrical anisotropy data.

TABLE 8.8.--M-7 (graywacke) electrical anisotropy data (not a least square tensor coefficient determination).

f (cps)	K Principal Values	K Principal Axes Direction Angles (°)			σ Principal Values $\times 10^9$ (mho/m)	σ Principal Axes Direction Angles (°)		
	7.108	76.4	110.8	154.8	562.3	71.9	65.3	148.6
30,000	6.155	99.0	25.2	113.4	301.8	101.4	24.9	68.2
	5.570	16.4	76.4	81.0	160.0	21.6	86.9	68.6
	7.297	76.8	106.1	159.0	211.61	80.0	56.0	144.1
10,000	6.274	99.7	21.2	108.6	112.32	109.9	36.3	61.0
	5.652	16.5	76.7	80.5	58.81	22.4	79.0	70.7
	7.572	76.9	101.7	162.3	86.95	78.8	55.6	143.3
3,000	6.394	101.6	18.7	104.5	52.84	113.7	37.6	62.6
	5.789	17.6	75.6	80.0	23.32	26.5	76.5	67.6
	7.979	76.8	94.3	166.1	41.747	77.1	2.2	139.4
1,000	6.578	103.6	15.6	97.4	22.406	108.6	38.6	57.6
	5.946	19.1	75.1	78.4	9.162	22.9	82.9	68.3
	8.598	76.3	85.5	165.6	21.173	72.6	49.6	134.4
300	6.823	103.5	13.6	88.8	10.127	105.0	40.4	53.5
	6.147	19.4	77.2	75.6	4.565	23.3	89.8	66.6
	9.084	76.4	79.6	162.8	11.988	75.5	51.7	138.1
150	7.030	104.6	16.2	83.1	5.978	106.6	38.6	56.3
	6.302	20.1	77.7	74.3	2.828	22.4	85.8	68.1
	9.446	76.2	77.3	161.1	9.091	76.6	51.7	138.6
100	7.171	104.4	17.2	80.8	4.521	108.5	39.0	57.1
	6.397	20.2	78.6	73.6	2.089	23.2	83.6	67.8
	9.978	75.8	73.8	158.2	6.580	75.8	51.5	138.0
60	7.398	104.7	19.5	77.5	3.225	108.4	39.1	56.9
	6.520	20.7	79.4	72.4	1.494	23.6	84.2	67.2
	10.841	76.1	68.1	153.6	4.3749	76.5	52.1	138.9
30	7.817	106.3	24.5	72.3	2.1417	109.3	38.8	57.8
	6.706	21.7	79.7	71.1	0.9717	23.9	82.8	67.3

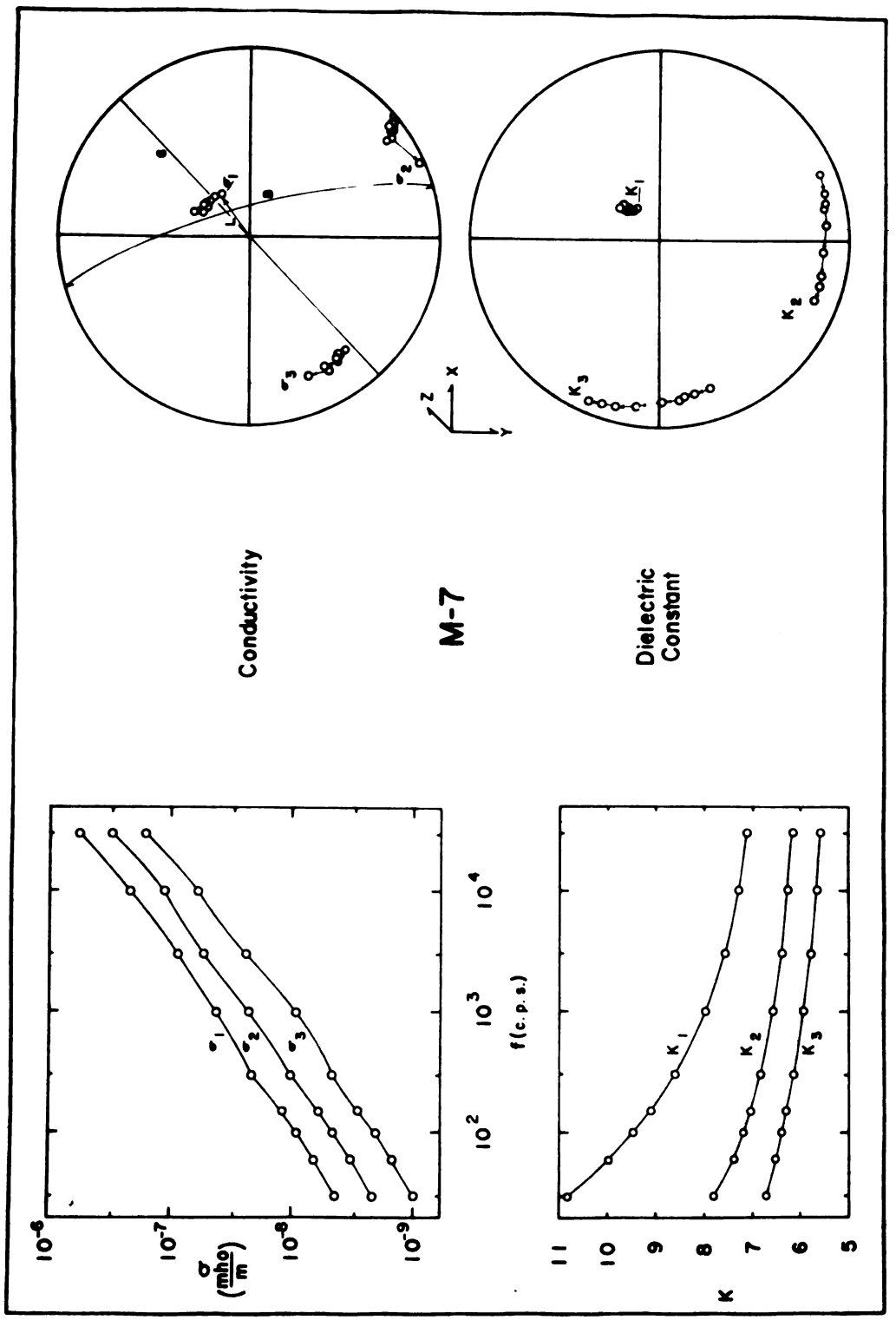

Fig. 8.7.--M-7 (graywacke) electrical anisotropy data.

TABLE 8.9.--M-8 (staurolite schist) electrical anisotropy data.

f (cps)	K Principal Values	K rms Error	K Principal Axes Direction Angles (°)			σ Principal Values $x10^9$ (mho/m)	σ rms Error $x10^9$ (mho/m)	σ Principal Axes Direction Angles (°)		
	10.427		17.7	95.6	73.2	4551.4		12.9	97.2	79.4
30,000	10.071	0.013	106.8	90.4	16.9	3085.2	68.7	100.8	90.2	10.8
	5.746		84.8	5.6	88.0	213.8		83.0	7.2	88.4
	12.613		16.2	96.2	75.1	1843.8		12.4	96.1	79.3
10,000	11.537	0.017	105.0	90.1	15.0	1229.4	21.6	100.8	90.4	10.8
	5.843		84.0	6.2	88.2	62.1		84.0	6.2	88.4
	15.495		15.5	97.4	76.5	676.38		11.7	94.2	79.1
3,000	13.459	0.020	103.6	89.9	13.6	449.34	3.63	101.0	91.5	11.1
	5.927		82.8	7.4	88.3	17.74		86.2	4.4	87.8
	18.663		13.9	95.2	77.2	259.55		11.1	91.3	78.9
1,000	15.543	0.056	103.0	90.7	13.0	174.29	1.01	101.1	92.4	11.4
	6.026		85.1	5.3	88.1	6.00		89.2	2.7	87.4
	22.450		13.0	93.8	77.6	94.622		168.7	88.0	78.9
300	18.120	0.057	102.5	91.3	12.6	64.798	0.022	79.0	94.0	11.7
	6.102		86.6	4.0	87.9	2.638		87.3	4.5	86.4
	25.043		12.5	92.7	77.8	50.406		167.8	85.8	78.6
150	19.894	0.065	102.3	91.7	12.4	34.582	0.110	79.0	94.8	12.4
	6.175		87.8	3.2	87.8	1.392		84.9	6.4	86.1
	26.725		12.1	91.5	78.0	35.655		167.3	84.2	78.7
100	21.042	0.034	102.1	92.2	12.3	24.247	0.023	79.3	95.5	12.1
	6.188		89.0	2.6	87.6	0.895		83.2	8.1	85.7
	28.868		12.0	90.6	78.0	23.541		166.3	82.2	78.7
60	22.531	0.028	102.0	92.5	12.2	15.632	0.158	79.5	95.7	12.0
	6.230		90.0	2.5	87.4	0.542		81.2	9.7	85.8
	32.100		168.2	89.0	78.2	13.268		164.5	79.6	78.6
30	24.662	0.030	78.3	93.1	12.1	9.076	0.080	80.0	98.2	12.9
	6.319		88.4	3.3	87.1	0.353		78.2	13.3	83.9

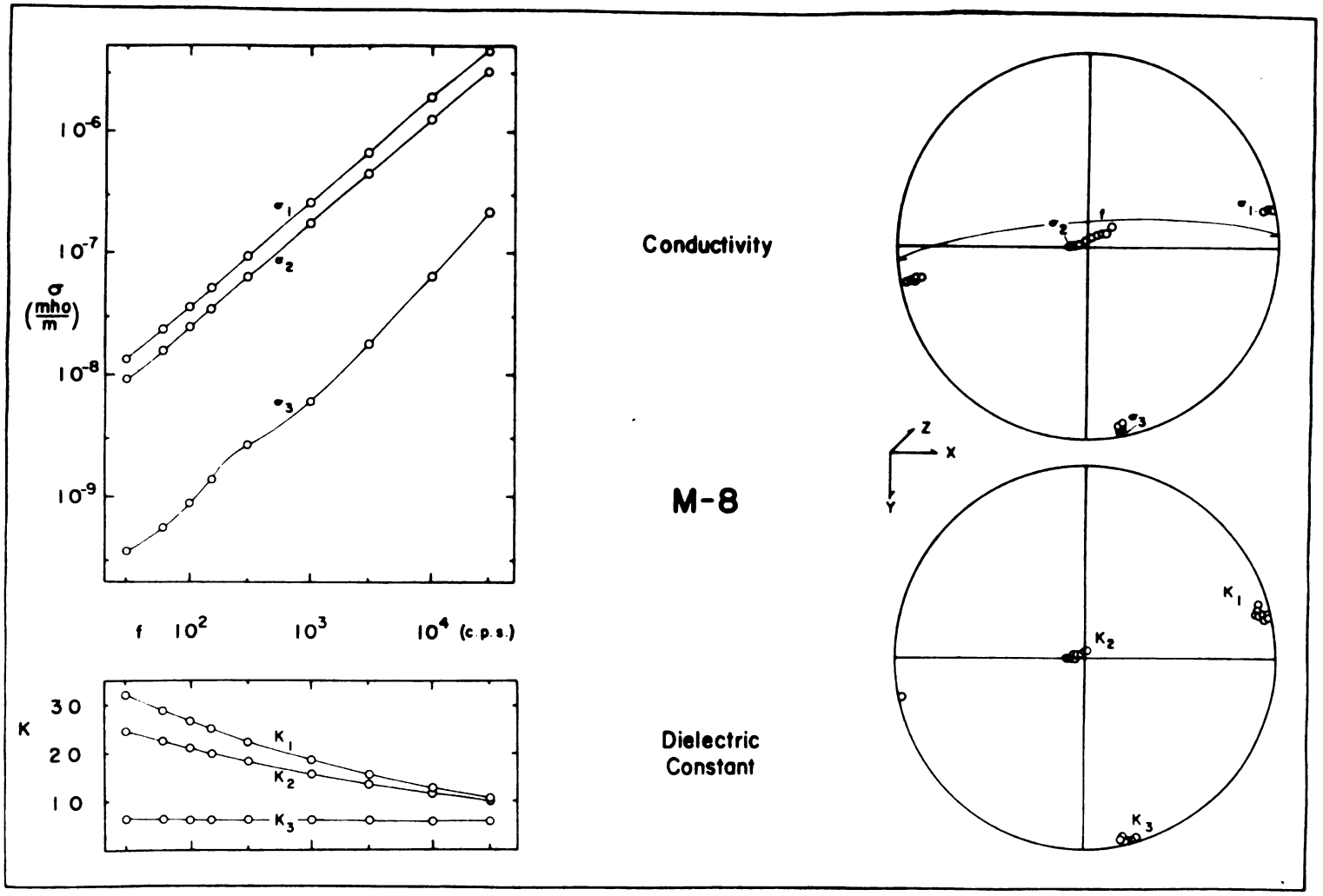

Fig. 8.8.--M-8 (staurolite schist) electrical anisotropy data.

TABLE 8.10.--M-9 (Hemlock formation) electrical anisotropy data.

f (c ps)	K Principal Values	K rms Error	K Principal Axes Direction Angles (°)			σ Principal Values $x10^9$ (mho/m)	σ rms Error $x10^9$ (mho/m)	σ Principal Axes Direction Angles (°)		
	11.474		133.6	79.5	134.5	1350.1		48.2	86.1	138.0
30,000	10.566	2.458	45.4	93.8	135.1	1012.6	300.3	138.2	85.8	131.5
	5.954		79.8	11.2	85.3	637.2		89.5	5.7	84.3
	12.048		134.1	81.0	134.5	458.5		48.4	88.8	138.4
10,000	10.964	2.583	45.3	92.8	135.2	319.8	101.1	138.1	83.8	131.2
	6.225		81.7	9.4	85.6	209.0		86.2	6.3	85.0
	12.688		135.0	84.2	134.4	153.82		50.4	84.4	139.8
3,000	11.394	2.743	45.2	89.5	135.2	113.61	32.21	140.3	82.6	128.7
	6.483		86.2	5.8	85.6	66.61		87.9	9.3	80.9
	13.354		134.6	84.4	134.8	60.72		128.1	81.0	140.4
1,000	11.853	2.888	44.8	89.0	134.8	45.34	12.26	38.1	83.2	127.3
	6.777		86.7	5.7	85.3	24.74		89.7	11.3	78.7
	14.201		134.2	84.2	135.2	26.28		52.0	83.3	141.2
300	12.459	3.050	44.4	88.6	134.3	18.99	5.14	141.9	81.8	126.8
	7.116		87.0	5.9	84.9	10.43		87.7	10.6	79.6
	14.844		133.9	84.5	135.5	15.377		52.7	80.8	141.2
150	12.964	3.181	44.0	88.1	134.0	11.261	2.912	142.7	81.2	125.9
	7.391		87.5	5.8	84.7	5.790		88.6	12.8	77.3
	15.291		133.8	85.0	135.8	11.628		53.0	82.3	141.9
100	13.259	3.265	43.8	87.3	133.7	8.525	2.122	142.9	81.6	125.8
	7.560		88.5	5.6	84.6	4.383		87.9	11.4	78.8
	15.902		133.4	85.0	136.1	8.201		54.4	82.5	143.3
60	13.739	3.382	43.5	87.3	133.3	6.168	1.497	144.2	81.0	124.3
	7.820		88.5	5.7	84.5	3.023		87.0	11.7	78.7
	16.946		133.2	85.3	136.4	5.490		53.0	83.3	142.2
30	14.517	3.585	43.2	86.2	133.0	3.815	0.960	142.6	79.0	125.2
	8.222		89.6	6.1	83.9	1.953		85.2	12.9	78.0

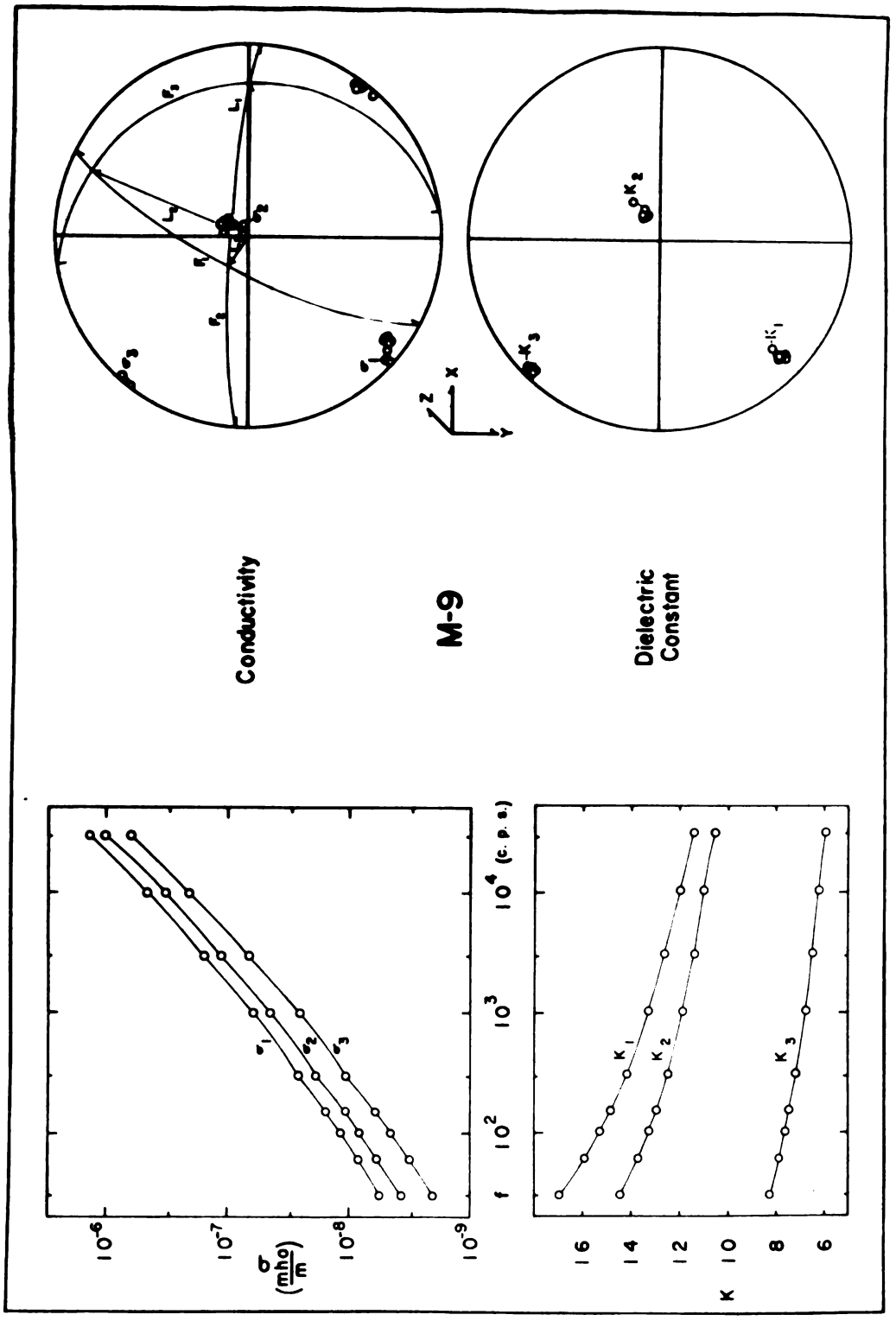

Fig. 8.9.--M-9 (Hemlock formation) electrical anisotropy data.

TABLE 8.11.--M-10 (amphibole schist) electrical anisotropy data.

f (cps)	K Principal Values	K rms Error	K Principal Axes Direction Angles (°)			σ Principal Values $x10^9$ (mho/m)	σ rms Error $x10^9$ (mho/m)	σ Principal Axes Direction Angles (°)		
	8.976		65.3	139.7	60.4	777.1		84.7	143.1	53.6
30,000	8.748	0.395	38.0	88.1	128.0	423.0	224.9	18.1	96.2	107.0
	7.983		63.0	49.7	52.1	316.5		72.7	53.8	41.4
	9.292		67.7	140.3	59.0	298.7		84.9	152.7	63.2
10,000	8.914	0.506	33.8	87.8	123.7	147.0	88.9	15.0	91.9	104.9
	8.129		66.0	50.3	49.2	107.9		75.9	62.8	31.2
	9.708		71.8	143.8	59.9	110.32		96.6	165.8	77.4
3,000	9.103	0.633	29.9	88.4	119.8	60.42	26.71	15.9	99.4	102.7
	8.283		67.2	53.8	44.9	46.67		75.6	79.4	18.0
	10.002		74.2	145.3	60.0	56.30		90.3	156.2	66.2
1,500	9.269	0.715	28.0	89.6	118.0	33.76	14.86	14.0	95.9	102.7
	8.393		67.5	55.3	43.3	24.6[illegible]		76.0	67.0	27.3
	10.166		75.6	147.4	61.5	40.55		91.2	156.6	66.6
1,000	9.396	0.752	26.9	89.5	116.9	25.92	9.75	17.7	98.0	105.7
	8.511		67.9	57.5	41.0	18.85		72.3	68.2	28.7
	10.341		77.3	147.5	60.6	32.48		90.4	157.5	67.5
600	9.456	0.800	26.0	91.2	116.0	22.52	5.92	20.0	97.9	108.3
	8.583		67.7	57.5	41.2	17.07		70.0	69.0	29.7
	10.681		78.8	147.9	60.4	16.036		98.2	159.1	70.9
300	9.743	0.901	24.3	91.7	114.2	11.973	3.069	23.1	104.3	107.7
	8.797		68.8	58.0	40.0	9.401		68.6	75.1	26.5
	11.113		80.5	150.6	62.5	9.046		105.2	156.7	72.8
150	10.019	0.970	24.4	92.6	114.2	6.911	1.447	30.6	111.2	110.9
	9.021		67.8	60.8	38.1	5.633		64.2	80.8	27.6
	11.370		82.3	151.2	62.5	6.757		109.1	154.8	74.2
100	10.237	1.010	24.2	94.2	113.8	5.297	0.962	36.9	114.8	115.5
	9.174		67.2	61.6	37.8	4.092		59.8	85.6	30.6
	11.692		83.6	152.8	63.6	4.712		115.3	28.0	78.8
60	10.525	1.088	23.7	94.7	113.2	3.892	0.582	42.7	62.3	119.6
	9.385		67.3	63.2	36.4	2.906		58.3	86.0	32.0
	12.210		86.0	153.9	64.3	2.996		118.3	28.3	88.9
30	11.015	1.168	23.8	96.6	112.7	2.572	0.342	49.3	68.5	131.6
	9.766		66.6	64.9	35.5	1.929		53.7	72.4	41.6

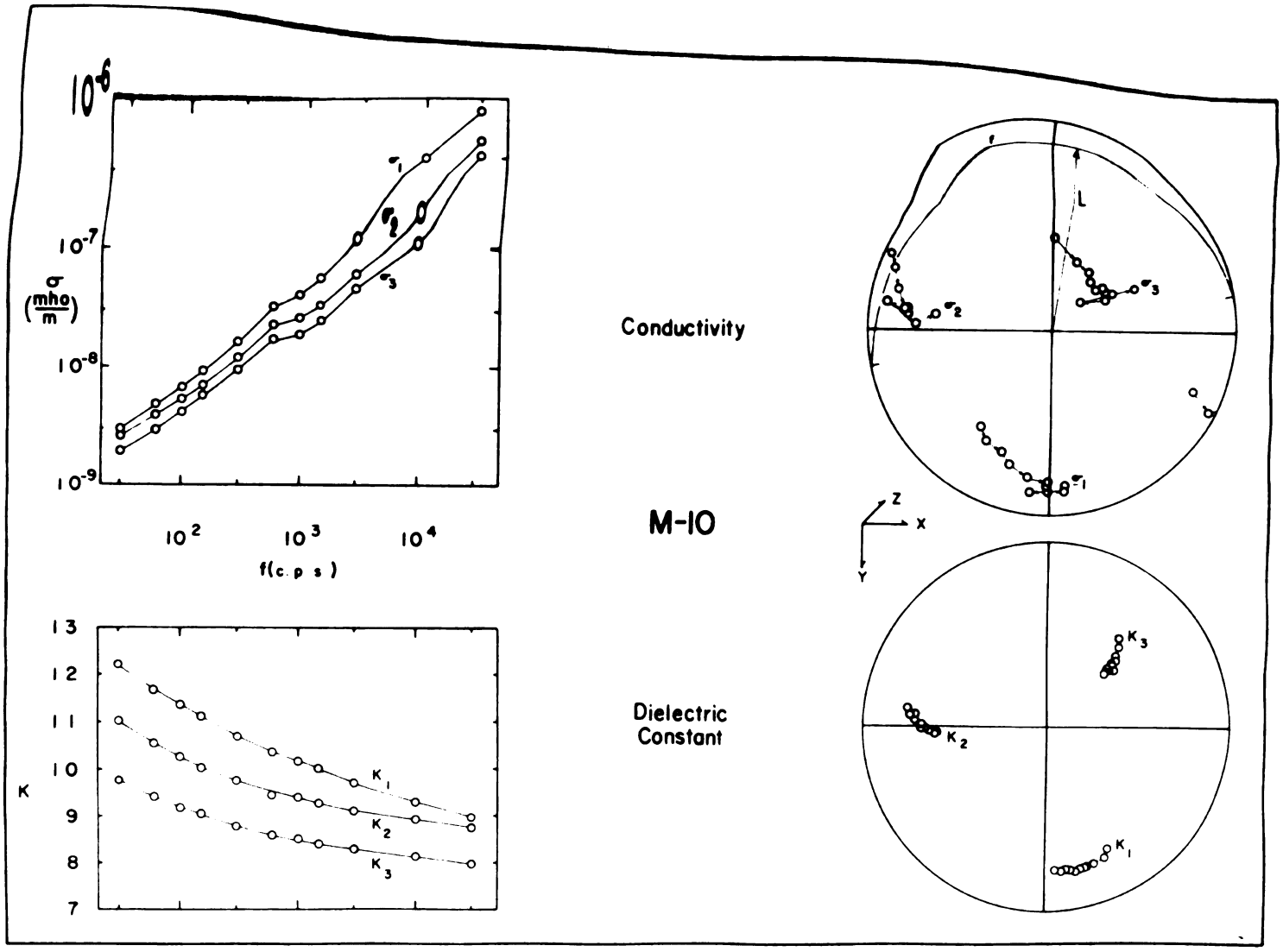

Fig. 8.10.--M-10 (amphibole schist) electrical anisotropy data.

TABLE 8.12.--M-11 (siltstone) electrical anisotropy data.

f (cps)	K Principal Values	K rms Error	K Principal Axes Direction Angles (°)			σ Principal Values $x10^9$ (mho/m)	σ rms Error $x10^9$ (mho/m)	σ Principal Axes Direction Angles (°)		
	7.865		28.6	117.9	95.8	1429.1		176.8	92.8	88.5
30,000	7.452	0.519	115.6	149.9	75.3	1047.4	156.8	86.9	163.9	74.2
	6.087		78.1	79.7	15.8	269.5		89.3	74.2	15.8
	8.500		21.0	110.5	93.9	525.1		174.9	94.3	87.3
10,000	7.930	0.557	108.9	155.6	75.2	350.5	39.1	85.1	161.3	72.0
	6.220		81.2	77.5	15.3	122.3		88.8	71.8	18.2
	9.246		14.8	104.6	92.4	180.43		172.5	96.4	86.0
3,000	8.441	0.564	103.4	159.0	74.2	113.58	14.71	82.6	155.9	67.2
	6.408		83.8	75.3	16.0	48.71		88.8	66.8	23.2
	10.057		12.5	102.5	91.1	66.39		12.8	102.8	89.8
1,000	8.942	0.578	101.6	159.4	73.3	40.25	6.45	101.9	155.2	68.6
	6.653		85.4	73.9	16.8	1 .36		85.6	69.1	21.4
	10.997		11.9	101.9	90.2	25.611		15.0	104.5	86.2
300	9.480	0.618	101.2	158.6	72.0	14.973	2.061	104.6	149.4	63.7
	6.979		86.2	72.4	18.0	8.507		86.9	63.6	26.6
	11.656		12.6	102.6	89.8	13.911		18.7	108.3	86.4
150	9.848	0.660	102.0	157.7	71.5	7.709	1.347	108.5	148.0	64.5
	7.200		86.2	71.9	18.5	4.758		85.3	64.7	25.8
	12.101		13.6	103.6	90.2	10.164		20.5	110.5	88.4
100	10.052	0.689	102.8	156.5	70.7	5.397	1.040	109.2	148.0	65.4
	7.436		85.4	71.3	19.3	3.307		83.0	66.5	24.6
	12.646		13.7	103.7	89.5	6.874		22.2	112.2	90.8
60	10.405	0.750	103.0	156.3	70.6	3.530	0.832	110.4	150.0	69.0
	7.583		85.9	71.1	19.4	2.125		81.5	71.0	21.0
	13.520		15.1	105.1	89.6	4.262		25.9	115.6	93.7
30	10.866	0.856	104.3	155.7	70.8	2.008	0.614	113.3	150.4	72.8
	7.867		85.4	71.4	19.2	1.218		79.4	76.2	17.6

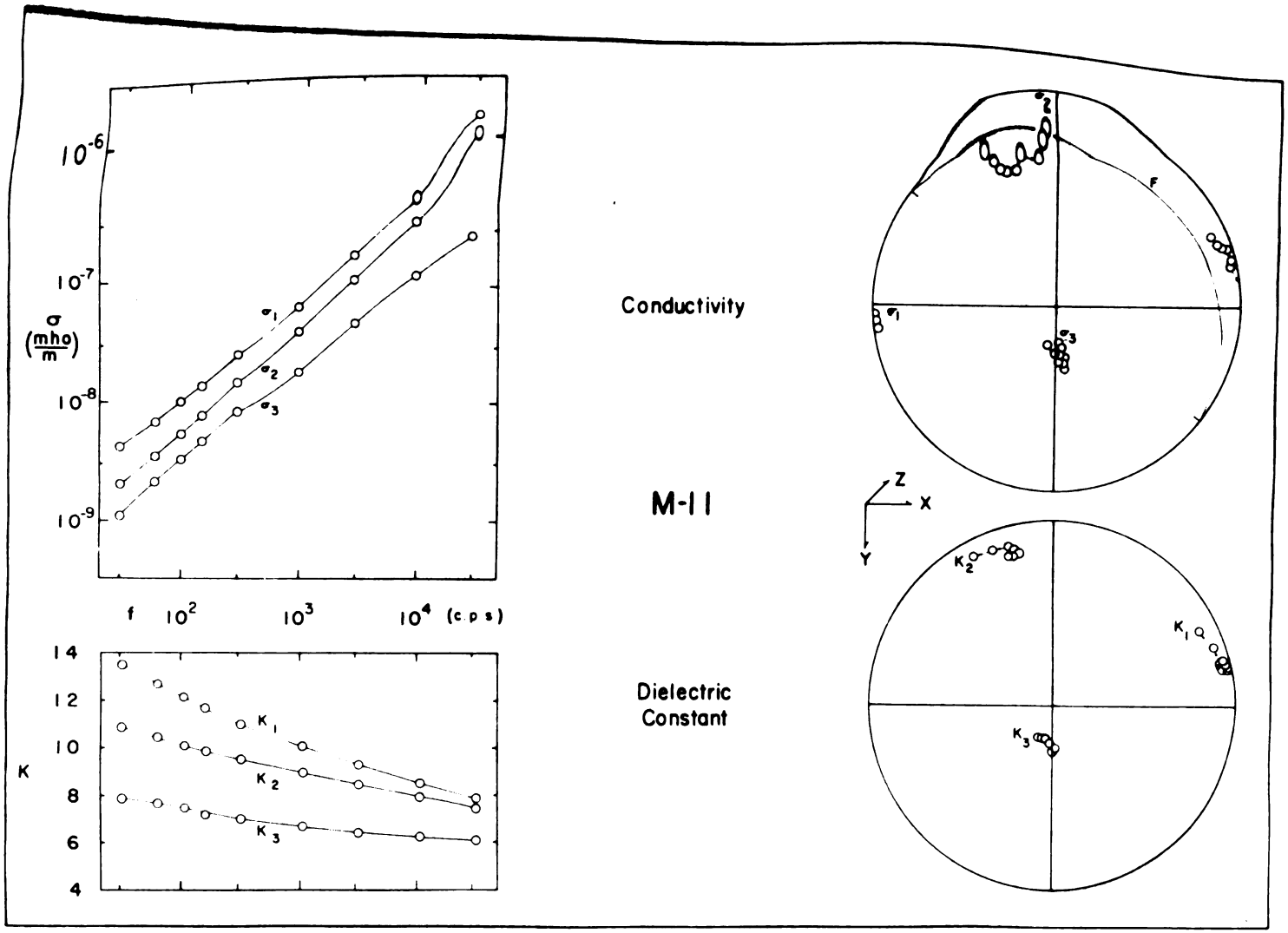

Fig. 8.11.--M-11 (siltstone) electrical anisotropy data.

TABLE 8.13.--M-2A (greenstone with atmospheric moisture) electrical anisotropy data.

f (cps)	K Principal Values	K rms Error	K Principal Axes Direction Angles (°)			σ Principal Values x10⁸ (mho/m)	σ rms Error x10⁸ (mho/m)	σ Principal Axes Direction Angles (°)		
	11.107		92.4	114.6	24.7	1291.0		95.2	69.8	159.1
100,000	9.042	0.186	16.7	106.0	94.6	589.2	13.7	13.2	99.6	99.0
	8.170		73.5	29.9	65.8	430.1		77.8	22.6	71.3
	12.886		90.6	112.7	22.7	503.3		80.1	81.0	166.6
30,000	10.074	0.206	9.0	98.5	92.8	242.4	11.4	170.1	88.1	99.7
	8.819		81.1	24.4	67.5	162.5		89.6	9.2	80.8
	15.077		92.7	103.4	13.6	222.12		77.8	87.0	106.4
10,000	11.040	0.223	7.5	97.4	89.0	106.19	9.04	106.7	87.8	102.1
	9.619		83.0	15.4	76.4	64.92		88.4	3.7	86.6
	18.16		95.6	98.1	9.9	105.57		74.9	89.7	164.9
3,000	12.58	0.24	7.0	94.9	85.0	48.69	5.52	164.8	88.1	105.1
	10.62		85.9	9.5	81.4	27.63		88.3	1.9	89.2
	23.14		98.5	94.5	9.7	56.27		72.4	86.6	162.1
1,000	14.73	0.53	8.8	93.1	81.7	24.63	3.41	162.4	88.0	107.5
	12.01		87.6	5.5	85.0	13.06		89.2	4.0	86.1
	24.42		99.2	93.2	9.7	48.16		72.2	86.0	161.7
700	15.28	0.63	9.4	92.6	81.0	21.17	2.87	162.2	88.6	107.7
	12.30		87.9	4.2	86.4	11.35		89.9	4.3	85.7
	27.50		100.3	91.4	10.4	40.318		107.0	82.4	161.2
500	16.50	0.70	10.9	93.9	79.8	17.583	2.119	17.6	92.0	107.5
	12.79		86.4	4.2	88.0	8.545		85.8	7.9	83.3
	31.69		102.6	91.3	12.6	28.740		108.5	82.5	160.0
300	18.28	1.24	12.6	90.4	77.4	12.820	1.664	18.8	91.2	108.8
	14.05		89.9	1.3	88.7	6.248		86.5	7.6	83.3
	36.22		76.0	89.6	166.0	22.326		109.3	83.8	159.7
200	20.40	1.56	166.0	89.2	103.9	10.036	1.536	19.7	91.9	109.6
	14.95		89.3	0.9	89.4	4.748		86.1	6.5	84.8
	46.48		74.3	87.3	164.0	14.345		109.3	84.3	159.8
100	23.96	2.35	164.2	88.2	105.6	6.540	1.245	20.2	94.1	109.7
	17.07		89.0	3.2	86.9	3.237		84.3	7.0	86.0
	53.38		72.8	86.4	162.4	11.394		108.6	84.2	160.4
70	27.04	3.00	162.8	87.6	107.1	5.218	1.147	20.4	96.4	109.3
	18.07		88.8	4.3	85.9	2.669		82.0	8.7	86.6
	60.52		72.5	86.7	162.2	8.923		107.1	85.2	162.2
50	30.31	3.43	162.4	87.2	107.3	4.291	1.035	21.4	101.6	107.8
	19.40		88.3	4.3	86.0	2.262		77.5	12.6	88.9
	71.56		108.4	83.4	160.3	6.193		105.9	85.8	16.5
30	36.11	4.33	18.4	88.1	108.3	3.063	0.878	27.5	111.5	73.6
	21.87		89.7	6.9	83.1	1.624		68.2	21.9	87.9

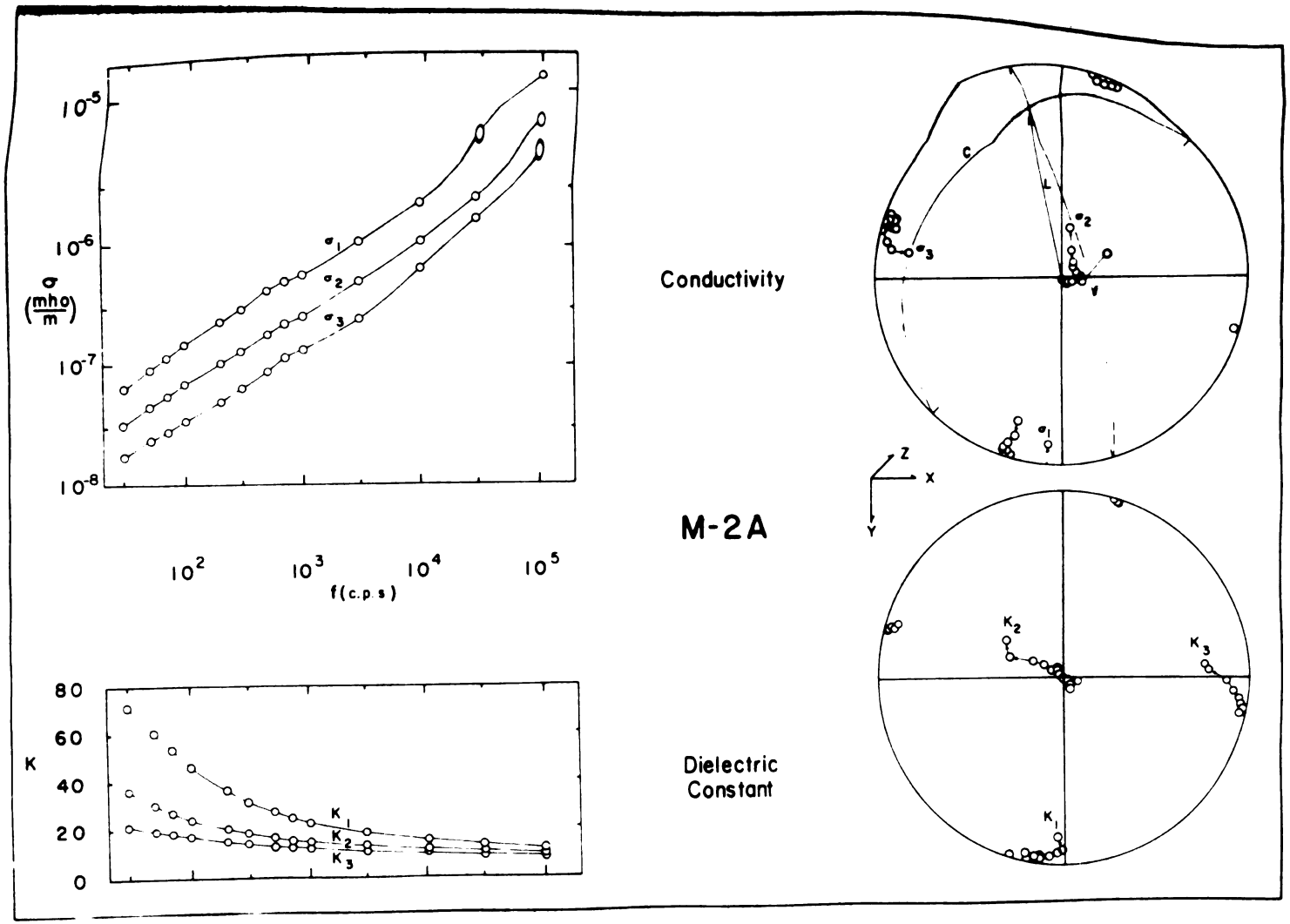

Fig. 8.12.--M-2A (greenstone) electrical anisotropy data.

The direction angle, α_{ij}, in Table 8.1 is the angle between the i^{th} principal direction (i = 1, 2, 3, for the maximum, intermediate, and minimum principal axes, respectively) and the j^{th} laboratory coordinate axis (j = 1, 2, 3, for the x, y, and z axes, respectively).

The graphical presentations of Figures 8.1 through 8.12 consist of dispersion (frequency variation) curves of the principal K and (effective) σ values and principal axis poles on equal area, or Schmidt net, projections. The Schmidt net projections are relative to the laboratory coordinate system and utilize the lower reference hemisphere. To indicate the systematic principal axis dispersion observed for some samples, successive principal axis poles on the Schmidt net projections are connected with arrows proceeding from low to high frequency. Also, each principal axis pole set is identified at the highest frequency pole. The maximum, intermediate, and minimum principal values and axis poles are indicated in Figures 8.1 through 8.12 with the subscripts 1, 2, and 3, respectively. All structural controls (e.g., lineations, foliation, cleavage, etc.) observed in the field sample are plotted on the conductivity Schmidt net projection for each sample.

Conductivity and Dielectric Constant Magnitudes

The dielectric constant values obtained for the vacuum dried rocks considered in this study ranged from

a low of 5.570, for the M-7 graywacke (see Figure 8.7 and Table 8.8) at 30,000 cps, to a high of 38.29, for the M-2 greenstone schist (see Figure 8.2 and Table 8.3) at 30 cps. The dielectric constant values at 30 cps ranged from 6.319 to 38.29, while at 30,000 cps, the values were spread from 5.570 to 12.316. The K values obtained in this study are consistent with those reported by Keller and Licastro (1959), Howell and Licastro (1961), Keller (1966), and Parkhomenko (1967) for rocks measured under similar conditions to those used for this study.

The lowest K values were observed for the sub-graywacke of M-1 (see Figure 8.1 and Table 8.2) and the graywacke of M-7 (see Figure 8.7 and Table 8.8). The highest K values were observed for the greenstone schist of M-2 (see Figure 8.2 and Table 8.3) and the staurolite-muscovite schist of M-8 (see Figure 8.8 and Table 8.9). The coarse grained samples (M-3, B-4, M-5, M-9, and M-10) had intermediate K values, as did the M-6 graywacke and the M-11 graywacke.

Most I.P. models for rocks yield a maximum polarization condition for an optimum grain size, due to the combined effects of surface resistivity and surface polarization (Keller and Frischknecht, 1966). The optimum grain size will depend upon the electrical properties of the model medium and the polarizing inhomogenities (Sillars, 1937; Wait, 1959). The combined effect of grain size and electrical properties on the bulk electrical polarization

explains why there seems to be no consistent grouping of the K values with respect to rock type or grain size, based upon magnitudes alone.

The effective conductivity values obtained for these same rocks ranged from a low of $2.925 \cdot 10^{-10}$mho/m, for the B-4 syenite gneiss (see Figure 8.4 and Table 8.5) at 30 cps to a high of $1.0648 \cdot 10^{-5}$mho/m, for the M-2 greenstone schist (see Figure 8.2 and Table 8.3) at 100,000 cps. The effective conductivity values at 30 cps ranged from $2.925 \cdot 10^{-10}$mho/m to $4.653 \cdot 10^{-8}$mho/m, while the range at 30,000 cps is from $1.600 \cdot 10^{-7}$mho/m to $3.896 \cdot 10^{-6}$mho/m. The σ values obtained in this study are consistent with those reported by Keller and Licastro (1959), Grant and West (1965) and Parkhomenko (1967) for rocks measured under similar conditions.

The lowest σ values were generally observed for the B-4 syenite gneiss (see Figure 8.4 and Table 8.5) and the M-6 sub-graywacke (see Figure 8.6 and Table 8.7). The highest σ values were observed for the M-2 greenstone schist (see Figure 8.2 and Table 8.3). The σ data for sample M-8 are rather unusual. Because of the very large σ anisotropy for this sample, its minimum σ values are among the lowest of those studied, while its intermediate and maximum principal values are among the highest. The σ values for the remaining samples (exclusive of M-2A) were intermediate in nature, although those for M-1 and M-7 tended to be lower than the others.

The electrical measurements of this study were made on vacuum dried rocks containing little conducting minerals. Thus, the (effective) conductivity values obtained represent displacement current power loss, rather than the transport of charge carriers. For this situation, the lossy dielectric model of Chapter IV is very appropriate. Thus, the (effective) conductivity may be discussed with the aid of the imaginary components of lossy dielectric polarization models (cf., Sillars, 1937; von Hippel, 1954a, 1954c; Wait, 1959; Wert and Thompson, 1964; Beam, 1965; and Appendix A). These models yield effective conductivities which depend upon the polarizing inhomogenity size and spatial density, as well as the electrical properties of the medium and polarizing inhomogenities. As was the case for K, the bulk σ represents the combined effects of the grain size and electrical properties. This does not allow the rocks studied in this investigation to be grouped on the basis of σ.

The lossy dielectric model for rocks (see Chapter IV) predicted K and σ dispersion curves similar to 4.2, with only the lowest resonance frequency within the range of the present study. The dispersion curves of Figures 8.1 through 8.12 do confirm this qualitative model. The σ values increased with frequency while the K values decreased with frequency, as predicted in Chapter IV. With some exceptions (e.g., B-4, M-6), those samples with high K values also had high σ values and those with low K

values also had low σ values. This may be explained with the aid of the lossy dielectric model of Chapter IV. Because the effective conductivity is due to displacement current power loss, those materials with large polarizations would be expected to exhibit large loss.

Discussion of Error

It is desirable to have an estimate on the variability of the tensor principal value and directions determined by the methods of Chapter VI. The principal value uncertainty is the rms error, given by equation 6.9. The reduction procedures of Chapter VI offer no estimate of the uncertainty in the principal directions. However, some indication of the principal direction uncertainty may be gained from the following approach. The principal values and directions are calculated for all possible combinations of the directional measurement data using one less measurement direction than actually measured. For the purposes of this study, these results will be referred to as the less determined cases. The results for the less determined cases can then be compared to the results using all the directional measurement data for the sample. This can also be used to check the usefulness of the rms error. The combined results for such a study using the directional data for M-2, M-3, M-6, and M-11 at 1000 cps is presented in Figure 8.13. The frequency of 1000 cps was chosen because it is in the center

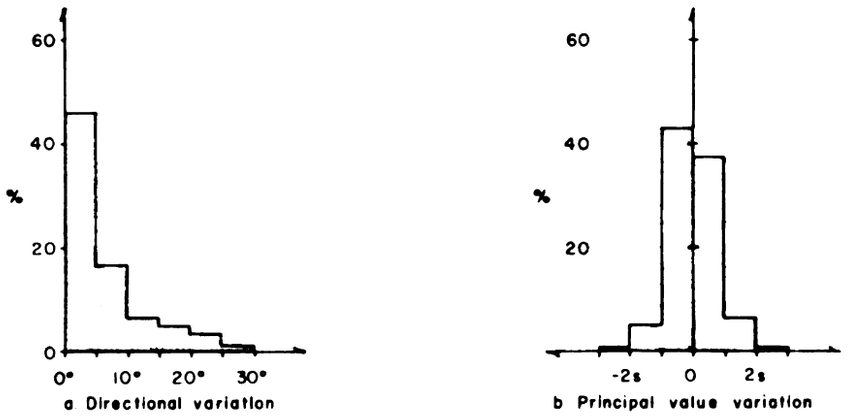

Fig. 8.13.--Variation of the less determined data about the results obtained using all directional measurements.

of the frequency spectrum used for this study. These samples were chosen because they exhibited low symmetry at 1000 cps and used either eight or nine measurement directions.

The data of Figure 8.13 indicate that about 80 per cent of the principal values for the less determined cases lie within one rms error of the principal value estimates obtained using all measurement directions. The data of Figure 8.13 also indicate that about 75 per cent of the principal direction estimates for the less determined cases lie within 20° of the principal direction estimates using all measurement directions. The directional scatter of M-3 (which has large rms errors) contributes heavily to this apparent poor correspondence. If the M-3 data are removed from consideration, about 87 per cent of the less determined principal directions are

within 20° of the principal direction estimates obtained using all directional measurements.

If the above variations of the principal value and direction estimates are a good indication of random error in these estimates, then the random errors should show up on the dispersion curves of Figures 8.1 through 8.12 as scatter. There is some apparent scatter on these plots (e.g., the K_2 and K_3 values and directions of Figure 8.1, the σ_2 values and σ_3 directions of Figure 8.5, and all the σ directions of Figure 8.10). However, the apparent scatter in these cases is rather small. In particular, the directional scatter is much less than the 20° discussed above. In general, the dispersion curves of Figures 8.1 through 8.12 vary smoothly with frequency. This would indicate that the errors discussed above are not random, or that they are much less than the above discussion would lead us to believe. This is similar to the conclusions reached in the discussion of experimental limitations in Chapter V. The actual variation observed in repeated measurements was much less than that predicted on the basis of a statistical propagation of error. If such large errors are indeed present, they are apparently not random.

The ratios of the rms errors to the principal values vary from sample to sample and, to a certain extent, with frequency within any particular sample. The coarse grained samples, such as the M-3 amphibolite, the B-4

syenite gneiss, the M-5 granite gneiss, the M-9 Hemlock formation, and the M-10 amphibole schist consistently exhibit large error ratios. By contrast, the finer grained samples, such as the M-1 sub-graywacke, the M-2 greenstone schist, the M-6 sub-graywacke, the M-8 staurolite-muscovite schist, and the M-11 graywacke consistently exhibit small error ratios.

The σ error ratios are generally larger than the K error ratios. This can be traced to their magnitudes at input to the least square tensor coefficient determination procedure (see Chapter V).

Only six measurement disks were prepared for the M-7 graywacke. Thus, its principal value and direction estimates do not involve least square determinations.

Anisotropy Ratios

The electrical anisotropy information for this study is summarized in Table 8.14 for measurements at 30, 1,000, and 30,000 cps, which effectively span the three decades of signal frequency used in this study. The results for these three signal frequencies can be used to summarize the results for the study because the dispersion curves of Figures 8.1 through 8.12 are very smooth.

It is desirable to have criteria with which to compare the electrical anisotropies of rocks. No precedents for these criteria were found in the literature, because the present study appears to be the first in which the σ

TABLE 8.14.--Electrical anisotropy summary.

Sample	Lithology	Structural Controls	(Approx.) f_c (cps)	30,000 cps	
				$K_1:K_2:K_3$ $\sigma_1:\sigma_2:\sigma_3$	Maximum Symmetry
M-1	Michigamme fm. sub-graywacke--meta-argillite	Slaty cleavage $\perp K_3,\sigma_3$ (except for high f K_3)	350	1.047:1.000:0.984 1.276:1.000:0.649	Isotropic Orthorhombic
M-2	Mona fm. greenstone schist	Foliation $\perp K_3$, σ_3 slaty cleavage $\perp K_2$, σ_2 lineation $\parallel K_1$, σ_1	200	1.219:1.000:0.947 2.454:1.000:0.934	Cylindrical, $\parallel K_1$ Cylindrical, $\parallel \sigma_1$
M-3	Amphibolite	Fracture set (no good correlation)	350	1.109:1.000:0.907 1.975:1.000:0.356	Cylindrical, $\parallel K_1$ or K_3 Cylindrical, $\parallel \sigma_1$ or σ_3
B-4	Syenite gneiss	Gneissic banding $\perp K_3,\sigma_3$	400	1.013:1.000:0.912 1.686:1.000:0.671	Cylindrical, $\parallel K_1$ or K_3 Cylindrical, $\parallel \sigma_1$ or σ_3
M-5	Granite gneiss	Gneissic banding $\perp K_3,\sigma_3$	400	1.091:1.000:0.948 1.551:1.000:0.861	Orthorhombic Cylindrical, $\parallel \sigma_1$
M-6	Michigamme fm. sub-graywacke	Slaty cleavage $\perp K_3,\sigma_3$	300	1.090:1.000:0.896 2.923:1.000:0.419	Orthorhombic Orthorhombic
M-7	Negaunee fm. quartzite-graywacke	Quartz C axis lineation $\parallel K_1$, σ_1	300	1.155:1.000:0.905 1.863:1.000:0.530	----- -----
M-8	Michigamme fm. staurolite-muscovite schist	Foliation $\perp K_3$, σ_3	200	1.035:1.000:0.571 1.475:1.000:0.693	Orthorhombic Orthorhombic
M-9	Hemlock fm.	One fracture set $\perp K_3,\sigma_3$ (no good correlations with the other fracture sets)	400	1.086:1.000:0.564 1.333:1.000:0.628	Cylindrical, $\parallel K_1$ or K_3 Cylindrical, $\parallel \sigma_1$ or σ_3
M-10	Amphibole-chlorite schist	Amphibole lineation $\parallel K_1$, σ_1	600	1.026:1.000:0.912 1.837:1.000:0.748	Cylindrical, $\parallel$, K_1 or K_3 Cylindrical, $\parallel$, σ_1 or σ_3
M-11	Michigamme fm. sub-graywacke-siltstone	Fracture set $\perp K_3$, $_3$	300	1.055:1.000:0.817 1.364:1.000:0.257	Cylindrical, $\parallel K_3$ Orthorhombic
M-2A	Mona fm. greenstone schist	Same as for M-2	500	1.279:1.000:0.875 2.077:1.000:0.670	Orthorhombic Orthorhombic

1,000 cps		30 cps		Comments
$K_1:K_2:K_3$ $\sigma_1:\sigma_2:\sigma_3$	Maximum Symmetry	$K_1:K_2:K_3$ $\sigma_1:\sigma_2:\sigma_3$	Maximum Symmetry	
1.074:1.000:0.972 1.302:1.000:0.674	Cylindrical, $\parallel K_1$ or K_3 Orthorhombic	1.091:1.000:0.907 1.230:1.000:0.610	Orthorhombic Orthorhombic	
1.542:1.000:0.941 2.614:1.000:0.792	Cylindrical, $\parallel K_1$ Orthorhombic	1.900:1.000:0.904 2.542:1.000:0.484	Orthorhombic Orthorhombic	
1.251:1.000:0.863 2.099:1.000:0.422	Cylindrical, $\parallel K_1$ or K_3 Cylindrical, $\parallel \sigma_1$	1.394:1.000:0.793 2.012:1.000:0.727	Cylindrical, $\parallel K_1$ Cylindrical, $\parallel \sigma_1$	High σ, K errors
1.116:1.000:0.897 2.956:1.000:0.462	Cylindrical, $\parallel K_1$ Cylindrical, $\parallel \sigma_1$	1.396:1.000:0.850 3.258:1.000:0.176	Cylindrical, $\parallel K_1$ Cylindrical, $\parallel \sigma_1$	High σ errors
1.206:1.000:0.206 1.720:1.000:0.757	Cylindrical, $\parallel K_1$ Cylindrical, $\parallel \sigma_1$	1.329:1.000:0.891 1.529:1.000:0.771	Cylindrical, $\parallel K_1$ Isotropic	High σ errors
1.298:1.000:0.835 2.763:1.000:0.273	Orthorhombic Orthorhombic	1.462:1.000:0.720 2.153:1.000:0.291	Orthorhombic Orthorhombic	
1.213:1.000:0.904 1.863:1.000:0.409	----- -----	1.387:1.000:0.858 2.043:1.000:0.454	----- -----	Not a least square tensor coefficient determination
1.201:1.000:0.388 1.489:1.000:0.344	Orthorhombic Orthorhombic	1.302:1.000:0.256 1.462:1.000:0.389	Orthorhombic Orthorhombic	
1.127:1.000:0.572 1.339:1.000:0.546	Cylindrical, $\parallel K_1$ or K_3 Cylindrical, $\parallel \sigma_1$ or σ_3	1.167:1.000:0.566 1.439:1.000:0.512	Cylindrical, $\parallel K_1$ or K_3 Cylindrical, $\parallel \sigma_1$ or σ_3	High σ, K errors
1.082:1.000:0.906 1.912:1.000:0.727	Cylindrical, $\parallel K_o$ or K_3 Cylindrical, $\parallel \sigma_1$ or σ_3	1.108:1.000:0.886 1.165:1.000:0.750	Cylindrical, $\parallel K_1$ or K_3 Cylindrical, $\parallel \sigma_1$ or σ_3	High σ, K errors
1.125:1.000:0.744 1.650:1.000:0.456	Cylindrical, $\parallel K_3$ Orthorhombic $\parallel$	1.244:1.000:0.724 2.122:1.000:0.606	Orthorhombic Cylindrical, $\parallel \sigma_1$	
1.571:1.000:0.815 2.285:1.000:0.530	Orthorhombic Orthorhombic	1.982:1.000:0.606 2.022:1.000:0.530	Orthorhombic Cylindrical, $\parallel \sigma_1$	Sample M-2 at equilibrium with atmospheric moisture

and K tensors were completely defined. As a result, two criteria were established during the present study. One of these, here called tensor symmetry, will be discussed in the next section. The other criterion is the use of anisotropy ratios. The anisotropy ratios used in this study and presented in Table 8.14 are the ratios of the maximum and minimum principal tensor values to the intermediate principal value (R_{12} and R_{32}, respectively). The greater the departure of these ratios from unity, the greater the anisotropy.

The $R_{32}(K)$ range from 0.256, for M-8 at 30 cps to 0.984, for M-1 at 30,000 cps, and the $R_{12}(K)$ from 1.013, for B-4 at 30,000, to 1.900, for M-2 at 30 cps. The $R_{32}(\sigma)$ range from 0.257, for M-11 at 30,000 cps to 0.934, for M-2 at 30,000 cps, and the $R_{12}(\sigma)$ range from 1.165, for M-10 at 30 cps, to 3.258, for B-4 at 30 cps.

The anisotropy ratios of Table 8.14 indicate that σ generally shows greater anisotropy than K at all frequencies. The conductivity of materials may vary over several orders of magnitude, while the dielectric constant varies over only two or three (Wert and Thompson, 1964; Beam, 1965; Keller, 1966). Thus, the physical property which has a wider range in possible values might be expected to show greater anisotropy (as judged by anisotropy ratios).

With some exceptions (e.g., B-4 and M-11), the anisotropy of both K and σ is generally greater at lower

frequencies than at the higher frequencies. The occurrence of resonance frequencies between 200 and 600 cps for all samples indicates that one of the polarization mechanisms present at low frequencies is dormant at high frequencies. These polarization mechanisms will add their anisotropic polarizabilities to the bulk polarization of the rock, which will cause greater K and σ anisotropy at low frequencies over that at high frequencies.

Figure 8.14 shows plots of R(σ) versus R(K) taken from Table 8.14. There appear to be linear relationships between these ratios for each of the three plots. These

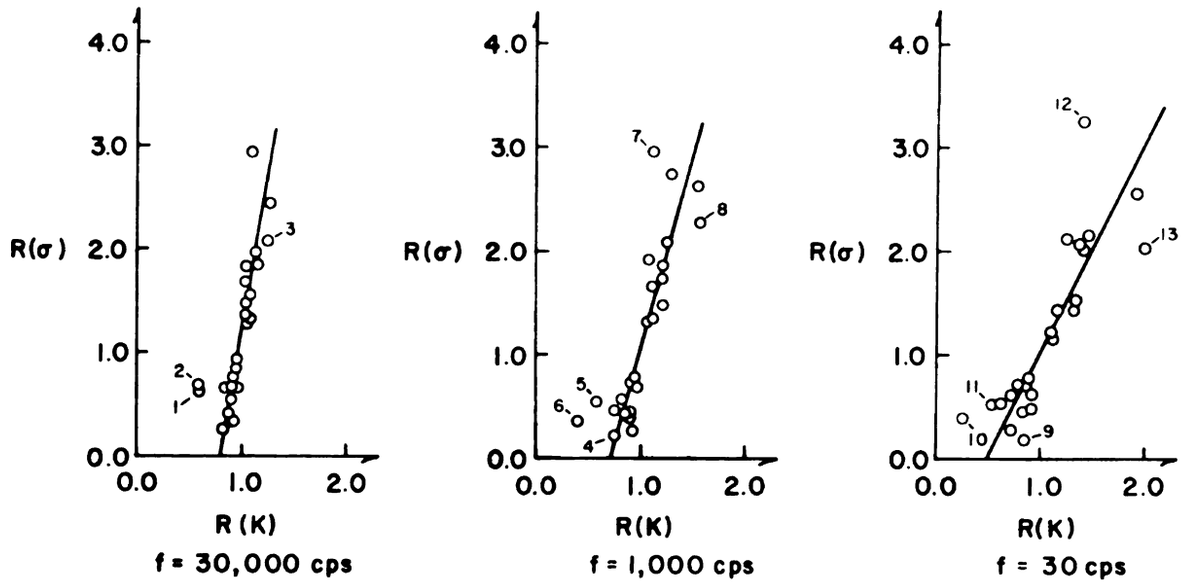

Fig. 8.14.--Anisotropy ratio relationships.

linear relationships pass very close to the point (1.0, 1.0). The scatter about the least square lines for each of these plots is also slight. The slopes of these linear

relationships vary with frequency. At 30,000 cps, the slope of the least square line is 6.182, while at 1,000 cps it is 3.714, and at 30 cps it is 2.019. This change in slope is a reflection that both the K and σ anisotropy are greater at lower frequencies and that the σ variation is greater than that for K.

Plots such as those in Figure 8.14 are helpful for identifying poor data. Points 1, 5, and 11, in Figure 8.14, are from M-9 (Hemlock formation), which has very large σ and K errors. Points 7, 9, and 12 are from B-4 (syenite gneiss) and point 4 is from M-5 (granite gneiss), both of which have large σ errors.

Points 2, 6, and 10 in Figure 8.14 are from M-8 (staurolite-muscovite schist). Both the σ and K errors for the M-8 data are quite low. However, the minimum principal σ values (sub-normal to the foliation) are more than an order of magnitude smaller than the maximum and intermediate principal values at all frequencies. This is a much greater spread than was observed for any of the other samples. The K principal value separation, by contrast, does not seem to be much different from that of the other samples studied. Thus, the $R_{32}(\sigma)$, $R_{32}(K)$ points plot well off the least square lines for all three frequencies. These anomalous results for one sample are not sufficient for generalization. However, they do offer the possibility that plots of R(σ) versus R(K) may be helpful in separation of rock types.

Tensor Symmetry

The tensor symmetry is the second criterion used to compare electrical anisotropy of rocks. The maximum symmetry of the symmetric second-rank σ and K tensors is dependent upon the number of distinguishable principal values. This, in turn, is determined by the rms error.

For the purposes of the present study, the σ and K tensors will have orthorhombic symmetry at a particular frequency, if their maximum, intermediate, and minimum principal tensor values are separated by more than twice the rms error at that frequency. The representation surface (for both σ and K) in this case will be a tri-axial ellipsoid. This representation surface has the same symmetry as the holohedral (2/m, 2/m, 2/m) orthorhombic crystal class (see Berry and Mason, 1959). Orthorhombic symmetry is the lowest symmetry which a symmetric second-rank tensor can exhibit. Thus, a material which exhibits orthorhombic symmetry in its σ and K tensors need not exhibit 2/m, 2/m, 2/m symmetry in its fabric or crystal lattice. It may exhibit even lower symmetry in these respects. However, it cannot exhibit symmetry higher than 2/m, 2/m, 2/m in its fabric or crystal lattice (Nye, 1964). An alternative approach would be to follow the convention used in optical crystallography and call this symmetry biaxial (see Walstrom, 1962), for a tri-axial ellipsoid has two circular (isotropic) cross-sections.

The author prefers not to use this term, for the analogy to optical properties may not be a good one. The optical indicatrix is a geometrical representation surface for the index of refraction in optical materials. The index of refraction in a given direction is proportional to the radius vector of the indicatrix in that direction. By contrast, the value of a symmetric second-rank tensor in a given direction is proportional to the inverse square of the representation surface radius vector in that direction. The index of refraction, which is the ratio of the velocity of light in free space to that in the material is not a symmetric second-rank tensor, but depends upon σ, K, and the magnetic permeability of the material (Corson, and Lorrain, 1962). Electromagnetic radiation uses transverse wave motion. Thus, the isotropic cross-sections (isotropic directions) assume more importance for optical properties than they do for electrical properties. The angle, 2V, between the two isotropic directions in optical materials is often measured directly and used as an aid in identification. The author does not feel that the two circular (isotropic) cross-sections of the σ and K representation surfaces and their relative orientations will be as important to electrical anisotropy as are the similar features to optical anisotropy. The term, biaxial symmetry, may be helpful for those with a strong background in crystal optics and is included for that reason.

If two of the principal values (i.e., the intermediate and either the maximum or minimum principal value) are separated by less than twice the rms error, then they are not distinct. If the remaining principal value is distinct, in the above sense, then the tensor has cylindrical symmetry about this unique axis. The representation surface (for both σ and K) in this case is an ellipsoid of revolution (about the unique axis). An alternative name for this symmetry would be uniaxial, as would be used for the parallel optical discription. Cylindrical symmetry is well established in the literature of electrical properties of rocks. Also, the above objections to the use of biaxial symmetry also hold for the use of uniaxial symmetry. For these reasons, the author prefers the term, cylindrical symmetry. However, the term, uniaxial symmetry, may be useful for those with a strong background in crystal optics and is included for that reason. If the intermediate principal value is separated from both the maximum and minimum principal values by less than twice the rms error, but the maximum and minimum principal values are separated by more than twice the rms error, then the tensor has cylindrical symmetry about either the maximum or minimum principal direction.

If the maximum and minimum principal values are separated by less than twice the rms error, then none of the principal values are unique and the tensor is

isotropic. The representation surface (for both σ and K) in this case will be a sphere.

The maximum K and σ tensor symmetry, based upon the above definitions, are also given in Table 8.14 for each sample at the signal frequencies of 30,000 cps, 1,000 cps, and 30 cps. The symmetry axes are denoted for the cases of cylindrical symmetry.

The tensor symmetry depends upon whether the individual principal values can be distinguished above the rms error. Thus, the tensor symmetry will be controlled by the anisotropy ratios of the principal value estimates and the corresponding rms error estimates. The rms error definitely increases the symmetry of those samples with high error, even when the anisotropy ratios indicate rather strong anisotropy (e.g., M-3, B-4, M-5, and M-9 in Table 8.14 and Tables 8.4, 8.5, 8.6, and 8.10, respectively).

Both σ and K tend to have higher symmetry at higher frequencies. This tendency is much less pronounced for σ than for K. This tendency is a reflection of the combined effects of greater (ratio) anisotropy at low frequencies and the relatively consistent error ratios. The fine grained samples (e.g., M-1, M-2, M-6, and M-11) generally exhibit lower symmetry for both σ and K than the coarse grained rocks. This is a reflection of the lower rms errors found for these fine grained rocks.

Rock Fabric and Structural Control

The extension of Neumann's principle developed in Chapter IV predicted that the symmetric second-rank tensor symmetry would be controlled by the symmetry of the rock fabric and structural control. Thus, the principal directions should parallel any lineations and be normal to any planar structural controls present in the rock. If multiple structural controls are present in a rock which are not mutually parallel or normal, then the above statement breaks down. This is analogous to the orientation of symmetric second rank tensors for monoclinic and triclinic crystals. The principal tensor directions, which are, by definition, mutually perpendicular, cannot simultaneously parallel all lineations and be normal to all planar structural controls.

In general, the principal tensor directions, as shown in Figures 8.1 through 8.12, do relate to structural controls very well. The maximum principal σ and K directions are sub-parallel to the lineation of the amphibole crystals in M-10 (amphibole schist, see Figure 8.11). The correspondence between the maximum principal directions and the quartz C-axis maximum for the M-7 graywacke (see Figure 8.8) is even better. This is very encouraging in view of the fact that only six directional measurement sets were available for this sample. There is also good correlation between the maximum principal

directions and the lineation due to the intersection of the foliation and slaty cleavage in M-2 (greenstone schist, see Figure 8.3).

For the sub-graywackes of M-1 and M-6, the minimum principal σ and K directions are sub-normal to the slaty cleavage, where these principal directions are distinct (see Figures 8.1 and 8.6). This correspondence is very good except for the high frequency K_3 directions for M-1, where K_2 and K_3 are not distinct (see Figure 8.1). The intermediate principal directions are sub-normal to the slaty cleavage in M-2 (see Figure 8.2).

The minimum principal K and σ directions for the greenstone schist of M-2 and the staurolite-muscovite schist of M-8 are sub-normal to the foliation with good correspondence (see Figures 8.2 and 8.8). The correspondence for K_3 in M-2 is not as good as the others, however.

In the syenite gneiss of B-3 and the granite gneiss of M-5, the minimum principal directions are sub-normal to the gneissic banding (see Figures 8.4 and 8.5). However, the correspondence is not very good. This poor correspondence may be due to the heterogeneity in mineral content and grain size in both of these samples.

There appears to be very poor correspondence between the principal directions and structural controls in the amphibolite of M-3 (see Figure 8.3). The large

rms errors for the data from this sample may indicate heterogenity. Such heterogenity, if present, may confuse any relationship between the tensor principal directions and the structural control. Also, the observed fracture set (F in Figure 8.3) is not a particularly strong one. Thus, it may not be a true indication of rock fabric.

The minimum principal σ and K directions are subnormal to fracture sets in the M-9 Hemlock formation sample and the graywacke of M-11 (see Figures 8.9 and 8.10). However, the intermediate and maximum principal directions in M-9 do not show good correspondence to the other structural controls present in that sample.

Principal Direction Dispersion

For some of the samples investigated, the principal directions remained relatively constant (see Figures 8.3, 8.4, 8.8, and 8.9) with variations in signal frequency. This, together with good correspondence between the σ and K principal directions (to be discussed in the next section), may indicate a strong preferred orientation of the constituent dipole sources in the rock. The lack of directional dispersion also may indicate that the relative contributions of the various dipole sources to the bulk σ and K of the rock do not vary appreciably with frequency.

Some samples exhibit considerable systematic variation in the orientation of the principal directions with frequency (see Figures 8.2, 8.5, 8.10, and 8.11). This

may be a manifestation of the multiple anisotropic polarization species model proposed in Chapter IV. The polarization centers of this model may have different preferred orientations and resonance frequencies. Thus, their various frequency dependent properties will contribute to the bulk σ and K values, causing the orientation dispersion.

Some samples show uniformity for a single principal direction with dispersion in the other principal axes (see Figures 8.6, 8.7, and 8.11). This may indicate one common principal polarization direction for the constituent polarization centers of the rock, with the others free to vary.

Parallelism of the σ and K Tensors

The qualitative model for the electrical properties of rocks, developed in Chapter IV, did not require that the σ and K principal directions be parallel. However, the dependence of the effective conductivity on the imaginary component of the lossy dielectric polarizability models would lead us to expect that. Inspection of Figures 8.1 through 8.12 shows that, in general, the σ and K principal axes are sub-parallel. The best examples of this are shown in Figures 8.4, 8.6, 8.8, 8.9, 8.11, and 8.12. Some samples have good correlation for only one principal direction. The best examples of this type of correlation are shown in Figures 8.2, 8.3, and 8.7. In these cases, the principal directions with good correlation are usually

directly related to structural control. For example, the maximum principal directions for M-2 and M-7 (those with good correlation) are parallel to lineations.

Good correlation between the σ and K principal directions may indicate close alignment of the principal directions of the constituent dipole centers of the rock. Poor correlation, by contrast, may indicate misalignment of the principal directions of the constituent dipole centers. It would be difficult to go beyond the above comments because the bulk electrical properties of a rock represent a composite of the properties of the constituent mineral grains.

Resonance Frequencies

The resonance frequencies, f_c, for the bulk electrical properties of the rock are obtained by observation of the local maximas on the σ dispersion curves and the inflection points on the K dispersion curves. The approximate resonance frequencies given in Table 8.14 were obtained from Figures 8.1 through 8.12 by this method. These f_c are only approximate in nature because of the lack of detailed control near most of them. They are definitely real, as can be seen from the data in Figures 8.10 and 8.12, which have good control near the f_c.

The f_c in Table 8.14 vary from about 200 cps, for the M-2 greenstone schist and the M-8 staurolite-muscovite schist, to about 600 cps, for the M-10 amphibole schist.

These resonance frequencies are probably due to the mechanism of interfacial polarization because of their low values. Interfacial polarization models, such as those of Sillars (1937) and Wait (1959), have resonance frequencies which depend upon the electrical properties of the inhomogenities and the medium, the inhomogenity spatial density, and the grain size. The coarse grained samples studied in this investigation (M-3, M-4, M-5, M-9, and M-10) have consistently higher approximate resonance frequencies than the fine grained samples (M-1, M-2, M-6, M-8, and M-11). By contrast, Wait (1959) predicts that for rocks of similar mineral composition, those with larger grain size will have longer relaxation times and thus lower resonance frequencies. However, variations in mineral content between rocks can cause the exact opposite to occur. This, then, may be the explanation for the apparent f_c-grain size relationships of the present study.

Effects of Moisture

The great danger in using vacuum dried samples was that they might show significant orthorhombic anisotropy, while their saturated equivalents might not. In the early portions of the laboratory investigation, some of the samples were measured after being dried in air at room temperature, so they were effectively in equilibrium with the atmospheric moisture. This technique was later

abandoned in favor of vacuum drying at 60° C to gain repeatability in the measurements. While the data obtained from these early measurements were not repeatable, it may be used as an indication of the effects that moisture might have on anisotropy. With this in mind, the results for the M-2 greenstone schist (marked M-2A, to avoid confusion) in this slightly moistened condition are included as Figure 8.12 and Table 8.13.

This slight increase in moisture content raised the σ values nearly one-half order of magnitude and nearly doubled the low frequency K_1 values over their vacuum dried equivalents. This served to increase the anisotropy ratios for both σ and K and increase the scatter of the $R(\sigma)$ versus R(K) plots of Figure 8.14. Points 3, 8, and 13 in Figure 8.14 are from the M-2A data. This anomalous behavior of the $R(\sigma)$ versus R(K) plot with the addition of water suggests the possibility that anisotropy ratio plots may also be used to evaluate the saturation of rocks. The resonance frequency was increased for the slightly moistened sample over its vacuum dried equivalent and the principal directions changed slightly.

The results for M-2 and M-2A are not sufficient to generalize on the effects of moisture on electrical anisotropy. However, they do offer the interesting possibility that metamorphic rocks may exhibit even greater electrical anisotropy in the saturated state than in the vacuum dried condition.

Consequences of the Laboratory Results

Strong orthorhombic electrical anisotropy was observed for many of the samples investigated in this study. Thus, the assumptions of electrical isotropy, or even anisotropy with cylindrical symmetry, often made in theoretical geoelectric data interpretation may not be valid for some rocks. This implication is more important than the specific values obtained for twelve sets of measurements on eleven samples of vacuum dried Precambrian rocks of Michigan and Ontario.

When strong orthorhombic anisotropy is present in rocks, theoretical geoelectric interpretation methods should be highly suspect. This is because the B.V.P. upon which the theoretical master curves are based is no longer analogous to the physical problem found in nature. In such cases, all geological control available should be applied to the curve matching results to obtain a final interpretation.

The laboratory portion of this study was concerned with micro-anisotropy, or that anisotropy which is observed in small samples. In a field situation, the macro-anisotropy, due to the structural attitude and thickness of the various lithologic units, would also be of interest. The observation of strong micro-anisotropy in the laboratory does not mean that strong total (micro- plus macro-) anisotropy will be observed in the field. However, Dowling

(1967) and Tammemogi (1969a, 1969b) observed striking anisotropy in their respective magneto-telluric investigations over Precambrian rocks in the Lake Superior region. While Dowling was unable to make a direct correlation of his anisotropy with geological structure, Tammemogi was able to make very good correlations. Schlumberger et al. (1934) indicate that the total anisotropy observed in the field is usually much greater than the micro-anisotropy of the individual lithologic units.

A very significant consequence of this study is that it can no longer be safely assumed that three mutually perpendicular σ and K directional measurements serve to completely define these tensor properties. In order to be able to use only three mutually perpendicular directional values, the principal tensor directions must be precisely known in advance. As indicated in Chapter V, the laboratory reference systems for the present study were oriented with respect to any observed fabric in the field samples. The principal direction plots of Figures 8.1 through 8.12 indicate that the principal directions so determined did not coincide with the tensor principal directions. Thus, to completely define the symmetric second-rank σ and K tensors, all six of the independent coefficients of the representation matrix must be determined. This requires that directional measurements of these tensor properties be made in six, or more directions.

CHAPTER IX

CONCLUSIONS

The addition of strong orthorhombic anisotropy to the boundary value problems used in theoretical geoelectrical interpretation methods makes them very difficult, if not impossible, to solve analytically. This is illustrated very well with the horizontally layered earth B.V.P. commonly used to develop master apparent resistivity curves used for interpretation of resistivity and I.P. field data.

The lossy dielectric provides a very good qualitative model for a macroscopic (in the solid-state sense) study of electrical anisotropy of rocks. The lossy dielectric model requires that the dielectric constant, K, and electrical conductivity, σ, tensors be completely defined. To completely define these symmetric second-rank tensors, directional measurements must be made of the effective directional properties in at least six different directions. Measurement of the effective directional properties in more than six different directions allows a least square determination of the tensor coefficients to be made.

Electrical anisotropy of rocks is studied by determining the principal values and directions of the σ and K tensors. The anisotropy is measured by the departure of the anisotropy ratios from unity. The degree of symmetry of the σ and K tensors is determined by the number of principal values which are distinguishable above the rms errors.

There appear to be linear relationships between the corresponding σ and K anisotropy ratios at each frequency. Departures from these linear relationships may indicate poor data, variations in lithology, or variations in moisture content.

The coarse grained samples exhibited larger rms errors in the principal values, higher symmetry, and higher resonance frequencies than the fine grained samples.

The anisotropy of both σ and K tended to be greater at lower frequencies. Also, the symmetry of these tensors tended to be lower at lower frequencies. However, this latter tendency was very weak for σ.

The symmetry of the σ and K tensors of rocks is related to the symmetry of the structural controls of the rocks. These structural controls can be statistical microscopic rock fabrics or macroscopically observable features, such as cleavage, joints, and foliation. Thus, electrical anisotropy may be used to infer rock fabric symmetry.

Some of the samples investigated exhibited significant dispersion (frequency variation) of the principal axes. This may be related to the variation in the relative contributions of the various dipole centers to the bulk electrical properties at various frequencies.

Generally speaking, the principal axes for K and σ were sub-parallel. This may be attributed to the dependence of the effective conductivity on the imaginary components of the lossy dielectric polarizability models.

Comparison of the electrical anisotropy results for a greenstone schist (M-2) in the vacuum and air dried states indicate that the presence of moisture in these metamorphic rocks may increase the electrical anisotropy.

CHAPTER X

RECOMMENDATIONS FOR FURTHER STUDY

The present study did achieve its primary goals. It demonstrated that strong orthorhombic electrical anisotropy may be present in some rocks. It also developed and tested a method for the laboratory determination of the σ and K tensors. In addition, it proposed a field method for the determination of these tensors. However, it did not provide a comprehensive catalog of electrical anisotropies for various rocks.

A study which would provide such a comprehensive catalog of rock electrical anisotropies of a given geological province is a logical follow-up study for the present investigation. Such a follow-up study should also include measurements on saturated and high metallic content rocks. This would require slightly different instrumentation than that used for the present study. However, the problems involved are not insurmountable.

Studies specifically aimed at investigating the effects of moisture content and electrolyte variations on electrical anisotropy would also be very worthwhile. Any investigation involving saturated rocks must deal

with the problem of non-polarizing electrodes. A very significant advance for petrophysics would be the development of a successful non-polarizing electrode system with a high degree of acceptability to those working in the field.

Now that the possibility of strong orthorhombic electrical anisotropy has been established, it is very desirable to extend as many as possible of the isotropic boundary value problems, used for theoretical geoelectric data interpretation, to include the condition of anisotropy. Numerical solutions may be necessary for these extensions where analytical solutions cannot be obtained.

Finally, a very logical follow-up of the present study would be a field electrical anisotropy investigation. It could also evaluate the field procedures suggested in Chapter II.

LIST OF REFERENCES

LIST OF REFERENCES

American Society for Testing Materials, 1965 Tentative methods of test for A-C loss characteristics and dielectric constant (permittivity) of solid electrical insulating materials: A.S.T.M. Standards: D150-65T, p. 47-72.

Arbogast, J. L., Fay, C. H., and Kaufman, S., 1960, Method and apparatus for determining directional dielectric anisotropy in solids: U.S. Patent No. 2,963,642.

Bacon, L. O., 1965, Induced polarization logging in the search for native copper: Geophysics, v. 30, p. 246-256.

Bailey, C. B., 1961, Matrix inversion by Gauss's method: Michigan State University Computer Laboratory Computer Program Description 00000048.

Bayley, R. W., 1959, Geology of the Lake Mary quadrangle, Iron County, Michigan: U.S. Geol. Surv. Bull. 1077.

Beam, W. R., 1965, Electronics of solids: New York, McGraw-Hill Book Co.

Berry, L. G. and Mason, B., 1959, Mineralogy: San Francisco, W. H. Freeman and Company.

Bewley, L. V., 1948, Two-dimensional fields in electrical engineering: New York, MacMillian Co.

Billings, M. P., 1954, Structural geology: Englewood Cliffs, Prentice Hall, Inc.

Bowman, F., 1958, Introduction to Bessel functions: New York, Dover Publications, Inc.

Boyce, W. E., and DiPrima, R. C., 1965, Elementary differential equations and boundary value problems: New York, John Wiley and Sons, Inc.

Boyum, B. H., 1963, The Marquette Iron Range, in Second summer conference, geology of the Lake Superior region, J. M. Neilson, director: Houghton, Michigan, College of Mining and Technology.

Buchheim, W., 1947, Die Bestimmung des Spezifischen Elektrischen Widerstandes von Anisotrop Leitenden Homogenen Medien Nach der Vier-Punkt-Methode: Geofisica Pura e Applicata, v. 10, p. 102-113.

Byerly, W. E., 1893 (1959 reprint), An elementary treatise on Fourier series and spherical, cylindrical, and ellipsoidal harmonics with applications to problems in mathematical physics: New York, Dover Publications, Inc.

Callen, H. B., 1961, Thermodynamics: New York: John Wiley and Sons, Inc.

Casimir, H. B. G., 1945, On Onsager's principle of microscopic reversibility: Rev. Modern Phys., v. 17, p. 343-350.

Collett, L. S., 1959, Laboratory investigations of overvoltage, in Overvoltage research and geophysical applications, J. R. Wait, editor: New York, Pergamon Press.

Cook, K. L., and Van Nostrand, R. G., 1954, Interpretation of resistivity data over filled sinks: Geophysics, v. 19, p. 761-790.

Corson, D. R. and Lorrain, P., 1962, Introduction to electromagnetic fields and waves: San Francisco, W. H. Freeman and Company.

Courant, R. and Hilbert, D., 1962, Methods of mathematical physics, vol. II: New York, Interscience Publishers.

Davis, H. F., 1961, Introduction to vector analysis: Boston, Allyn and Bacon, Inc.

De Groot, S. R., and Mazur, P., 1954a, Extension of Onsager's theory of reciprocal relations, I: Phys. Rev., v. 94, p. 218-224.

_____, 1954b, Extension of Onsager's theory of reciprocal relations II: Phys. Rev., v. 95, p. 224-226.

Deppermann, K., 1954, Die Abhängigkeit des scheinbaren Widerstandes vom Sondenabstand bie der Vierpunkt-Methode: Geophys. Prosp., v. 2, p. 262-273.

Dowling, F. L., 1967, Preliminary magnetotelluric resistivity results across the Wisconsin Arch, in Thirteenth annual institute on Lake Superior geology abstracts: East Lansing, Michigan State University.

_____, 1969, Personal communication.

Faddeeva, V. N., 1959, Computational methods of linear algebra: New York, Dover Publications Inc., (translated by: C. D. Benster).

Field, R. F., 1954a, Permittivity--lumped circuits, in Dielectric materials and applications, A. von Hippel, editor: Cambridge, the M.I.T. Press.

_____, 1954b, Errors occurring in the measurement of dielectric constant: Proc. A.S.T.M., v. 54, p. 456-478.

Grant, F. S., and West, G. F., 1965, Interpretation theory in applied geophysics: New York, McGraw-Hill Book Co.

Gray, A., and Mathews, G. B., 1922 (1966 reprint), A treatise on Bessel functions and their applications to physics: New York, Dover Publications Inc.

Halliday, D., and Resnick, R., 1961, Physics for students of science and engineering: New York: John Wiley and Sons.

Hartshorn, L., and Ward, W. H., 1936, The measurement of the permittivity and power factor of dielectrics at frequencies from 10^4 to 10^8 cycles per second: Proc. Instn. Elect. Engrs. (London), v. 79, p. 598-609.

Harvey, R. D., 1928, Electrical conductivity and polished mineral surfaces: Econ. Geology, v. 23, p. 778-803.

Heiland, C. A., 1940, Geophysical Exploration: Englewood Cliffs, Prentice-Hall, Inc.

Henrickson, E. L., 1956, A study of the metamorphism of the upper Huronian rocks of the western portion of the Marquette District, Northern Peninsula, Michigan: Unpublished Ph.D. thesis, University of Minnesota, Minneapolis.

Hewitt, D. F., 1959, Geology of Cardiff and Faraday Townships: Sixty-sixth annual report of the Ontario Department of Mines, v. 66, part 3.

Howell, B. F., and Licastro, P. H., 1961, Dielectric behavior of rocks and minerals: Am. Mineralogist, v. 46, p. 269-288.

Hummel, J. N., 1932, A theoretical study of apparent resistivity in surface potential methods: A.I.M.E. Trans., v. 97, p. 392-422. (Translation by J. A. Malkovsky of two articles by the author under the title: Der scheinbare spezifische Widerstand: Zeitschr. f. Geophysik, v. 5, 1929, p. 89 and 228).

Jakosky, J. J., 1950, Exploration geophysics: Newport Beach, Trija Publishing Co.

James, H. L., 1955, Zones of regional metamorphism in the Precambrian of Northern Michigan: Geol. Soc. America Bull., v. 66, p. 1455-1488.

Jenkins, G. M., and Watts, D. G., 1968, Spectral analysis and its applications: San Francisco, Holden-Day.

Katchalsky, A., and Curran, P. F., 1965, Nonequilibrium thermodynamics in biophysics: Cambridge, Harvard University Press.

Keck, W. G., and Colby, W. F., 1942, The depth dependence of earth conductivity upon surface potential data: Jour. of Applied Physics, v. 13, p. 179-188.

Keevil, N. B., and Ward, S. H., 1962, Electrolite activity: Its effect on induced polarization: Geophysics, v. 27, p. 677-690.

Keller, G. V., 1966, Electrical properties of rocks and minerals, in Handbook of physical constants, S. P. Clark, Jr., editor, Geol. Soc. America Mem. 97.

_____, 1967, Personal communication.

_____, and Frischknecht, F. C., 1966, Electrical methods in geophysical prospecting, New York, Pergamon Press.

_____, and Licastro, P. H., 1959, Dielectric constant and electrical resistivity of natural state cores: U.S. Geol. Surv. Bull. 1052-H.

Kellogg, O. D., 1929 (1959 reprint), Foundations of potential theory: New York, Dover Publications, Inc.

Knox, W. P., 1964, A comparison of the Schlumberger and Wenner geoelectrical sounding systems: Unpublished M.S. thesis, University of Minnesota, Minneapolis.

Kreyszig, E., 1967, Advanced engineering mathematics: New York, John Wiley and Sons, Inc.

Liessman, G., 1964, Messung elektrisher Eigenschaften von Gestein: Gerlands Beitr. z. Geophysik, v. 73, p. 317-327.

McEuen, R. B., Berg, J. W., Jr., and Cook, K. L., 1959, Electrical properties of synthetic metalliferous ore: Geophysics, v. 24, p. 510-530.

MacInnes, D. A., 1961, The principles of electrochemistry: New York, Dover Publications, Inc.

Mandel, P., Jr., Berg, J. W., Jr., and Cook, K. L., 1957, Resistivity studies of metalliferous synthetic cores: Geophysics, v. 22, p. 398-411.

Marcus, M., and Minc, H., 1965, Introduction to linear algebra: New York, The MacMillian Co.

Martin, H. M., 1937, The centennial geological map of Michigan (1:500,000); Part I--Northern Peninsula: Michigan Geol. Survey, Pub. 39, Ser. 33.

Mayper, V., 1959, The normal effect--part I, in Over-voltage research and geophysical applications, J. R. Wait, editor: New York, Pergamon Press.

Merritt, D. W., 1963, Velocity anisotropy studies in Precambrian lamellar formations: The Compass, v. 41, p. 28-39.

Mooney, H. M., Orellana, E., Pickett, H., and Tornheim, L., 1966, A resistivity computation method for layered earth models: Geophysics, v. 31, p. 192-203.

Moore, W. J., 1964, Physical chemistry: Englewood Cliffs, Prentice-Hall, Inc.

Nye, J. F., 1964, Physical properties of crystals: Oxford, Clarendon Press.

Onsager, L., 1931a, Reciprocal relations in irreversible processes, I: Phys. Rev., v. 37, p. 405-426.

_____, L., 1931b, Reciprocal relations in irreversible processes, II: Phys. Rev., v. 38, p. 2265-2279.

Orellana, E., and Mooney, H. M., 1965, Master tables and curves for geoelectrical sounding over layered structures: Madrid, Instituto de Geofisica.

Orr, W. R., 1964, Method for determining directional inductive anisotropy of materials by measuring Q factor: U.S. Patent No., 3,151,292.

Parasnis, D. S., 1956, The electrical resistivity of some sulphide and oxide minerals and their ores: Geophys. Prosp., v. 4, p. 249-278.

Parkhomenko, E. I., 1967, Electrical properties of rocks: New York, Plenum Press, (translated by: G. V. Keller).

Peters, L. J., and Bardeen, J., 1932, Some aspects of electrical prospecting applied in locating oil structures: Physics, v. 2, p. 103-122.

Quraishi, R., 1967, Laboratory determination of electrical properties of mineralized porphyry by the induced polarization method: Unpublished M.S. thesis, University of Arizona, Tucson.

Rao, D. A. A. S. N., 1948, Dielectric anisotropy of rocks: Proc. Indian Acad. Sci., v. 28A, p. 26-29.

Robinson, E. A., 1967, Multichannel time series analysis with digital computer programs: San Francisco, Holden-Day, Inc.

Roman, I., 1931, How to compute tables for determining electrical resistivity of underlying beds and their application to geophysical problems: U.S. Bur. Mines, Tech. Paper 502.

Schlumberger, C., Schlumberger, M., and Leonardon, 1934, Some observations concerning electrical measurements in anisotropic media and their interpretation: A.I.M.E. Trans., v. 110, p. 159-182.

Scott, J. H., Carroll, R. D., and Cunningham, D. R., 1967, Dielectric constant and electrical conductivity measurements of moist rock: A new laboratory method: J. Geophys. Res., v. 72, p. 5101-5115.

Scott, W. J., and West, G. F., 1969, Induced polarization of synthetic, high-resistivity rocks containing disseminated sulfides: Geophysics, v. 34, p. 87-100.

Seigel, H. O., 1959a, A theory of induced polarization effects (for step-function excitation), in Overvoltage research and geophysical applications, J. R. Wait, editor: New York, Pergamon Press.

Seigel, H. O., 1959b, Mathematical formulation and type curves for induced polarization: Geophysics, v. 24, p. 547-565.

Sharbaugh, A. H., and Roberts, S., 1959, Dielectric measurement procedures, in Methods of experimental physics--Solid state physics, v. 6, pt. B, K. Lark-Horvitz and V. A. Johnson, editors: New York, Academic Press.

Sherwood, G. E. F., and Taylor, A. E., 1957, Calculus: Englewood Cliffs, Prentice-Hall, Inc.

Shaub, Y. B., 1964, Measurement of rock resistivity in alternating electric and magnetic fields: Izv. Geophysics Ser., no. 10, p. 920-923.

Sillars, R. W., 1937, The properties of a dielectric containing semiconducting particles of various shapes: Proc. Instn. Elect. Engrs. (London), v. 80, p. 378-394.

Simmons, G., and Nur, A., 1968, Granites: Relations of properties insitu to laboratory measurements: Science, v. 162, p. 789-791.

Simandoux, P., 1963, Measures diélectriques en milieu poreux, Application a la mesure des saturations en eau étude du comportment des massifs argileux: Revue de L'Institut Francais du Petrole, supplementary issue, p. 193-214.

Slichter, L. B., and Telks, M., 1942, Electrical properties of rocks and minerals, in Handbook of physical constants, Birch, Schairer, and Spicer, editors: Geol. Soc. America, Spec. Paper 36.

Sokolnikoff, I. S., 1951, Tensor analysis, theory and applications: New York, John Wiley and Sons, Inc.

Smith, A. C., Janak, J. F., and Adler, R. B., 1967, Electric conduction in solids: New York, McGraw-Hill Book Co.

Stacey, F. D., 1961, Dielectric anisotropy and fabric of rocks: Geofisica Pura e Applicata, v. 48, p. 40-48.

Stefanesco, S., Schlumberger, C., and Schlumberger, M., 1930, Sur la distribution électrique potentielle autour dúne prise de terre ponctuelle dans un terrain a couches horizontales homogenes et isotropes: Jurnal de Physique el la Radium, v. 1, p. 132-140.

Stonehouse, H. B., 1967, Institute on Lake Superior geology guidebook for field trip to the Grenville of Southeastern Ontario: East Lansing, Michigan State University.

Stout, M. B., 1960, Basic electrical measurements: Englewood Cliffs, Prentice-Hall, Inc.

Strangway, D. W., 1969, Moon: Electrical properties of the uppermost layers: Science, v. 165, p. 1012-1013.

Tammemogi, H., 1969a, A magnetotelluric study in the Lake Superior area: Unpublished M.S. thesis, University of Toronto, Toronto.

_____, 1969b, A magnetotelluric study of the Northeastern Lake Superior area, in Fifteenth annual institute on Lake Superior geology abstracts: Oshkosh, Wisconsin State University.

Tranter, C. J., 1966, Integral transforms in mathematical physics: London, Methuen and Co., Ltd.

Turner, F. J., and Weiss, L. E., 1963, Structural analysis of metamorphic tectonites: New York: McGraw-Hill Book Co.

Vacquier, V., Holmes, C. R., Kintzinger, P. R., and Lavergne, M., 1957, Prospecting for ground water by induced electrical polarization: Geophysics, v. 22, 1957, p. 660-687.

Van Hise, C. R., and Bayley, W. S., 1897, The Marquette iron bearing district of Michigan: U.S. Geol. Surv. Monograph 28.

_____, and Lieth, C. K., 1911, The geology of the Lake Superior region: U.S. Geol. Surv. Monograph 52.

Van Nostrand, R. G., and Cook, K. L., 1966, Interpretation of resistivity data: U.S. Geol. Surv. Prof. Paper 499.

Villar, J. W., 1965, Metamorphic petrology of the Animikie Series in the Republic Trough area, Marquette County, Michigan: Unpublished Ph.D. thesis, Michigan State University, East Lansing.

v. Hippel, A., 1954a, Macroscopic properties of dielectrics, in Dielectric materials and applications, A. v. Hippel, editor: Cambridge, M.I.T. Press.

v. Hippel, A., 1954b, Molecular properties of dielectrics, in Dielectric materials and applications, A. v. Hippel, editor, Cambridge, M.I.T. Press.

_____, 1954c, Dielectrics and waves: Cambridge, M.I.T. Press.

Wait, J. R., 1959, A phenomenological theory of overvoltage for metalic particles, in Overvoltage research and geophysical applications, J. R. Wait, editor: New York, Pergamon Press.

Walstrom, E. E., 1962, Optical crystallography: New York, John Wiley and Sons, Inc.

Ward, S. H., 1953, A method for measuring the electrical conductivity of diamond drill core specimens: Geophysics, v. 17, p. 434-447.

_____, and Fraser, D. C., 1967, Conduction of electricity in rocks, in Society of Exploration Geophysics Mining geophysics, Volume II, Hansen, Heinrichs, Holmer, MacDougall, Rogers, Sumner, and Ward, editors: Tulsa, The Society of Exploration Geophysicists.

Watson, G. N., 1944, A treatise on the theory of Bessel functions: London, Cambridge University Press.

Weeg, G. P., and Reed, G. B., 1966, Introduction to numerical analysis: Waltham, Mass., Blaisdell Publishing Company.

Wert, C. A., and Thompson, R. M., 1964, Physics of solids: New York, McGraw-Hill Book Co.

Whitaker, J. T., 1966, Ultrasonic velocity measurements of Precambrian metamorphic rocks and their correlation with field measurements: Unpublished M.S. thesis, Michigan State University, East Lansing.

Wyllie, M. R. J., 1963, The fundamentals of well log interpretation: New York, Academic Press.

GENERAL REFERENCES

GENERAL REFERENCES

Aldredge, R. F., 1937, The effect of dipping strata on earth resistivity determinations: Colo. School of Mines Quart., v. 32, p. 169-186.

Astrakhantsev, G. V., 1962, The relation between the specific inductive capacitance and the polarization capacity of rocks: Izv. Geophysics Ser., no. 12, p. 1128-1129.

Belluigi, A., 1934, Über den Effekt der Anisotropie bie Gleichstrommessungen: Beiträge zur Angewandte Geophysik, v. 4, p. 400-406.

Birnbaum, A., 1962, On the foundations of statistical inference: Jour. Am. Stat. Assoc., v. 57, p. 269-326.

Bridgman, P. W., 1961, The thermodynamics of electrical phenomena in metals and a condensed collection of thermodynamic formulas: New York, Dover Publications, Inc.

Brunschwig, M., and Ahrens, T. J., 1960, Estimation of the physical constants of the lunar surface: University of Michigan Research Institute Report 3544-1-F.

Card, R. H., 1940, Correlation of earth resistivity with geological structure and age: A.I.M.E. Trans., v. 138, p. 380-398.

Daniel, V. V., 1967, Dielectric relaxation: New York, Academic Press.

Dunlap, W. C., Jr., 1959, Conductivity measurements on solids, in Methods of experimental physics--Solid state physics, v. 6, pt. B, K. Lark-Horvitz and V. A. Johnson, editors: New York: Academic Press.

Fraser, D. C., Keevil, N. B., Jr., and Ward, S. H., 1964, Conductivity spectra of rock from the Craigmont ore environment: Geophysics, v. 29, p. 832-847.

Fricke, H., 1924, A mathematical treatment of the electric conductivity and capacity of disperse systems: Phys. Rev., v. 24, p. 575-587.

Frische, R. H., and von Buttlar, H., 1957, A theoretical study of induced electrical polarization: Geophysics, v. 22, p. 688-706.

Hammond, S. B., 1961, Electrical engineering: New York, McGraw-Hill Book Co.

Hinze, W. J., Parsons, W. H., and Secor, G. B., 1964, Chemical and physical properties of possible lunar materials: Bendix Corporation preliminary report SMSS-60.

Hungerford, E. T., 1965, Electromagnetic well surveying method and apparatus for obtaining bith dip and conductivity anisotropy of a formation: U.S. Patent No. 3,187,252.

Kendal, M. G., 1959, Hiawatha designs an experiment: The Am. Statistician, v. 13, No. 5, p. 23-24.

Kerr, P. F., 1959, Optical mineralogy: New York, McGraw-Hill Book Co.

Kunz, K. S., and Moran, J. H., 1958, Some effects of formation anisotropy on resistivity measurements in boreholes: Geophysics, v. 23, p. 770-794.

Langbein, D., 1961, Elektrische Leitungsphänomene in anisotropen Medien I: Zeit. f. Physik, v. 162, p. 542-556.

_____, 1962, Elektrische Leitungsphänomeme in anisotropen Medien II: Zeit. f. Physik, v. 166, p. 22-41.

Langer, R. E., 1933, An inverse problem in differential equations: Bull. Am. Math. Soc., v. 22 (ser. 2), p. 814-820.

Leonardon, E. G., and Kelly, S. F., 1929, Some applications of potential methods to structural studies: A.I.M.E. Trans., v. 81, p. 180-198.

Maxwell, J. C., 1891 (1954 reprint), A treatise on electricity and magnetism: New York, Dover Publications, Inc.

Maeda, K., 1955, Apparent resistivity for dipping beds: Geophysics, v. 20, p. 123-139.

Maillet, R., 1947, The fundamental equations of electrical prospecting: Geophysics, v. 12, p. 529-556.

Manning, M. F., and Bell, M. E., 1940, Electrical conduction and related phenomena in solid dielectrics: Rev. of Modern Physics, v. 12, p. 215-256.

Marshall, D. J., and Madden, T. R., 1959, Induced polarization, a study of its causes: Geophysics, v. 24, p. 790-816.

Mooney, H. M., 1954, Effect of a variable surface layer on apparent resistivity data: Min. Eng., v. 6, p. 1210-1212.

_____, 1955, Depth determinations by electrical resistivity: Min. Eng., v. 7, p. 915-918.

_____, and Wetzel, W. W., 1956, The potentials about a point electrode and apparent resistivity curves for a two-, three-, and four-layered earth: Minneapolis, University of Minnesota Press.

Morse, P. M., and Feshbach, H., 1953, Methods of theoretical physics: New York, McGraw-Hill Book Co.

Müller, M., 1931, Der Einfluss der Anisotropie der Gesteinsmedien auf die Verteilung niederperiodischer eledtromagnetischer Wechselfelder: Gerlands Beitr. z. Geophysik, v. 30, p. 142-195.

Muskat, M., 1933, Potential distribution about an electrode on the surface of the earth: Physics, v. 4, p. 129-147.

Pirson, S. J., 1935, Effect of anisotropy on apparent resistivity curves: Bull. A.A.P.G., v. 19, p. 37-57.

Roman, I., 1957, An image analysis of multiple-layer resistivity problems: Geophysics, v. 24, p. 485-509.

Scott, A. H., and Curtis, H. L., 1939, Edge correction in the determination of dielectric constant: Jour. of Research, National Bur. of Standards, v. 22, p. 747-775.

Stratton, J. A., 1941, Electromagnetic theory: New York, McGraw-Hill Book Co.

Tagg, G. F., 1964, Earth resistances: New York, Pitman Press.

Unz, M., 1953, Apparent resistivity curves for dipping beds: Geophysics, v. 18, p. 116-137.

Van der Pauw, L. J., 1958, A method of measuring specific resistivity and Hall effect of disks of arbitrary shape: Philips Research Reports, v. 13, p. 1-9.

_____, 1961, Determination of resistivity tensor and Hall tensor of anisotropic conductors: Philips Research Reports, v. 16, p. 187-195.

Wait, J. R., Frische, R. H., and von Buttlar, H., 1958, Discussions on a theoretical study of induced electrical polarization: Geophysics, v. 23, p. 144-153.

Weeks, J. R., Jr., 1922, The dielectric constant of mica: Physical Review, v. 19, p. 319-322.

Wood, W. W., 1964, Regional metamorphism of Southeast Iron County, Michigan: Unpublished term paper, Michigan State University, East Lansing.

APPENDICES

APPENDIX A

REVIEW OF POLARIZATION MECHANISMS

REVIEW OF POLARIZATION MECHANISMS

Introduction

The present laboratory investigation is macroscopic in nature (at least in the solid state physics sense). As such, quantitative microscopic polarization models are not required. However, qualitative microscopic polarization models are very useful for predicting experimental results before experimentation is commenced and explaining experimental observations after experimentation is completed. For these reasons, a catalog of the microscopic polarization models of others has been included as an appendix.

Electronic Polarization

The classical idea of an atom consists of a dense, positively charged nucleus surrounded by a diffuse cloud of negatively charged electrons. In the presence of an $\underline{E}$ field, the centers of gravity for the nucleus and electron cloud undergo a relative shift, which produces a microscopic electric dipole. The magnitude of this shift depends upon the field strength, $\underline{E}$, atomic number of the atom, Z, and the radius of the electron cloud, von Hippel (1954b, 1954c), Wert and Thompson (1964), and R. Beam (1965) assume a simple spherical atomic model

with the polarization displacement reaching equilibrium between forces due to the external $\underline{E}$ field and the coulombic attraction of the shifted charge centers. In the presence of an oscillating $\underline{E}$ field the polarization of this model is analogous to the motion of a driven damped harmonic oscillator. With this somewhat simplified model, they obtain:

$$\alpha_e = \sqrt{\frac{e^2/m}{\omega_o'^2 - \omega^2 + j\omega 2\alpha}}\ , \qquad \text{A.1}$$

where: e and m are the electronic charge and mass, respectively, $j = \sqrt{-1}$,

$\omega_o' = \sqrt{\omega_o^2 - \frac{Ne^2}{3m\varepsilon_o}}$, is the resonance (angular) frequency of the damped harmonic oscillators, of density, N,

$\omega_o = \sqrt{k/m'}$ is the resonance (angular) frequency of the corresponding simple harmonic oscillator model with elastic constant (bonding strength), k,

$2\alpha = \frac{\mu_o e^2 \omega_o^2}{6\pi mc}$ is the electromagnetic attenuation (damping) factor,

μ_o is the magnetic permeability of free space and c is the velocity of light, respectively,

for the steady state electric polarizability. The relationship of equation A.1 yields a frequency dependent, or dispersive, polarizability.

For D.C. $\underline{E}$ fields, $\omega = 0$ and equation A.1 becomes:

$$\alpha_e = \frac{3\varepsilon_o e^2}{3\varepsilon_o k - Ne^2} \cong \frac{e^2}{k} = 4\pi\varepsilon_o R^3, \qquad \text{A.2}$$

for low N. The polarizability models given by equations A.1 and A.2 apparently agree with observations quite well (Wert and Thompson, 1964). The polarization mechanism described by the models of equations A.1 and A.2 is called induced, or electronic, polarization and its polarizability is indicated by α_e. The term, induced polarization, is undesirable, both from the standpoint that geophysicists also use this term to describe a different polarization mechanism and because all polarization mechanisms due to an external field are, in fact, induced. For this reason, the polarization mechanism described by equations A.1 and A.2 will be referred to as electronic polarization in this paper.

Ionic Polarization

When atoms combine into molecules, there is generally an unequal distribution of charge, giving rise to positive and negative charge centers. In the presence of an $\underline{E}$ field, these charge centers undergo a relative shift

from their equilibrium positions (in the absence of $\underline{E}$). This mechanism is really similar to that for electronic polarization, however, the charge center geometries and masses are different. The damped harmonic oscillator model for electronic polarization was assumed to be isotropic and thus have three degrees of vibrational freedom. A dipolar molecule requires an anisotropic damped oscillator model, with only one degree of vibrational freedom. Von Hippel (1954c) and Beam (1965) use an anisotropic damped harmonic oscillator and obtain:

$$\alpha_I = \frac{q^2/3m}{\omega_o'^2 - \omega^2 + j\omega 2\alpha} , \qquad A.3$$

as the steady state polarizability for multivalent diatomic molecules where ω_o', j, and 2α are as was defined for the electronic polarization model, q is the dipole charge, and 1/3 is the factor needed to convert from three to one degree of vibrational freedom.

For static $\underline{E}$ fields, $\omega = 0$ and equation A.3 becomes:

$$\alpha_I = \frac{q^2}{3k} , \qquad A.4$$

for low N. This type of polarization is called ionic, or atomic, polarization and is indicated by α_I. The term, ionic polarization will be used for this paper.

Dipole Relaxation Polarization

Some molecules, such as water and HCl, are highly dipolar. In the gaseous, liquid, and, to a lesser extent, solid state, such molecules attempt to physically align themselves parallel to any $\underline{E}$ field. Opposing this alignment will be intermolecular and thermal forces. For diffuse fluids with negligible intermolecular forces, von Hippel (1954b) and Beam (1965) obtained:

$$\alpha_d = \frac{\underline{p}_p^2/3k\theta}{1 + j\omega\tau} , \qquad \text{A.5}$$

for the steady state polarizability, where $\tau = \frac{4\ \pi a^3 \eta}{k\theta}$ is the relaxation time constant for a spherical molecular model of radius, a, k is Boltzman's constant, θ, is the temperature in ^{o}K, η is the viscosity of the fluid, and $\underline{p}_p$ is the permanent dipole moment of the molecule. This mechanism is called dipole relaxation, molecular, or orientation, polarization and its polarizability is indicated as α_d. Dipole relaxation appears to be the most commonly used name for this mechanism and will be used in this paper. Dipole relaxation in solids will be similar to that in fluids, however, the polarizability will be more complicated than that given by equation A.5 and include the effects of intermolecular forces. I could find no treatment of this more complicated problem.

For static $\underline{E}$ fields, $\omega = 0$ and equation A.5 becomes:

$$\alpha_d = \frac{p^2}{3k\theta} , \qquad \text{A.6}$$

for models assuming negligible intermolecular forces. Models, which consider intermolecular forces, should have more complicated static α_d than that given by equation A.6.

Interfacial Polarization

The above polarization mechanisms (electronic, ionic, and dipole relaxation polarization) are sufficient to describe electric polarization within a homogeneous material. For such materials, the total polarizability is simply the sum of the above polarizabilities.

Most rocks, however, are far from homogeneous. For such inhomogeneous materials, an additional polarization mechanism must be added to account for the collection of charge at the boundaries of the inhomogenities in the presence of an $\underline{E}$ field. Such a mechanism is called space-charge, or interfacial, polarization and its polarizability is indicated as α_i. This is one of the primary mechanisms involved in what geophysicists refer to as induced polarization. Keller and Freschknecht (1966) mention this phenomena, but do not pursue the matter further. The term, interfacial polarization, will be used in this paper, for its initials (I.P.) can then be

used in geophysical literature without causing further confusion.

Wait (1959) describes an interfacial polarization model consisting of spherical particles of conductivity, σ_p, and radius, a, coated with an insulating film of thickness, t_m, and dielectric constant, K_m, suspended uniformly in a medium of conductivity, σ. With this model, he obtained:

$$\alpha_i = \frac{3v}{N}\left(\frac{1 - \delta}{1 + 2\delta}\right), \qquad \text{A.7}$$

for the steady state polarizability, where $v = 4\ \pi a^3 N/3$, N is the inhomogenity density, and $\delta = \frac{\sigma}{\sigma_p} + \frac{t_m \sigma}{j\omega\varepsilon_m a}$.

Sillars (1937) obtained the results for an ideal dielectric of dielectric constant, K_1, containing spheroidal inhomogenities of conductivity, σ_2, and dielectric constant, K_2, with semi-axes, a, parallel to $\underline{E}$, and b = c, normal to $\underline{E}$. With such a model, he obtained:

$$\alpha_i = \frac{1}{N}\left[K + \frac{K_1 N}{1 + \omega^2\tau^2} - 1 - j\,\frac{K_1 N\omega\tau}{1 + \omega^2\tau^2}\right], \qquad \text{A.8}$$

for the steady state polarizability where $\tau \equiv \frac{K_1(n-1) + K_2}{4\pi\sigma_2}$

$$N \equiv q\,\frac{n^2 K_1}{K_1(n-1) + K_2}, \quad K = K_1\left[1 + q\,\frac{n(K_2 - K_1)}{K_1(n-1) + K_2}\right],$$

$$n = 4\pi/l_a,$$

q is the spheroid volume fraction of the dielectric,

$$l_a = 4\pi\left\{\frac{1}{e^2} - \left[\frac{\sqrt{(1-e^2)}}{e^3}\sin^{-1}e\right]\right\}, \text{ for oblate spheroids}$$

$(l_a \cong 4\pi$ when a << b, c),

$$l_a = 4\pi\left(\frac{1}{e^2} - 1\right)\left(\frac{1}{2e}\log\frac{1+e}{1-e} - 1\right), \text{ for prolate}$$

spheroids $\left(l_a \cong 4\pi\frac{b^2}{a^2}\left(\log\frac{2a}{b} - 1\right)\right.$ when a >> b, c),

$e = \sqrt{1 - \frac{a^2}{c^2}} = \sqrt{1 - \frac{a^2}{b^2}}$ is the eccentricity of the spheroids.

The coefficient, n, is a function of the eccentricity of the spheroids and varies from a value of unity, for a very flat oblate spheroid, to infinity, for a very long prolate spheroid. For a sphere, n = 3.

APPENDIX B

COMPUTER PROGRAM AND SUBROUTINE DESCRIPTIONS

COMPUTER PROGRAM AND SUBROUTINE DESCRIPTIONS

Introduction

This appendix contains the program and subroutine discriptions for only one rather involved program. The input for this program (ELECT) consists of the Schering bridge balance readings, the sample disk dimensions, the disk orientations, and the measurement frequencies. The final output is the principal values and directions, of the K and σ tensors, with respect to the laboratory axis system.

The main program, ELECT, exists primarily to call the semi-autonomous subroutines: KRD, TENSØR, and REDUCE, which apply successive reduction steps to the laboratory data. The program and subroutines of this appendix were written in FØRTRAN for the CDC 3600 computer available at Michigan State University. They may need some revision if used on some other system.

Some of the subroutines described in this appendix were obtained from the book by Robinson (1967) and the Michigan State University Computer Library, but most were written by the author. Robinson (1967) uses the ingeneous

device of storing multiple dimensioned arrays as column vectors in his calling program, or subroutines. The author found this to be an invaluable aid in conserving storage space, for then the respective arrays could be dummy dimensioned in the called subroutines.

The three major working subroutines, mentioned above, were written and debugged separately before insertion into the main program. They were combined into a single program, because the final principal values and directions were what was most desired from the original data. Combining these successive data reduction operations end-to-end in a single program eliminated the need for intermediate physical data handling. As an aid in interpretation and quality control, the results of three stages in the data reduction operations are printed out.

Program ELECT and the three major subroutines were written specifically for the problem described in Chapters III, IV, and V of this paper. However, most of the smaller subroutines are perfectly general in nature and may easily be adapted for use in other programs. This is a great advantage in modular programming, for subroutines developed for one program can then also be used for other programs.

Program Description: ELECT

Purpose

To convert directional measurements of σ and K into the respective tensor coefficients and to obtain their principal directions and values.

Usage

The input deck order for program elect is shown in Figure B.1. The input variables are:

NØSPLS--number of data sets which are to be processed.
NAME--data set identification.
NØDXN--number of directions in which the electrical properties were measured.
NØFQ--number of frequencies at which the electrical properties were measured.
NM--measurement direction identification.
SDM--sample disk diameter, in inches.
T--sample disk thickness, in mills.
A(I,NTM)--direction angles of the NTM measurement direction (NTM = 1, NØDXN; I = 1, 3).
INDC--corrected-uncorrected capacitance value indicator (if INDC ≠ 0, the capacitance values are pre-corrected).
F--the measurement signal frequency, in cps.
FO--bridge frequency range setting, in cps.
C1--initial capacitance balance reading (see Chapter V), in pf.
C2--second capacitance balance reading, in pf.
D1--initial dissipation factor balance reading.
D2--second dissipation factor balance reading.
L(I)--direction cosines of the arbitrary direction used to initiate the iterative rotation procedure of Chapter VI (I = 1, 3).

Only cards 1 and 2 are read by the main program, ELECT. The rest of the data deck of Figure B.1 is read by KRD and REDUCE.

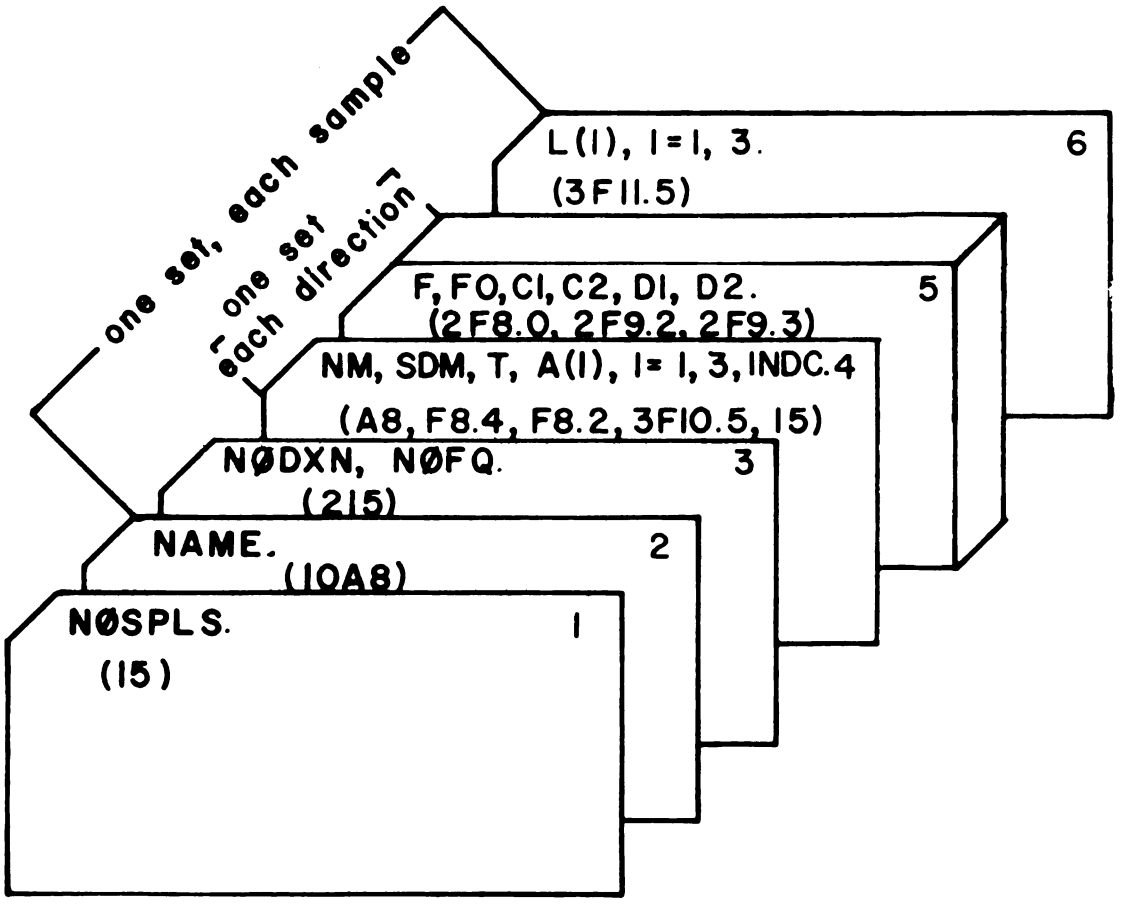

Fig. B.1.--Deck order for program ELECT.

Method

Program ELECT is really a dummy program which combines the operations of the three semi-autonomous major subroutines: KRD, TENSØR, and REDUCE. It is these three major subroutines which actually do the operations required to accomplish the purpose of program ELECT.

Restrictions

The carriage controls used in FØRMAT statements 1 and 4 may only be valid for the Michigan State University

CDC 3600. This program requires the use of three scratch units (here numbered 25, 26, and 27). Program ELECT requires subroutines: KRD, TENSØR, and REDUCE. Other restrictions will be listed with each of the individual subroutines.

```
      PROGRAM ELECT
      DIMENSION NAME (10)
    1 FORMAT (*1*/*4ROCK ELECTRICAL PROPERTIES*//)
    2 FORMAT (I5)
    3 FORMAT (10A8)
    4 FORMAT (*1PROGRAM COMPLETED*)
C     *****   MAIN PROGRAM   *****
      READ 2, NOSPLS                                              READ
      DO 31 NOTIM = 1, NOSPLS
      PRINT 1                                                     PRINT
      READ 3, NAME                                                READ
      PRINT 3, NAME                                               PRINT
      REWIND 25
      REWIND 26
      REWIND 27
      CALL KRD (NODXN, NOFQ)
      IT = 0
      CALL TENSOR (NODXN, NOFQ, NAME)
      CALL REDUCE (NOFQ, NAME)
   31 CONTINUE
      PRINT 4                                                     PRINT
      END
```

Subroutine Description: KRD

Purpose

To convert the initial laboratory data obtained from the General Radio 716-C capacitance bridge, available in the Michigan State University Department of Geology, into directional values for σ and K.

Usage

The calling sequence is:

CALL KRD (NØDXN, NØFQ)
NØDXN--number of directions in which the electrical properties were measured.
NØFQ--number of frequencies at which the electrical properties were measured.

Subroutine KRD reads NØDXN, NØFQ, NM, SDM, T, A(I,NTM), F(J), FO(J), C1(J), C2(J), D1(J), and D2(J) from the data deck.

Method

The measurement direction angles are converted to direction cosines by:

$$l = \cos^{-1}\phi.$$

If the Schering bridge balance C values are uncorrected, they are corrected by subroutine CØRRECT. The corrected C values and D values are converted into CP and corrected dissipation factors, D, by means of subroutine BRIDGE. The CP and corrected D values for both balances (see

Chapter V) along with the sample disk dimensions and measurement frequencies, are input into subroutine CAP to obtain the directional σ and K values at each measurement frequency. The measurement frequencies, direction cosines, and directional values of σ and K are then stored on scratch unit 25 until further use.

Restrictions

The variables, KE and SIG are specified to be double precision. Measurements can be made in no more than ten directions, and at no more than twenty frequencies without changing the dimension statements. Subroutine KRD calls subroutines: CØRRECT, BRIDGE, and CAP. Subroutine KRD uses a scratch unit (here, numbered 25). Care must be exercised to see that the data is read from the scratch unit in exactly the same manner in which it was written. The carriage controls used in the print formats may only be valid for the Michigan State University CDC 3600 computer.

```
      SUBROUTINE KRD (NODXN,NOFQ)
      TYPE DOUBLE KE,SIG
      DIMENSION NAME(10), F(20), F0(20), C1(20), C2(20)
      DIMENSION D1(20), D2(20), KE(20,10), SIG(20,10), A(3,10)
    1 FORMAT (2I5)
    2 FORMAT (A8, F8.4, F8.2, 3F10.5, I5)
    3 FORMAT (2F8.0, 2F9.2, 2F9.3)
    4 FORMAT (*1*/*4*,13X,* DIELECTRIC MATERIAL DATA REDUCTION*)
    5 FORMAT (*0*, 13X,* MEASURED IN DIRECTION,*, A8, *,* 3F12.5)
    6 FORMAT (*-*, 13X,* SAMPLE DIAMETER = *, F8.4, *   INCHES*)
    7 FORMAT (*0*, 13X, * SAMPLE THICKNESS = *, F8.2, *   MILLS*)
    8 FORMAT (*-*,17X,* F*,5X,* F0*, 5X,* C1*, 6X,* C2*, 7X,* D1*,
     1 6X,* D2*/)
    9 FORMAT (13X, 2F8.0, 2F9.2, 2F9.3)
   10 FORMAT (*-*,17X,* F*, 7X, * K*,5X,* CONDUCTIVITY (IN MHO/METER)*)
   11 FORMAT (13X, F8.0, F10.3, 8X, E14.3)
C     *****   MAIN   *****
      PI = 3.14159265358979
      READ 1, (NODXN, NOFQ)                                          READ
      DO 31 NTM = 1, NODXN
      READ  2, NM, SDM, T, (A(I,NTM), I = 1, 3), INDC                READ
      READ 3, (F(J), F0(J), C1(J), C2(J), D1(J), D2(J), J = 1, NOFQ)  READ
      PRINT 4                                                        PRINT
      PRINT 5, NM, (A(I,NTM), I = 1, 3)                              PRINT
      PRINT 6, SDM $      PRINT 7, T                                 PRINT
      DO 27 I = 1, 3
```

```
      PHI = PI*A(I,NTM)/180.00000
   27 A(I,NTM) = COS(PHI)
      PRINT 8                                                          PRINT
      PRINT 9, (F(J), F0(J), C1(J), C2(J), D1(J), D2(J), J = 1, NOFQ)  PRINT
      IF (INDC .NE. 0) GO TO 29
      DO 28 J = 1, NOFQ
      CALL CORRECT (C1(J))
   28 CALL CORRECT (C2(J))
   29 SDM = SDM*(2.540005E-02)
      T = T*(2.540005E-05)
      CNST = 1.000000000E-12
      DO 30 J = 1, NOFQ
      C1(J) = C1(J)*CNST      $      C2(J) = C2(J)*CNST
      CALL BRIDGE (F(J), F0(J), C1(J), D1(J), CP1)
      CALL BRIDGE (F(J), F0(J), C2(J), D2(J), CP2)
   30 CALL CAP (CP1,CP2,D1(J),D2(J),T,SDM,F(J),SIG(J,NTM),KE(J,NTM))
      PRINT 10                                                         PRINT
   31 PRINT 11, (F(J), KE(J,NTM), SIG(J,NTM), J = 1, NOFQ)             PRINT
C     *****   STORING DATA ON SCRATCH DRUM   *****
      REWIND 25
      WRITE (25), ((A(I,J), J = 1, NODXN), I = 1, 3)                   WRITE
      DO 32 I = 1, NOFQ
   32 WRITE (25), F(I), (KE(I,J), SIG(I,J), J = 1, NODXN)              WRITE
      REWIND 25    $      RETURN      $      END
```

Subroutine Description: CØRRECT

Purpose

To correct the capacitance readings on the General Radio 716-C capacitance bridge available in the Michigan State University Department of Geology, to calibrated values.

Usage

The calling sequence is:

CALL CØRRECT (RD)
RD--capacitance balance dial reading, in pf.

Method

If RD is between two calibration points, D_i, and D_{i+1}, the correction, CR is given by

$$SLP = (C_{i+1} - C_i)/(D_{i+1} - D_i),$$

$$CR = C_i + SLP(RD - D_i),$$

where the C_i and C_{i+1} are the corrections for the calibration points, D_i and D_{i+1}, respectively. The corrected value is then:

$$RD = RD + CR.$$

Restrictions

The C_i are valid only for the 716-C capacitance bridge available in the Michigan State University

Department of Geology. They will vary for each specific bridge and, perhaps with each calibration of the same bridge. The allowable range in RD is: 100 pf $\leqslant$ RD $\leqslant$ 1150 pf.

```
      SUBROUTINE CORRECT (RD)
C     *****   CAPACITANCE BRIDGE CORRECTIONS   *****
      DIMENSION D(15), C(15)
    1 FORMAT (* RAD DATA*)
      DO 10 I = 1, 11
   10 D(I) = I*100.000
      D(12) = 1150.000
      C(1) = -2.2  $      C(2) = -2.02 $      C(3) = -2.3
      C(4) = -2.21 $      C(5) = -2.6  $      C(6) = -2.28
      C(7) = -2.5  $      C(8) = -2.16 $      C(9) = -2.4
      C(10) = -1.75$      C(11) = -2.0 $      C(12) = -1.50
      DO 11 I = 1, 12
   11 IF (RD .GE. D(I) .AND. RD .LE. D(I+1))GO TO 12
      GO TO 13
   12 SLP = (C(I+1) - C(I))/(D(I+1) - D(I))
      CR = C(I) + SLP*(RD - D(I))
      RD = RD + CR
      GO TO 14
   13 PRINT 1                                                    PRINT
   14 RETURN        $      END
```

Subroutine Description: BRIDGE

Purpose

To convert the General Radio 716-C bridge balance readings of C and D into appropriate dissipation factors and parallel capacitances for the unknown element.

Usage

The calling sequence is:

```
CALL BRIDGE (F, FO, C, D, CP)
F--measurement frequency, in cps.
FO--bridge frequency range selector position, in cps.
C--corrected bridge capacitance dial reading, in f.
D--uncorrected bridge reading at input and unknown
   dissipation factor value on output.
CP--unknown parallel capacitance.
```

Method

D is first corrected for the measuring frequency:

$$D = 0.01 \frac{F}{FO} D^{\cdot}$$

Then a correction for the dissipation of the standard capacitor is applied:

$$D = D + 0.04/C.$$

The unknown dissipation factor, D, and the series capacitance, CS, are obtained from:

$$D = D\left(1 - 0.026 \frac{F}{FO} D\right),$$

$$CS = C\left(1 - 0.026 \frac{F}{FO} D\right).$$

The unknown parallel capacitance, CP, is then obtained from the relationships between equivalent series and parallel RC circuits (Stout, 1960):

$$CP = \frac{CS}{1 + D^2} .$$

Restrictions

This subroutine is intended only for use with a General Radio 716-C Capacitance bridge with a type 722 internal capacitor.

Acknowledgments

The correction and reduction equations used in this subroutine were obtained from the 716-C instrument manual and verified by the author.

```
      SUBROUTINE BRIDGE (F,F0,C,D,CP)
C     *****   SCHERING BRIDGE DATA REDUCTION   *****
      D = 0.01*...(F/F0)
      D = D + 0.14/(C*(1.0000CE+12))
      CS = C*(1.0000000000 - 0.(20*D*(F/F0)))
      D = D*(1.0000000000 - 0.026*D*(F/F0))
      CP = CS/(1.0000000000 + D**2)
      RETURN
      END
```

Subroutine Description: CAP

Purpose

To calculate σ and K values for measurements using a micrometer dielectric sample holder.

Usage

The calling sequence is:

CALL CAP (C1, C2, D1, D2, T, SDM, F, SIGMA, K)
C1--initial balance unknown parallel capacitance, in f.
C2--second balance unknown parallel capacitance, in f.
D1--initial balance unknown dissipation factor.
D2--second balance unknown dissipation factor.
T--sample disk thickness, in m.
SDM--sample disk diameter, in m.
SIGMA--sample disk effective conductivity, σ, in mho/m.
K--sample disk dielectric constant.
F--measurement frequency, in cps.

Method

Using the sample dimensions and the C1, C2, D1, and D2 values obtained from the bridge balances with and without the sample disk in the holder, the sample conductivity and dielectric constant are obtained from:

$$K = \frac{(C1 - C2)T}{A\varepsilon_o} + 1,$$

$$\sigma = \frac{\omega T(D1C1 - D2C2)}{A},$$

where $\omega = 2\pi F$ is the measurement angular frequency and $A = \pi(SDM/2)^2$ is the sample disk area, and $\varepsilon_o = 8.85 \cdot 10^{-12}$ f/m.

Restrictions

This subroutine should only be used to reduce data obtained by using a micrometer sample holder in the manner described in Chapter V. SIGMA and K are specified as double precision.

```
      SUBROUTINE CAP (C1,C2,D1,D2,T,SDM,F,SIGMA,K)
C     *****   LOSSEY DIELECTRIC MATERIAL DATA REDUCTION   *****
      TYPE DOUBLE K, SIGMA
      PI = 2.000000*ASIN(1.0000000000)
      OMEGA = 2.0000000000*PI*F
      AX = PI*((SDM/2.000000)**2)
      EPV = 8.85E-12
      GX = OMEGA*(D1*C1 - D2*C2)
      K = ((C1 - C2)*T/(AX*EPV)) + 1.0000000000
      SIGMA = GX*T/AX
      RETURN
      END
```

Subroutine Description: TENSØR

Purpose

To calculate the K and σ least square tensor coefficients and rms errors from directional measurements of K and σ.

Usage

The calling sequence is:

CALL TENSØR (NØDXN, NØFQ, NAME)
NØDXN--number of directions in which the electrical properties were measured.
NØFQ--number of frequencies at which the electrical properties were measured.
NAME--sample identification.

Method

Subroutine TENSØR is really a dummy, or bookkeeping, subroutine. The actual least square determinations and rms error calculations are done by subroutine LSQ. Subroutine TENSØR reads the direction cosines, frequencies, and directional K and σ values from scratch units 25 and 26 and inputs this information to LSQ for reduction. The least square coefficients and rms error for each frequency are then printed out. The measurement frequencies, the least square K and σ tensor coefficients, and the rms errors are then stored on scratch unit 27 for later use.

Restrictions

There can be no more than twenty elements in arrays K, KE, SIGMA, and CØND without changing the dimension

statements. Array DXN cannot have more than twenty-five elements and NAME, ten, without changing the dimension statements.

Variables KE, SIGMA, KR, SR, K, and CØND are specified as double precision. Subroutine TENSØR calls subroutines LSQ and ØUTPUT. Subroutine TENSØR was intended only to be used for the measurement technique given in Chapters V and VI of the text. Its use for other purposes may require revision.

This subroutine reads input from scratch units 25 and 26. Thus, the data must be stored on these tapes in exactly the same manner in which this subroutine reads it. Subroutine TENSØR also stores data on scratch units 26 and 27. Thus, this data must be read from these scratch units in exactly the same manner that it is written by this subroutine.

Variables DXN, K, KE, SIGMA, and CØND are multiply dimensioned arrays stored in column mode. This allows the use of dummy dimensions for these variables in any subroutine called from TENSØR.

The carriage controls used in the FØRTRAN statements may only be valid for the Michigan State University CDC 3600 system.

```
      SUBROUTINE TENSOR (NODXN, NOFQ, NAME)
      TYPE DOUBLE KE, SIGMA, KR, SR, K, COND
      DIMENSION DXN(50), K(20), KE(20), SIGMA(20), COND(20), NAME(10)
    1 FORMAT (*1*,/*4*, 13X, * SAMPLE *, 10A8)
    2 FORMAT (*0*, 13X, * FREQUENCY,*, F9.0, * CPS*)
    3 FORMAT (*0*, 13X, * RELATIVE TO LABORATORY AXIS SYSTEM*)
    4 FORMAT (*0*,37X,* DIRECTION COSINES*,21X,* DIELECTRIC CONSTANT*,
     C3X, * CONDUCTIVITY*/)
    5 FORMAT (13X,5(5X,E15.7))
    6 FORMAT (*-*, 13X, * DIELECTRIC CONSTANT TENSOR*)
    7 FORMAT (*0*,13X,* RMS DIELECTRIC CONSTANT ERROR FROM THE*,
     1 * MODEL = *, E15.8)
    8 FORMAT (*-*, 13X, * CONDUCTIVITY TENSOR (IN MHO/METER)*)
    9 FORMAT (*0*,13X,* RMS CONDUCTIVITY ERROR FROM THE MODEL = *,
     1 E15.8,* MHO/M*)
C     *****   READING DATA FROM SCRATCH DRUM   *****
      REWIND 25     $       REWIND 26     $       REWIND 27
      ND = 3*NODXN
      READ (25), (DXN(I), I = 1, ND)                                    READ
      WRITE (26), (DXN(I), I = 1, ND)                                   WRITE
      REWIND 26
      DO 36 NOTM = 1, NOFQ
      READ (26), (DXN(I), I = 1, ND)                                    READ
      REWIND 26
      READ (25), FREQ, (K(I), COND(I), I = 1, NODXN)                    READ
      PRINT 1, NAME$       PRINT 2, FREQ                                PRINT
```

```
      PRINT 3        $      PRINT 4                                    PRINT
      DO 35 I = 1, NODXN
      J = I + NODXN
      JJ = I + 2*NODXN
   35 PRINT  5, DXN(I), DXN(J), DXN(JJ), K(I), COND(I)                 PRINT
C     *****   DIELECTRIC CONSTANT REDUCTION   *****
      CALL LSQ (DXN, K, NODXN, KE, KR)
      PRINT 6                                                         PRINT
      CALL OUTPUT (3,3,1,KE)
      PRINT 7, KR                                                     PRINT
C     *****   CONDUCTIVITY REDUCTION   *****
      CALL LSQ (DXN, COND, NODXN, SIGMA, SR)
      PRINT 8                                                         PRINT
      CALL OUTPUT (3,3,1,SIGMA)
      PRINT 9, SR                                                     PRINT
C     *****   STORING DATA ON SCRATCH DRUM   *****
      WRITE (27), FREQ                                                WRITE
      WRITE (27), KR                                                  WRITE
      WRITE (27), (KE(I), I = 1, 9)                                   WRITE
      WRITE (27), SR                                                  WRITE
   35 WRITE (27), (SIGMA(I), I = 1, 9)                                WRITE
      REWIND 26      $      REWIND 27
      RETURN         $      END
```

Subroutine Description: ØUTPUT

Purpose

To print out a multiply dimensioned array as a series of matrices.

Usage

The calling sequence is:

CALL ØUTPUT (NRX, NCX, NX, X)
NRX--number of rows in each matrix of X.
NCX--number of columns in each matrix of X.
NX--number of matrices in X.
X--the array to be printed.

Method

A multiply dimensioned array, stored by columns and in multiplexed mode (see Robinson, 1967) is printed out as a series of matrices.

Restrictions

Subroutine ØUTPUT assumes that the array, X, is stored such that each matrix is stored by columns and the different matrices are multiplexed (see Robinson, 1967). This subroutine is general in nature and can be used to print out any array stored in this manner. The only change which may be necessary will be in the print format.

The total dimension for X, NRX•NCS•NX, cannot exceed the dimension for this variable in the calling routine. NCX cannot exceed seven without changing format statement 1.

The present format 1 will print out the elements of X as floating point numbers. X is specified as double precision.

The carriage control in format 2 may only be valid for the Michigan State University CDC 3600 system.

```
      SUBROUTINE OUTPUT (NRX,NCX,NX,X)
      TYPE DOUBLE X
      DIMENSION X(NRX,NCX,NX)
    1 FORMAT (18X,7E15.6)
    2 FORMAT (* *)
      DO 10 K = 1, NX
      PRINT 2
      DO 10 I = 1, NRX
   10 PRINT 1, (X(I,J,K), J = 1, NCX)
      RETURN
      END
```

Subroutine Description: LSQ

Purpose

To calculate least square tensor coefficients and rms errors for a symmetric second-rank tensor, given directional tensor values.

Usage

The calling sequence is:

CALL LSQ (D, B, N, A, G)
D--direction cosine array, stored by columns.
B--measured value column vector.
A--least square tensor coefficient matrix, stored by columns.
G--rms error (see Jenkins and Watts, 1968).

Method

The direction cosines of the measurement directions are converted into a coefficient matrix, C, by:

$$c_{i1} = d_{i1}^2, \qquad c_{i4} = 2d_{i2}d_{i3},$$

$$c_{i2} = d_{i2}^2, \qquad c_{i5} = 2d_{i3}d_{i1},$$

$$c_{i3} = d_{i3}^2, \qquad c_{i6} = 2d_{i1}d_{i2}.$$

The least square coefficients are then given by:

$$A = (C^T C)^{-1} C^T B,$$

where:

$$A_{11} = A_1, \qquad A_{23} = A_{32} = A_4,$$

$$A_{22} = A_2, \qquad A_{31} = A_{13} = A_5,$$

$$A_{33} = A_3, \qquad A_{12} = A_{21} = A_6.$$

The least square error, E, is given by:

$$E = ((I - C(C^TC)^{-1}C^TB)^T(I - C(C^TC)^{-1}C^TB),$$

and the rms error, G, by:

$$G = \sqrt{\frac{E}{p + 2 - 6}},$$

where p is the number of directional values available.

Restrictions

Subroutine LSQ is written in completely general form. Thus, it may be used to give least square coefficients and rms errors for any symmetric second-rank tensor on which directional measurements have been made. Subroutine LSQ calls subroutines TRNSPS, MATMULT, INVERT, IDENT, and ADD.

The variables A, C, CT, Z, ZNV, CØEF, G, and B are specified to be double precision. All arrays are stored by columns. The number of elements in D, B, and A cannot exceed the dimensions of their respective arrays in the calling routine. The number of elements in C, Ct, Z, ZNV, and CØEF cannot exceed 100 without changing the dimension statements.

```
      SUBROUTINE LSQ (D, B, N, A, G)
C     *****   LEAST SQUARE DETERMINATION OF TENSOR COEFFICENTS   *****
      TYPE DOUBLE A, C, CT, Z, ZNV, COEF, G, B
C     *****   DIMENSION D(3*N), A(9)   *****
      DIMENSION D(1), B(N), A(1), C(100), CT(100), Z(100)
      DIMENSION ZNV(100), COEF(100)
   50 FORMAT (* LEAST SQUARE REDUCTION*)
   51 FORMAT (* FIRST MULTIPLICATION*)
   52 FORMAT (* SECOND MULTIPLICATION*)
   53 FORMAT (* THIRD MULTIPLICATION*)
   54 FORMAT (* LEAST SQUARE ERROR*)
C     *****   SETTING UP COEFFICENT MATRIX   *****
      DO 2 I = 1, N
      DO 1 J = 1, 3
    1 C((J-1)*N+I) = D((J-1)*N+I)**2
      C(3*N+I) = 2.0*D(N+I)*D(2*N+I)
      C(4*N+I) = 2.0*D(2*N+I)*D(I)
    2 C(5*N+I) = 2.0*D(I)*D(N+I)
C     *****   LEAST SQUARE VARIABLE DETERMINATION   *****
      CALL TRNSPS (N, 6, C, CT)
      CALL MATMULT (6, N, N, 6, CT, C, Z, IFLG)
      IF (IFLG .EQ. 0) PRINT 51
      IF (IFLG .EQ. 0) GO TO 30
      CALL INVERT (6, 0.00001, Z, ZNV, IFLG)
      IF (IFLG .EQ.2) GO TO 30
      CALL MATMULT (6,6,6,N, ZNV, CT, COEF, IFLG)
```

```
      IF (IF_G .EQ. 0) PRINT 52
      IF (IF_G .EQ. 0) GO TO 30
      CALL MATMULT (6, N, N, 1, COEF, B, A, IFLG)
      IF (IF_G .EQ. 0) PRINT 53
      IF (IF_G .EQ. 0) GO TO 30
      A(9) = A(3)  $       A(3) = A(7) = A(5)      $       A(5) = A(2)
      A(10) = A(4) $       A(2) = A(4) = A(6)$       A(6) = A(8) = A(10)
C     *****   ROOT MEAN SQUARE ERROR DETERMINATION   *****
      CALL MATMULT (N, 6, 6, N, C, COEF, Z, IFLG)
      IF (IF_G .EQ. 0) PRINT 51
      IF (IF_G .EQ. 0) GO TO 31
      CALL IDENT (N,ZNV)
      CALL ADD(N,N,ZNV,Z,COEF,-1.00000)
      CALL MATMULT (N,N,N,1, COEF, B, C, IFLG)
      IF (IF_G .EQ. 0) PRINT 52
      IF (IF_G .EQ. 0) GO TO 31
      CALL TRNSPS (N, 1, C, CT)
      CALL MATMULT (1,N,N,1, CT, C, Z, IFLG)
      IF (IF_G .EQ. 0) PRINT 53
      IF (IF_G .EQ. 0) GO TO 31
      XMSE = Z(1)/(N+2-6)     $       G = SQRT(XMSE)
      GO TO 32
   30 PRINT 50    $       STOP
   31 PRINT 54    $       STOP
   32 RETURN  $       END
```

Subroutine Description: TRNSPS

Purpose

To form a matrix transpose.

Usage

The calling sequence is:

CALL TRNSPS (NØRWX, NØCOLX, X, XT)
NØRWX--number of rows in X.
NØCØLX--number of columns in X.
X--matrix to be transposed.
XT--matrix transpose of X.

Method

Given a NØRWX by NØCOLX matrix, X, the NØCOLX by NØRWX matrix, XT, is formed by:

$$XT = X^T,$$

where

$$(XT)_{ij} = X_{ji}.$$

Restrictions

Subroutine TRNSPS is written in a general form. Thus, it may be used to form a matrix transpose under most circumstances. The variables, X and XT, are specified to be double precision. This subroutine uses dummy dimensions for X and XT. Thus they must be stored in column mode in the calling routine.

```
      SUBROUTINE TRNSPS(NORWX, NOCOLX, X, XT)
C     *****   MATRIX TRANSPOSE   *****
      TYPE DOUBLE X, XT
      DIMENSION X(NORWX,NOCOLX), XT(NOCOLX,NORWX)
      DO 2 I = 1, NOCOLX
      DO 1 J = 1, NORWX
    1 XT(I,J) = X(J,I)
    2 CONTINUE
      RETURN
      END
```

Subroutine Description: MATMULT

Purpose

To perform matrix multiplication.

Usage

The calling sequence is:

CALL MATMULT (NØRWX, NØCØLX, NØRWY, NØCØLY, X, Y, X, IM)
NØRWX--number of rows in matrix, X.
NØCOLX--number of columns in matrix, X.
NØRWY--number of rows in matrix Y.
NØCØLY--number of columns in matrix Y.
X--input matrix.
Y--input matrix.
Z--output matrix.
IM--error flag. When NØCØLX $\neq$ NØRWY, IM = 0.

Method

Given the NØRWX by NØCØLX matrix, X, and the NØRWY by NØCØLY matrix, Y, the NØRWX by NØCØLY matrix, Z, is obtained by:

$$Z = XY,$$

where:

$$z_{ij} = \sum_{k=1}^{N} x_{ik} y_{kj}, \quad N = \text{NØCØLX} = \text{NØRWY}$$

Restrictions

Subroutine MATMULT is written in general form. Thus, it may be used to perform matrix multiplication under most circumstances. The variables X, Y, and Z are specified to

be double precision. NØCØLX must equal NØRWX. The arrays X, Y, and Z are dummy dimensioned. Thus, they must be stored in column mode in the calling routine.

```
      SUBROUTINE MATMULT (NORWX,NOCOLX, NORWY, NOCOLY, X, Y, Z, IM)
C     *****   MATRIX MULTIPLICATION   *****
C     *****   Z = X*Y   *****
      TYPE DOUBLE X,Y, Z
      DIMENSION X(NORWX,NOCOLX), Y(NORWY,NOCOLY), Z(NORWX,NOCOLY)
    1 FORMAT (* MATRIX MULTIPLICATION ERROR*)
      IF (NOCOLX .EQ. NORWY) GO TO 2
      IM = 0
      PRINT 1                                                    PRINT
      RETURN
    2 IM = 1
      DO 4 I = 1, NORWX
      DO 4 J = 1, NOCOLY
      Z(I,J) = 0.0
      DO 3 N = 1, NOCOLX
    3 Z(I,J) = Z(I,J) + X(I,N)*Y(N,J)
    4 CONTINUE
      RETURN
      END
```

Subroutine Description: INVERT

Purpose

To invert a real matrix by Gaussian elimination and back substitution.

Usage

The calling sequence is:

CALL INVERT (N, EP, B, X, KER)
N--rank of the matrix.
EP--the zero test value for the singularity check.
B--the N by N input matrix.
X--the N by N output (inverse of B) matrix.
Ker--singularity flag. KER = 2 if B is singular.

Method

Given an N by N, non-singular matrix, A, it can be transformed into an upper triangular matrix, B, by simple row operations (Marcus and Minc, 1965). The matrix is first searched to find the row with the largest (magnitude) element in the first column. The magnitude of this element is then tested against EP to insure that the matrix is not singular. For non-singular matrices, the row containing this element is interchanged with the first row of the matrix. Next, the first column entries in all but the first row are eliminated by subtracting multiples of the first row such that their first column entries vanish. The appropriate multiplication factor, m_i, for the i^{th} row will be:

$$m_i = \frac{a_{i1}}{a_{11}} ,$$

and the elements of row i will be given by:

$$a'_{ij} = a_{ij} - \frac{a_{i1}}{a_{11}} a_{1j}.$$

Next, the above process is repeated on the (N-1) by (N-1) matrix remaining in rows 2 through N. The row of this new matrix with the largest (magnitude) element in the first column (column 2 of the original N by N matrix) is tested against Ef, rotated into the top row (second row of the original N by N matrix), and the first column elements eliminated in the remaining rows as above. This process is repeated until an upper triangular matrix is obtained, which will be called B. Simultaneously, the same elementary row operations applied to A to obtain B are also applied to an N by N identity matrix, I, to obtain an auxillary matrix, C.

When A has been transformed into B, back substitution (Faddeeva, 1959; Weeg and Reed, 1966) is used to obtain the elements of the inverse matrix, X. The recursion formulas for this back substitution are (Bailey, 1961; Weeg and Reed, 1966):

$$x_{Nj} = \frac{c_{Nj}}{b_{NN}} ,$$

$$x_{ij} = \frac{c_{ij} - \sum_{k=i+1}^{N} b_{ik} x_{kj}}{b_{ii}} , \quad i < N, \; j \leqslant N.$$

Restrictions

Subroutine INVERT is written in general form. Thus, it may be used to invert any non-singular matrix, under most circumstances. The rank of the matrix to be inverted may not be greater than ten without changing the dimension for A. Variables X and B have dummy dimensions. Thus, these variables must be stored in column mode in the calling routine. The variables A, X, Z, RATIØ, S, and B are specified to be double precision.

The test for singular matrices will depend upon the input value of EP. Care must be taken in determining it.

Subroutine INVERT calls subroutine IDENT.

Acknowledgments

Subroutine INVERT was obtained from the Michigan State University Computer Laboratory Library (Bailey, 1961), as subroutine GAUSS. It was verified and modified by the author.

```
      SUBROUTINE INVERT (N, EP,B,X,KER)
C     *****   MATRIX INVERSION BY GAUSIAN ELIMINATION   *****
      TYPE DOUBLE A, X, Z, RATIO, S ,B
      DIMENSION B(N,N), X(N,N), A(10,10)
    1 FORMAT (* SINGULAR MATRIX*)
      DO 2 I = 1, N
      DO 2 J = 1, N
    2 A(I,J) = B(I,J)
      CALL IDENT (N,X)
      DO 10 L = 1, N
      KP = 0   $        Z = 0.000000
      DO 3 K = L, N
      IF (Z .GE. DABS(A(K,L))) GO TO 3
      Z = DABS(A(K,L))   $        KP = K
    3 CONTINUE
      IF (L .GE. KP) GO TO 6
      DO 4 J = L, N
      Z = A(L,J)    $        A(L,J) = A(KP,J)
    4 A(KP,J) = Z
      DO 5 J = 1, N
      Z = X(L,J)
      X(L,J) = X(KP,J)
    5 X(KP,J) = Z
    6 IF (DABS(A(L,L)) .LE. EP) GO TO 13
      IF (L .GE. N) GO TO 10
```

```
      LP1 = L + 1
      DO 9 K = LP1, N
      IF (A(K,L) .EQ. 0.0) GO TO 9
      RATIO = A(K,L)/A(L,L)
      DO 7 J = LP1, N
    7 A(K,J) = A(K,J) - RATIO*A(L,J)
      DO 8 J = 1, N
    8 X(K,J) = X(K,J) - RATIO*X(L,J)
    9 CONTINUE
   10 CONTINUE
      DO 12 I = 1, N
      II = N + 1 - I
      DO 12 J = 1, N
      S = 0.0
      IF (II .GE. N) GO TO 12
      IIP1 = II + 1
      DO 11 K = IIP1, N
   11 S = S + A(II,K)*X(K,J)
   12 X(II,J) = (X(II,J) - S)/A(II,II)
      KER = 1 $          GO TO 14
   13 KER = 2 $          PRINT 1
   14 CONTINUE
      RETURN $          END
```

Subroutine Description: IDENT

Purpose

To create an N by N identity matrix.

Usage

The calling sequence is:

CALL IDENT (N, X)
N--rank of the identity matrix, X.
X--array in which the identity matrix will be stored.

Method

The N by N matrix, X, is first set equal to zero and then the x_{ii} elements set equal to 1.000000.

Restrictions

Subroutine IDENT is general in form. Thus, it may be used to create identity matrices in most cases. The array, X, is dummy dimensioned. Thus, it must be stored in column mode in the calling routine. The array, X, may not have more elements than allowed by its dimension in the calling routine. The variable, X, is specified to be double precision. Subroutine IDENT calls subroutine ZERØ.

```
      SUBROUTINE IDENT (N,X)
C     *****   N X N IDENTITY MATRIX    *****
      TYPE DOUBLE X
      DIMENSION X(N,N)
      NN = N*N
      CALL ZERO (NN,X)
      DO 10 I = 1, N
   10 X(I,I) = 1.000000
      RETURN
      END
```

Subroutine Description: ZERØ

Purpose

To fill an array with zero elements.

Usage

The calling sequence is:

CALL ZERØ (LX, X)
LX--number of elements in the array, X.
X--the array to be set equal to zero.

Method

All elements in the array, X, are set equal to 0.000000.

Restrictions

Subroutine ZERØ is general, so it may be used to set arrays equal to zero in most cases. The array, X, is dummy dimensioned. Thus all multiply dimensioned arrays to be zeroed by this routine must be stored in column mode in the calling routine. The variable, X, is specified to be double precision. The number of elements in X cannot exceed the dimension of X in the calling routine.

Acknowledgments

Subroutine ZERØ was obtained from Robinson (1967).

```
      SUBROUTINE ZERO (LX,X)
      TYPE DOUBLE X
      DIMENSION X(LX)
      IF (LX .LE. 0) RETURN
      DO 1 I = 1, LX
    1 X(I) = 0.00
      RETURN
      END
```

Subroutine Description: ADD

Purpose

To perform matrix addition.

Usage

The calling sequence is:

CALL ADD (NR, NC, X, Y, Z, CNST)
RN--number of rows in the matrices to be added.
NC--number of columns in the matrices to be added.
X--matrix to be added.
Y--matrix to be added.
Z--matrix sum of X and Y.
CNST--a multiplicitive constant for Y

Method

Given the NR by NC matrices, X and Y, and a constant, CNST, the NR by NC matrix, Z is obtained by:

$$Z = X + CNST \cdot Y.$$

Restrictions

Subroutine ADD is general in form, so that it may be used to perform real matrix addition under most circumstances. The arrays X, Y, and Z are dummy dimensioned. Thus, they must be stored in column mode in the calling routine. The arrays X, Y, and Z, may not contain more elements than dimensioned in the calling routine. The arrays X, Y, and Z must all be NR by NC matrices. The variables X, Y, and Z are specified to be double precision.

```
      SUBROUTINE ADD (NR, NC, X, Y, Z, CNST)
C     *****   MATRIX ADDITION   *****
C     *****   Z = X + CNST*Y   *****
      TYPE DOUBLE X, Y, Z
      DIMENSION X(NR,NC), Y(NR,NC), Z(NR,NC)
      DO 10 I = 1, NR
      DO 10 J = 1, NC
   10 Z(I,J) = X(I,J) + CNST*Y(I,J)
      RETURN
      END
```

Subroutine Description: REDUCE

Purpose

To obtain the principal directions and values of the σ and K tensors by rotation to their principal axes.

Usage

The calling sequence is:

CALL REDUCE (NØFQ, NAME)
NØFQ--number of frequencies at which the electrical properties were measured.
NAME--sample identification.

Method

The arbitrary initial direction, L, is read in and stored on scratch unit 26. Then the measurement frequency, σ and K tensors, and rms errors are read from scratch unit 27. The σ and K data are processed separately.

The iteration cut-off value, CTF, for the tensor, T, is obtained by:

$$CTF = \frac{\sqrt{\sum_{i=1}^{3} T_{ii}^2}}{10^9}.$$

The maximum principal direction for the symmetric second-rank tensor, T, is obtained by inputting CTF and T into subroutine MAXCF. The minimum principal direction is obtained by taking the inverse of T, calculating a

new cut-off value, based on its main diagonal and inputting it to subroutine MAXCF.

The intermediate principal direction is obtained by taking the cross product of the maximum and minimum principal directions.

These principal directions are used as in equations 3.5 and 6.13.

$$T_{||}\ \hat{1} = \hat{1}^T\ T\ \hat{1}.$$

This procedure is repeated for σ and K at each frequency and the results printed out, along with the rms errors.

Restrictions

Subroutine REDUCE was written specifically for the problem described in Chapters II, IV, and VI of the text. It will have to be rewritten if used for any other purpose. The variables T, TIV, L, Ll, and AT are specified as double precision. The variables T, TIV, L, AT, AA, and Ll are multiply dimensioned arrays stored by column mode.

Subroutine REDUCE calls subroutines ØUTPUT, MAXCF, INVERT, CRØSS, and MATMULT. This subroutine reads input from scratch units 26 and 27. Thus, care must be taken to see that these tapes are written in exactly the same manner as they are read.

The carriage controls in the print formats may only be valid for the Michigan State University CDC 3600 system.

```
      SUBROUTINE REDUCE (NOFQ, NAME)
      TYPE DOUBLE T, TIV, L, L1, AT
C     *****   ITERATIVE REDUCTION TO PRINCIPAL DIRECTIONS   *****
      DIMENSION T(20), TIV(20), L(20), NAME(10), AT(20), AA(20), L1(20)
    1 FORMAT (3F11.5)
    2 FORMAT (*1*/*4*, 13X, * SAMPLE *, 10A8)
    3 FORMAT (*0*, 13X, * FREQUENCY = *, F8.0, * CPS*)
    4 FORMAT (*0*, 13X, * DIELECTRIC CONSTANT*)
    5 FORMAT (*0*,13X,* CONDUCTIVITY (IN MHO/METER)*)
    6 FORMAT (*0*,13X,* TENSOR INPUT*)
    7 FORMAT (*0*,13X,* DIRECTION COSINES AND DIRECTION ANGLES OF*,
     1 * PRINCIPAL DIRECTIONS*)
    8 FORMAT (13X,3F11.5,10X,3F11.5)
    9 FORMAT (*0*,13X,33H *** MAXIMUM PRINCIPAL COEFFICENT,5X,* = *,
     1 E13.6, 4H ***)
   10 FORMAT (14X,42H *** INTERMEDIATE PRINCIPAL COEFFICENT  = ,E13.6,
     1 4H ***)
   11 FORMAT (14X,33H *** MINIMUM PRINCIPAL COEFFICENT,6X,* = *,
     1 E13.6, 4H ***)
   12 FORMAT (*0*, 13X, * RMS ERROR FROM THE MODEL = *,E13.5)
C     *****   MAIN   *****
      PI = 3.14159265358979
      REWIND 25     $       REWIND 27
      READ 1, (L(I), I = 1, 3)                                        READ
      WRITE (25), (L(I), I = 1, 3)                                    WRITE
      REWIND 25
      DO 44 NOTM = 1, NOFQ
```

```
      READ (27), FQ                                                    READ
      PRINT 2, NAMES       PRINT 3, FQ                                 PRINT
      DO 44 NTM = 1, 2
      READ (26), (L(I), I = 1, 3)                                      READ
      REWIND 26
      READ (27), ERROR
      READ (27), (T(I), I = 1, 9)                                      READ
      IF (NTM .EQ. 1) PRINT 4 $       IF (NTM .EQ. 2) PRINT 5          PRINT
      PRINT 6 $       CALL OUTPUT (3,3,1,T)                            PRINT
C     *****   MAXIMUM PRINCIPAL DIRECTION   *****
      CUTOFF = 0.000000000000
      DO 33 I = 1, 3
   33 CUTOFF = CUTOFF + (T(3*(I-1)+I))**2
      CUTOFF = (SQRT(CUTOFF))/1000000000.000
      CALL MAXCF (T,L,CUTOFF,L1)
      DO 34 I = 1, 3
   34 AT(I) = L1(I)
C     *****   MINIMUM PRINCIPAL DIRECTION   *****
      CUTOFF = CUTOFF/1000000000.0
      IS = 0  $       CALL INVERT (3,CUTOFF,T,TIV,IS)
      IF (IS .EQ. 2) STOP $       CUTOFF = 0.000000000
      DO 35 I = 1, 3
   35 CUTOFF = CUTOFF + (TIV(3*(I-1)+I))**2
      CUTOFF = (SQRT(CUTOFF))/1000000000.000
      CALL MAXCF (TIV,L,CUTOFF, L1)
      DO 36 I = 1, 3
   36 AT(6+I) = L1(I)
C     *****   INTERMEDIATE PRINCIPAL DIRECTION   *****
      CALL CROSS (AT)
```

```
      DO 37 I = 1, 3
   37 AT(3+I) = -1.000000*AT(3+I)
      PRINT 7                                                        PRINT
      DO 39 J = 1, 3
      IF (AT(3+J) .GE. 0.000000) GO TO 39
      DO 38 I = 1, 3
   38 AT(3*(J-1)+I) = -1.000000*AT(3*(J-1)+I)
   39 CONTINUE
      DO 40 I = 1, 9
   40 AA(I) = (180.000*ACOS(AT(I)))/PI
      DO 41 I = 1, 3
   41 PRINT  8, AT(I), AT(I+3), AT(I+6), AA(I), AA(I+3), AA(I+6)     PRINT
C     *****   PRINCIPAL VALUES   *****
      IM = 1  $       CALL MATMULT (3,3,3,1,T,AT,L,IK)
      IF (IK .LE. 0) STOP $       CALL MATMULT (1,3,3,1,AT,L,L1,IK)
      IF (IK .LE. 0) STOP     $       PRINT 9, L1(1)               PRINT
      DO 42 I = 1, 3
   42 L1(I) = AT(3+I)
      CALL MATMULT(3,3,3,1,T, L1, L, IK)
      IF (IK .LE. 0) STOP $       CALL MATMULT (1,3,3,1,L1,L,AT,IK)
      IF (IK .LE. 0) STOP     $       PRINT 10, AT(1)              PRINT
      DO 43 I = 1, 3
   43 L1(I) = AT(6+I)
      CALL MATMULT(3,3,3,1,T, L1, L, IK)
      IF (IK .LE. 0) STOP $       CALL MATMULT (1,3,3,1,L1,L,AT,IK)
      IF (IK .LE. 0) STOP
      PRINT 11,AT(1)
   44 PRINT 12, ERROR                                                PRINT
      RETURN  $       END
```

Subroutine Description: MAXCF

Purpose

To determine the maximum principal direction of a symmetric second-rank tensor.

Usage

The calling sequence is:

CALL MAXCF (T, L, CLF, L1)
T--the symmetric, second-rank tensor.
L--direction cosine column vector for an initial arbitrary direction.
CLF--test cut-off value for the iteration procedure.
L1--the maximum principal direction of T.

Method

The method used is the iterative procedure described in Chapter VI of the text. Starting with an arbitrary unit direction, L, the unit normal to the representation surface at the point of intersection of L and the surface is determined by:

$$\hat{n} = \frac{T \cdot L}{||T \cdot L||}.$$

This unit direction is now used to determine the unit normal to the representation at its point of intersection. This process is repeated, each time testing the difference between successive representation surface normals ($||\hat{n}_i - \hat{n}_{i+1}||$) against the iteration cut-off value, CLF.

When this difference falls within CLF, the last $\hat{n}_i$ is then taken to be the maximum principal direction of the symmetric second-rank tensor.

Restrictions

Subroutine MAXCF is general in nature and can be used to obtain the maximum principal direction of any symmetric second-rank tensor.

Variables T, Ll, and M are specified to be double precision, while CLF is single precision. The arrays T, Ll, and L are dummy dimensioned and so must be stored in column mode in the calling routine. Variable M is a multiply dimensioned array stored in column mode as a singly dimensioned array of 20 elements. Subroutine MAXCF calls subroutine MATMULT.

```
      SUBROUTINE MAXCF (T, L, CLF, L1)
C     *****   ITERATIVE ROTATION TO MAXIMUM PRINCIPAL DIRECTION   *****
      TYPE DOUBLE T, L, CTF, L1, M, TEST, DENOM, DENOM1
      DIMENSION T(1), L(1), L1(1), M(20)
      CTF = CLF
      DO 21 I = 1, 3
   21 L1(I) = L(I)
      DENOM = 0.0000000000
   22 DENOM1 = DENOM
      IK = 1
      CALL MATMULT (3,3,3,1, T, L1, M)
      IF (IK .LE. 0) STOP
      DENOM = 0.0000000000
      DO 23 I = 1, 3
   23 DENOM = DENOM + (M(I)**2)
      DENOM = DSQRT(DENOM)
      TEST = DABS(DENOM - DENOM1)
      DO 24 I = 1, 3
   24 L1(I) = M(I)/DENOM
      IF (TEST .GE. CTF) GO TO 22
   25 RETURN
      END
```

Subroutine Description: CRØSS

Purpose

To perform the (vector) cross product.

Usage

The calling sequence is:

CALL CRØSS (X)
X--the 3 by 3 array containing all three column vectors.

Method

Given two three-dimension column vectors stored as the first and third columns of a 3 by 3 matrix, X, the cross product is obtained by:

$$[X_1] \times [X_2] = \begin{vmatrix} i & j & k \\ x_{11} & x_{21} & x_{31} \\ x_{31} & x_{32} & x_{33} \end{vmatrix} = [X_2],$$

where the resulting column vector is stored as the second column of X.

Restrictions

Subroutine CRØSS can be used to perform the cross product between any two vectors stored as above. The variable, X, is specified to be double precision.

```
      SUBROUTINE CROSS (X)
C     *****   VECTOR (CROSS) PRODUCT    *****
      TYPE DOUBLE X
      DIMENSION X(3,3)
      DO 11 I = 1, 3
      J = I + 1
      IF (J .LE. 3) GO TO 10
      J = J - 3
   10 K = I + 2
      IF (K .LE. 3) GO TO 11
      K = K - 3
   11 X(I,2) = X(J,1)*X(K,3) - X(K,1)*X(J,3)
      RETURN
      END
```

MICHIGAN STATE UNIVERSITY LIBRARIES
3 1293 03085 2499